

Research & Development
2016

Mechanical Engineering Letters, Szent István University

Annual Technical-Scientific Journal of the Mechanical Engineering Faculty,
Szent István University, Gödöllő, Hungary

Editor-in-Chief:
Dr. István SZABÓ

Editor:
Dr. Gábor KALÁCSKA

Executive Editorial Board:

Dr. István BARÓTFI
Dr. János BEKE
Dr. István FARKAS
Dr. László FENYVESI
Dr. István HUSTI
Dr. László KÁTAI
Dr. Sándor MOLNÁR
Dr. Péter SZENDRŐ
Dr. Zoltán VARGA

Cover design:
Dr. László ZSIDAI

HU ISSN 2060-3789

All Rights Reserved. No part of this publication may be reproduced, stored in a retrieval system or transmitted in any form or by any means, electronic, mechanical, photocopying, recording, scanning or otherwise without the written permission of Faculty.

Páter K. u. 1., Gödöllő, H-2103 Hungary
dekan@gek.szie.hu, www.gek.szie.hu,

Volume 14 (2016)

Mechanical Engineering Letters



Professor Dr. László KÁTAI
Dean

Dear Reader,

The Mechanical Engineering Faculty of Szent István University is an important institution of the Hungarian higher education scene and has, for more than 60 years, taught students at BSc, MSc and PhD levels.

One of the most important basic activities of the Faculty operating within the framework of the higher education institute is education and training. In addition to education, other significant fields of its activity in focus are research, development and innovation. The Faculty of Mechanical Engineering has a significant potential in research, which is also supported by the laboratory infrastructure and equipment developments realised in recent years.

In national (and on given fields also international) comparison, our colleagues have achieved acknowledged results in research. Such topics of outstanding importance are for example:

- agricultural machinery and technology development;
- renewable energy utilization (solar, biomass, wind and geothermal energy);
- materials sciences (primarily application of polymer composites);
- biomechanics, mechanics of biological materials and systems;
- safe food production;
- applied mathematics and
- applied and engineering-agricultural informatics.

An important element of scientific activities is the dissemination of results, in other words publication. The periodical „Mechanical Engineering Letters” issued by the Mechanical Engineering Faculty now for the 14th time is dedicated to this purpose: to provide room for the publication of RDI results.

I commend the publications summarising the latest scientific results of the Faculty’s institutes to our dear readers.

Dr. László Kátai
dean

Contents

1. Institute for Environmental Engineering Systems (Professor Dr. István FARKAS, Director of the Institute)	7
Qudama AL-YASIRI, Márta SZABÓ: Solar absorption cooling systems versus traditional air-conditioning in hot climate	9
János Péter FEJES, János BUZÁS: Modeling of storage tank filling with boiling liquid	17
Attila SZILÁGYI, István FARKAS, István SERES: Development of a solar assisted absorption cooler	26
2. Institute for Mathematics and Informatics (Professor Dr. Sándor MOLNÁR, Director of the Institute)	33
Richárd KICSINY: Multiple linear regression based models for solar collectors	35
Márk MOLNÁR, Tamás TIMÁR, Zsuzsa TÓTH-NAÁR: Economic indicators and market prosperity - a new approach for the estimation of market uncertainty	47
Sándor MOLNÁR, Márk MOLNÁR: A new approach for the estimation of non-linear switching-type systems	54
3. Institute for Mechanical Engineering Technology (Professor Dr. Gábor KALÁCSKA, Director of the Institute)	63
Adrienn GODA, Viktor MEDINA, László ZSIDAI: Methodological development of the International Manufacturing Strategy Survey based on the case of the Hungarian maize pickers' manufacturer sector	64
Al-Maliki HAYDER, Zoltán SZAKÁL, Róbert KERESZTES, Gábor KALÁCSKA: Shear strength of polypropylene bonded joints using pristine and DBD plasma treated surfaces	71
Eszter SÁRKÖZI: Reduction of air consumption of positioned pneumatic drive by the optimization criteria of GA	78

4. Institute for Process Engineering	
(Professor Dr. Péter KISS, Director of the Institute)	89
Zoltán KURJÁK, Kornél BESSENYEI, János BEKE: Influence of energy and mass transport on microwave drying process of vegetables	91
Mohammed HUSSEIN ALI, Márta SZABÓ, János BEKE: Development of Earth-air heat exchanger based cooling system for building insubtropical conditions	101
László MÁTHÉ, György PILLINGER, Péter KISS: Determination of rolling losses of a towed vehicle	118
5. Institute for Engineering Management	
(Associate Professor Dr. Miklós DARÓCZI, Director of the Institute)	131
Imre KOVÁCS, Viktor MEDINA, István HUSTI: Partial examination of the influencing factors in the use of IT applications in agricultural mechanization	132
6. Institute for Mechanics and Machinery	
Professor Dr. István SZABÓ, Director of the Institute)	139
István KEPPLER, István OLDAL, Ferenc SAFRANYIK, Adrienn BABLENA: Calibration of discrete element models	140
Zoltán BLAHUNKA, Zoltán BÁRTFAI, Dezső FAUST: Terrain classification with IMU	152
Mohammad HUSHKI, Laszlo KÁTAI, Istvan SZABÓ: Experimental study: Operator's behavior measuring inside Off-road vehicle Cabin (Operator's focusing matrix and response time)	160
7. Invited Papers	171
Zsolt HORVÁTH, András EDELMAYER: LTI-modelling of the air path of turbocharged diesel engine for fault detection and isolation	172
Jozef RÉDL, Juraj MAGA, Gábor KALÁCSKA: Mathematical model of lateral stability of agricultural machine	189

Institute for Environmental Engineering Systems



Professor Dr. István FARKAS
Director of the Institute

Dear Reader,

The Institute for Environmental Engineering Systems consists of two departments as Department of Environmental and Building Engineering and Department of Physics and Process Control. There are several research activities going on in the Institute having interrelations in order to find new scientific solutions concerning to the environmental engineering requirements. It gives a strong opportunity for sustainable development and allowing common way of approach in the solution of different nature of problems.

Form the results of the current research activity the following topics are selected out to publish in the recent issues of the Journal:

Modeling of storage tank filling with boiling liquid

- This paper presents a mathematical model and a computer simulation of LPG (Liquefied Petroleum Gas), especially propane filling into a storage tank as a boiling liquid. To represent the physical process the equipment and the liquid was divided into homogeneous control volumes. Assuming open thermodynamic systems the governing equations were identified for each heat and mass transfer process occurring between the control volumes. Using the proper conservation of mass and energy equations along with the equations of state the values of the lumped parameters describing the system were determined. A measurement system built to validate the model and the simulation has also been introduced.

Development of a solar assisted absorption cooler:

- In this paper it was shown how the solar energy can be used for cooling. This is a very important topic nowadays, because summers are getting hotter and hotter, and numerous air conditioning system are working with electrical energy. This energy demand would be decreased with solar air conditioning devices, which can reduce also the environmental impact of the heat power plants. The energy demand for cooling can be collected from solar energy (with solar cells or solar collectors), so there is no need for energy storage. For this purpose, a solar collector combined with an absorption cooler can be a proper solution. In this paper the development of the experimental equipment is presented with some measurement results.

Solar absorption cooling systems versus traditional air-conditioning in hot climate:

- In building sector globally accounts more than 40% of the energy use. Especially in hot climates cooling and air-conditioning represent the highest share of the energy use. Use of solar energy is a key factors in minimizing the dependency on the power systems and maximizing the environmental effects having suitable indoor comfort for the occupants. A comparison of traditional and modern technology has been conducted for hot climate and presented by a case study for Iraq. According to the calculations building retrofitting contributed by 14% of reducing the need for cooling. It can also be concluded that solar AC systems contribute to a low electric power consumption (165 kWh) compared to the traditional one (around 1440 kWh) and results a CO₂ emission decrease by more than 88%.

Solar absorption cooling systems versus traditional air-conditioning in hot climate

Qudama AL-YASIRI, Márta SZABÓ

Department of Building Service and Environmental Engineering,
Institute for Environmental Systems

Abstract

Building sector globally accounts more than 40 % of the energy use, consuming more than industrial or transport sector. Especially in hot climates cooling – air conditioning represents the highest share of the energy used in buildings. Decreasing the cooling load and utilization of solar energy are key factors in minimizing the dependency on the power systems and maximizing the environmental effects having the suitable indoor comfort for the occupants.

A comparison of traditional and modern technology has been conducted for hot climate and presented by a case study for Iraq. According to the calculations building retrofitting contributed by 14 % of reducing the need for cooling. As a result, it can be concluded too that solar AC systems contribute to a low electric power consumption (165 kWh) compared to the traditional one (around 1440 kWh) and results a CO₂ emission decrease by more than 88 %.

Keywords

Absorption solar cooling, cooling load, HVAC systems, Building retrofitting

1. Introduction

The building sector in Iraq is one of the most important sectors responsible for energy consumption due to population growth and increasing of various other economic activities year after year. The share of energy consumption within the total supplied energy by residential buildings is high, in the capital- Baghdad alone was about 48% [1]. The buildings use high proportion (92 %) of total energy processed to operate air-conditioning and cooling systems [2]. The long summer season in Iraq is characterized by high-temperature and long day hours, and during the hot period in order to overcome the high temperature and reach the thermal comfort of the occupants there is a need for using efficient cooling system. The use of renewable energy becomes more relevant because of the electric power instability and because of the environmental impacts of the traditional air-conditioning systems and their refrigerants. In this paper energy efficiency measures and solar absorption air-conditioning system is introduced and discussed compared to the traditional air conditioning system in a given building.

2. Cooling load calculations Methodology

The calculations have been made according to two methods: Cooling Load Temperature Difference/ Solar Cooling Load/ Cooling Load Factor (CLTD/SCL/CLF) method of ASHRAE and then, by using Hourly Analysis Program (HAP 4.8).

CLTD/ SCL/ CLF method

This method is one of the most important traditional methods used to calculate the external and internal loads of the buildings based on set of parameters available by ASHRAE. It is an accurate method and address the aspects that are related to the building one by one, as following [3]:

Roofs load:

$$Q_{\text{Roof}} = A_r U_r \text{CLTD}_c \quad (1)$$

Q_{Roof} : heat gain of the roof (kW)

A_r : roof's area (m²)

U_r : overall heat transfer coefficient of the roof (W/m²K).

CLTD_c : correction of cooling load temperature difference of the roofs.

$$U_r = 1/R, R = L/k \quad (2)$$

R : thermal resistance of roof layers (m²K/W),

L : layer thickness (m),

k : layer thermal conductivity (W/mK)

$$\text{CLTD}_c = \text{CLTD} + (25.5 - T_r) + (T_o - 29.4) \quad (3)$$

T_r : inside temperature (comfort temp.) (°C).

T_o : mean outdoor temperature (°C).

$$T_o = t_o - \text{DR} / 2 \quad (4)$$

t_o : outdoor design temperature (°C).

DR : daily range during the day (°C).

Walls load:

– External walls

$$Q_{\text{Ext. wall}} = A_w U_w \text{CLTD}_c \quad (5)$$

A_w : net wall's area (excluding the windows and doors) (m²).

$A_w = \text{Width} \times \text{height}$, height= 3 m

U_w : overall heat transfer coefficient of the external wall (W/m²K)
 CLTD_c: correction of cooling load temperature difference of external walls.
 – Internal walls

$$Q_{\text{Int. wall}} = A_w U_w \Delta T \quad (6)$$

A_w : net wall's area (m²). $A_w = \text{Width (m)} \times \text{height (m)}$.
 U_w : overall heat transfer coefficient of the internal wall (W/m²K)
 ΔT : temperature difference between the adjacent space and the conditioned room.

Windows load:
 – Conductive load

$$Q_{\text{Cond. window}} = A_w U_w \text{CLTD}_c \quad (7)$$

A_w : window's area (m²), $A = \text{length (m)} \times \text{width (m)}$.
 U_w : overall heat transfer coefficient of the windows (W/m²K).
 CLTD_c: correction of cooling load temperature difference of windows.
 – Solar load through glass

$$Q_{\text{Solar window}} = A_w (\text{SC}) (\text{SCL}) \quad (8)$$

A_w : widow's area (m²).
 SC = shading coefficient.
 SCL = solar cooling load factor with no interior shade or with shade.

Occupants load:

$$Q_{\text{sensible}} = N \times q_s \times \quad (9)$$

N : number of occupants in space.
 q_s : Sensible heat gain for each person (kW).
 CLF: cooling load factor. CLF= 1.0 (cooling off at night and during weekends).

$$Q_{\text{latent}} = N \times q_L \quad (10)$$

q_L : latent heat gain for each person (kW).

Lighting load:

$$Q_{\text{lighting}} = (\text{watt} / \text{m}^2) \times \text{Space area} \quad (11)$$

Infiltration load:

$$Q_{\text{sensible}} = 1.23 \times V_{\text{inf}} \times \Delta T \quad (12)$$

$V_{inf} = ACH \times \text{Room volume} / 3600$, $ACH = 1$ (the room has window in one side)
 ΔT : outside & inside air temperature ($^{\circ}C$) = $50 - 24 = 26$ $^{\circ}C$.

$$Q_{Latent} = 3010 \times V_{inf} \times \Delta w \tag{13}$$

Δw : outside & inside air humidity ratio, kg (water)/kg (dry air).

Equipment load: Selected directly from the tables for all equipment in space.

Floor load: Neglected (the calculated space above conditioned area).

$$\text{Total Load} = Q_{Roof} + Q_{Wall (Ext. + Int.)} + Q_{Window (Cond. + Solar)} + Q_{Occupants} + Q_{Lighting} + Q_{Infiltration} + Q_{Equipment}$$

Hourly Analysis Program (HAP4.8)

HAP program is one of the widely used software programs in the design of air-conditioning systems in Iraq. The program was developed by Carrier Company where it is used to design HVAC systems of various buildings and makes selection of the appropriate system with all components on one hand, and uses to make an analysis of energy consumption and fuel on the other hand. The program has been used for estimating the cooling load of case study building according to the same data that have been applied with CLTD method in order to support the results.

3. Case study calculation and results

Iraq is located in the south-west region of the continent of Asia. It is part of the north-east of the Arab world and lies between latitudes 29 – 37 degrees north. The summer season is hot, longer daytime and the mean temperature is more than 45 $^{\circ}C$ most of the year.

The building is located in Maysan province to the north of Amarah city (center of Maysan province) on the main line linking the city to the capital Baghdad (Amarah city located south-east of Iraq, on a low ridge next to the Tigris River waterway south of Baghdad about 50 km from the border with Iran). The building shown in Figure 1. is used for educational purposes at Maysan University– Faculty of Engineering.

The calculations have done according to the conditions of Table 1:

The total load of the building calculated by CLTD/ SCL/ CLF method is 167.2 kW. While, it was 165.6 kW using HAP software.

Table 1. The boundary design conditions of the building.

Location	Al- Amarah city/ Maysan province	
Outdoor conditions	$t_d = 50$ $^{\circ}C$	$t_w = 26$ $^{\circ}C$
Indoor conditions	$t_d = 24$ $^{\circ}C$	RH = 50 %
Daily range	13.5*	

* Daily range of Al- Amarah city during July 2016. [4]



Figure 1. Building case study

Selection of solar absorption A/C system

The selection of appropriate solar cooling system can be done based on the total cooling load of the building. The solar cooling system consists of one chiller having cooling capacity covering the total cooling load required, or consists of a number of chillers having less cooling capacity can cover building total load combine with all other necessary accessories. Table 2 consists of the specifications of solar absorption chiller of (35 kW) cooling capacity. [5]

Table 2. The main technical data of a) solar absorption chiller and b) solar thermal system

a) Solar Absorption Chiller (LiBr - Water)		
Model		GRS-35
Cooling Capacity		35 kW
Hot Water	Inlet/ outlet temperature (°C)	90/85
	Flow Rate (m ³ /hr)	9.2
	Connection Diameter	DN40
Chilled Water	Inlet/ outlet temperature (°C)	15/10
	Flow Rate (m ³ /hr)	6
	Connection Diameter	DN32
Power Consumption (kW)		3
Total Cost (\$)		18,800

b) Solar Thermal System	
Solar Collector Type	Evacuated Tubes
Solar Collector Area (m ²)	45
Hot Water Buffer Storage Tank Volume (m ³)	2

The building needs to use 5 chillers of 35 kW to cover the total load.

Minimizing cooling loads of the building

Cooling loads of existing building can be minimized by several methods. Generally, these methods are applied for the building envelope (roofs, walls and windows) where costs should be taken under consideration. As following:

- **Roofs load:** Adding a compressed glass fiber layer of (30 mm).

Insulating material	Thickness (mm)	Thermal conductivity (W/m.K)
Compressed glass fiber	30	0.038

- **Walls load:** Covering the inner walls of each room with wood insulation of (14 mm) away from the wall by air gab of (~25 mm).

Insulating material	Thickness (mm)	Thermal conductivity (W/m.K)
Softwood- southern cypress	14	0.131

- **Windows load:** Replacing the existed single glazing windows by double glazing ones of (6.4 mm) thickness and (12.7 mm) air gab.

Glazing type	Thickness (mm)	Air gab (mm)	U (W/m2.K)	SC
Clear double glazing	6.4	12.7	3.26	0.81

The total building cooling load after applying those techniques has become 143.76 kW.

4. Evaluating of traditional A/C and solar absorption cooling systems

Electrical energy consumption and CO₂ emissions

Traditional air-conditioning systems consume a large electric power volume to work, unlike the solar absorption systems that rely on thermal energy produced from the solar system primarily, as well as using less electrical energy to operate some parts of the system such like solution pump and other measurement and control devices.

The amount of CO₂ emissions are linked with the electrical energy consumed by air-conditioning systems. In fact, the power plants in Iraq are still dependent on oil products and natural gas by a large margin. According to the International Energy Agency IEA [6], the value of CO₂ emissions that generated from each kWh in Iraq is 1002.8376 depending on the type of sources used to generate electrical power. Table 3 below shows the amounts of CO₂ emissions generated from the traditional and solar absorption systems for each single working day (11 hours).

Table 3. CO₂ emissions/ kWh consumption of the systems

A/C systems type	Energy kWh/ day	CO ₂ grammes/ kWh	CO ₂ kg emissions
Electricity driven A/C	1438.8	1002.8367	1442.88
Solar absorption chillers	165	1002.8367	165.47

Initial cost and operational lifetime

The traditional air-conditioning systems are very economic because they are widely available and there are many companies producing such systems. Unlike solar absorption systems, those are modern technologies that need a long time to be common and competitive.

In general, the cost of traditional systems is much lesser than the solar driven systems. The average cost of a conventional system/s of split unite type of 35 kW cooling capacity is around \$ 3000, while the cost of solar-powered absorption chiller which gives the same cooling capacity is about \$ 18,800 (excluding the cost of solar thermal system).

On the other hand, the expected mean operating lifetime of the traditional A/C systems ranging from 5 to 8 years depending mainly on the stability of the electrical power. While the average operating lifetime of the solar absorption chiller is about 23 years (according to the manufacturer company) because that the moving parts of the latter system is much lesser than the traditional one, which prolongs its operational lifetime.

Conclusions and recommendation

One of the most important goals of this paper is finding a way to take advantages of the available solar energy on one hand, and solve the problem of power shortage that affects negatively on people's comfort on the other hand.

The study has been studied for building in Iraq in order to assess the current situation of its air-conditioning systems and recommend the possibility of using other modern technology that has many advantages. Several conclusions have been derived and can be summarized as follow:

- The possibility of using environmentally friendly air-conditioning systems has been studied by conducting detailed calculations of overall cooling loads of the building. These calculations are very important to choose the number and size of A/C systems that have to be used as a substitute for traditional systems. The calculations of cooling loads have been made by two methods and the results were approximately equal.
- The calculations were carried out as a kind of building retrofitting are very important and reflect positively in reducing the need for cooling by 14%. That reduction is led to reduce the number of solar absorption chillers that need to cool the building from 5 to approximately 4 chillers. Although it was simple and a bit expensive but it is more economic if compared with the rationalization in the air-conditioning systems usage.
- It was found that the use of traditional A/C systems of the building consumed about 1,438.8 kWh of electric power for each day work. While the proposed solar absorption chillers are consume only 165 kWh. And from an environmental perspective, CO₂ emissions that linked to the amount of electricity consumed by the traditional systems were about 1442.88 kg, but the generated CO₂ emissions from solar ones were 165.47 kg only.

- The initial cost of traditional systems constitutes about 10% of the initial cost of solar A/C systems also, the fact that traditional systems are more efficient than those driven by solar and they are easy to install and maintain. On the other hand, the operating lifetime of the solar A/C systems represents approximately 3 times more than the operational lifetime of the traditional ones as they contain moving parts much lower than those found in conventional systems as well as other electrical problems associated with the traditional systems.

As a result, it can be concluded that the main problem facing the solar A/C systems in general is the cost. Also, they still need more improvements to increase the total system efficiency. But, it could be a rival to traditional systems when taking into consideration the electric power consumption, long operating lifetime and positive environmental impact. Likewise, the type of application is essential to examine the feasibility of their use, as applying such systems in buildings that have more daily working hours, like hospitals or airports; they are definitely going to be highly interesting.

References

- [1] Wael A. alaqily, Ibrahim J.K. Al-Yousif. 2008. Reduction Cooling Load Using Intelligent Envelope System. The Iraqi journal of architecture 4B, 76-96.
- [2] Economic and Social Commission for Western Asia (ESCWA), (rationalization of energy consumption in the building sector), the World Summit Sustainable Development, Johannesburg, for the period from 26.08 - 04.09. 2002, in Arabic.
- [3] ASHRAE Handbook. American Society of Heating, Refrigeration and Air-Conditioning Engineers. Fundamentals. Atlanta 1997.
- [4] {eosweb.larc.nasa.gov}. NASA Surface meteorology and Solar Energy 25 Sep. 2016.
- [5] Technical catalog of solar absorption chiller GRS-35. SHANGHAI GLORIOUS REFRIGERATION EQUIPMENTS CO., LTD.2016.
- [6] International Energy Agency. {www.iea.org/publications/freepublications}.

Modeling of storage tank filling with boiling liquid

János Péter FEJES, János BUZÁS
 Department of Physics and Process Control,
 Institute for Environmental Engineering Systems

Abstract

This paper presents a mathematical model and a computer simulation of LPG (Liquefied Petroleum Gas), especially propane filling into a storage tank as a boiling liquid. To represent the physical process the equipment and the liquid was divided into homogeneous control volumes. Assuming open thermodynamic systems the governing equations were identified for each heat and mass transfer process occurring between the control volumes. Using the proper conservation of mass and energy equations along with the equations of state the values of the lumped parameters describing the system were determined. A measurement system built to validate the model and the simulation has also been introduced.

Keywords

LPG transfilling, heat and mass transfer, vapor liquid equilibrium, open thermodynamic system, computer simulation

1. Introduction

LPG, like propane and butane are transported in pressurized tanks: inside the tank LPG is in vapor liquid equilibrium with temperature above its boiling point. During transport at transfilling stations or storage facilities LPG is transferred into storage tanks, or between tank cars. In Fig. 1 is a typical propane liquid transfer system with a compressor.

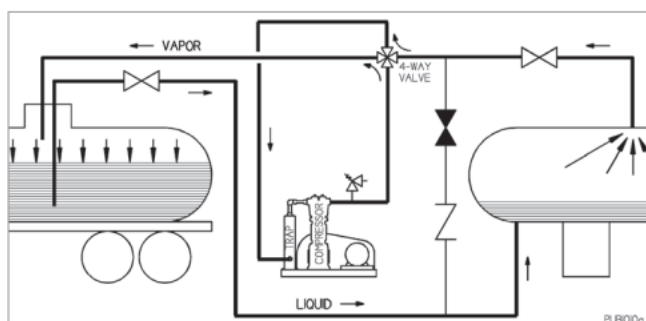


Figure 1. A typical propane liquid transfer system (PSG Grand Rapids, 2015)

In order to transfer the liquid from the railcar to the storage tank, the compressor will draw vapors from the storage tank vapor portion and into the compressor where they are compressed slightly. These compressed vapors, which are at a slightly elevated pressure, will be discharged into the top of the rail tank car. This action will slightly reduce the pressure in the storage tank while raising the pressure in the rail tank car. This difference in pressure will then cause the liquid to move through the liquid line from the railcar over to the storage tank.

This paper describes the physical phenomenon and a mathematical model with a computer simulation of the storage tank being filled with liquid propane.

2. Mathematical model

The storage tank was assumed as a horizontal cylinder. Inside the cylinder propane is in vapor liquid equilibrium, the liquid phase is located in the bottom side of the cylinder, the vapor phase is in the top side. The cylinder is divided into 4 control volumes: vapor phase (CV_v), liquid phase (CV_l), the tank wall in contact with the vapor ($CV_{w,v}$) and the tank wall in contact with the liquid ($CV_{w,l}$), see Fig. 2.

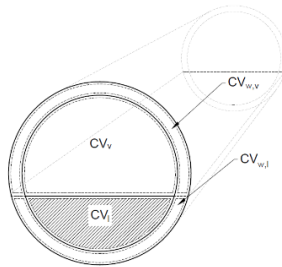


Figure 2. Control volumes of the cylindrical storage tank

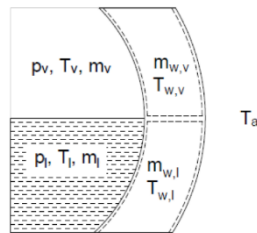


Figure 3. Lumped parameters of the CVs

In the model lumped parameters were used to describe the thermodynamic properties of the control volumes. The state of the vapor and the liquid is determined by its pressure, temperature and mass. The wall's state is determined

by its temperature and mass. And because of the heat exchange with the environment the ambient temperature is also needed as seen in Fig. 3.

Heat and mass transfer

Each control volume has its own mass and heat transfer (Fig. 4): mass and enthalpy flow from the vapor phase ($m_{v,o}, h_{v,o}$), to the liquid phase ($m_{l,i}, h_{l,i}$) and between the phases (m_e, h_e). Heat transfer between the tank wall and vapor phase ($Q_{v,w}$), the tank wall and the liquid phase ($Q_{l,w}$), between the phases (Q_p) and between the tank wall and the environment ($Q_{wv,a}, Q_{wl,a}$).

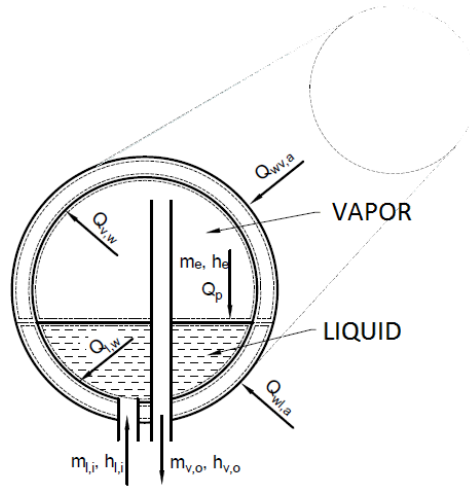


Figure 4. Heat and mass transfer of the tank

For the control volumes of the vapor (v) and liquid (l) phase the following equations were used for the conservation of mass and energy (Bergman, et al., 2011):

$$\frac{dm_{v(l)}}{dt} = \dot{m}_{v(l),i} - \dot{m}_{v(l),o} + \dot{m}_e \quad (1)$$

$$\frac{dE_{v(l)}}{dt} = \dot{Q}_{v(l),w} + \dot{Q}_p - \dot{m}_{v(l),i} h_{v(l),i} + \dot{m}_{v(l),o} h_{v(l),o} + \dot{m}_e h_e \quad (2)$$

where $m_{v(l)}$ is the mass $E_{v(l)}$ is the internal energy, $\dot{m}_{v(l),i}$ is the mass entering, $\dot{m}_{v(l),o}$ is the mass leaving the CV, \dot{m}_e is the mass of the evaporating liquid, $\dot{Q}_{v(l),w}$ is the heat transfer to the wall, \dot{Q}_p is the heat transfer between the phases, $\dot{m}_{v(l),i} h_{v(l),i}$ is the enthalpy flow into, $\dot{m}_{v(l),o} h_{v(l),o}$ is the enthalpy flow from the

CV, and $\dot{m}_e h_e$ is the enthalpy flow between the phases due to evaporation or condensation.

The tank mass was measured by a scale continuously, therefore the mass entering the liquid phase ($\dot{m}_{l,i}$) was approximated by a 6th degree polynomial, this polynomial was used to calculate the mass flow. Mass flow from the vapor phase ($\dot{m}_{v,o}$) is calculated from (Lee and Smith, 1980):

$$\dot{m}_{v,o} = C \cdot A_k \sqrt{(p_o - p_v) \rho_v} \quad (3)$$

where C is the discharge coefficient of the compressor, A_k is the cross-sectional area of the vapor pipe, p_o is the outgoing pressure from the compressor, p_v is the pressure of the vapor phase in the tank and ρ_v is the vapor density.

The enthalpy of the evaporating liquid Eq. (4), the assumption is the enthalpy of the saturated vapor at film temperature, where $T_f = \frac{T_v + T_l}{2}$:

$$h_e = h_v(T_f, p_{sat}(T_f)) \quad (4)$$

Saturation pressure ($p_{sat}(T_f)$) was calculated by the Antoine equation (Antoine, 1888). The mass flux of evaporation was calculated from the Hertz-Knudsen equation (Knudsen and Partington, 1935) and the mass flow from

$$\dot{m}_e = A_p \alpha_c \frac{\sqrt{M}}{\sqrt{2\pi R}} \left(\frac{p_v}{\sqrt{T_v}} - \frac{p_{sat}(T_l)}{\sqrt{T_l}} \right) \quad (5)$$

where A_p is the area of the phase interface, α_c is the evaporation rate multiplier, M is the molar mass of the fluid, R is the universal gas constant, p_v is the pressure of the vapor phase in the tank, $p_{sat}(T_l)$ is the saturated vapor pressure at T_l temperature, T_v is the temperature of the vapor and T_l is the temperature of the liquid.

The heat transfer between the CVs was treated as free convection and the rate was calculated from Newton's law of cooling (Bergman, et al., 2011):

$$\dot{Q} = \alpha A \Delta T \quad (6)$$

The α heat transfer coefficient was calculated from

$$\alpha = \frac{N_u k}{L} \quad (7)$$

Different Nusselt numbers were used for the heat transfer between the fluid and the wall, and between the phases. In the first case the assumption was the heat transfer is similar to the free convection from a horizontal cylinder (Bergman, et al., 2011) and the Nusselt number (Nu_D) is from Eq. (8). The Nusselt number for a horizontal flat plate (Bergman, et al., 2011) (Nu_L) was used to calculate heat transfer between the phases from Eq. (9).

$$Nu_D = \left[0,6 + \frac{0,387 Ra_D^{\frac{1}{6}}}{\left(1 + \left(\frac{0,559}{Pr} \right)^{\frac{9}{16}} \right)^{\frac{8}{27}}} \right]^2 \quad (8)$$

$$Nu_L = 0,52 Ra_L^{\frac{1}{5}} \quad (9)$$

Where Ra_D , Ra_L and Pr are the corresponding Rayleigh and Prandtl numbers.

Equations of state

To calculate the thermodynamic properties of the CVs the vapor phase as real gas, and the liquid as real liquid was treated. The vapor's state is governed by the Peng-Robinson equation of state developed in 1976 (Peng and Robinson, 1976):

$$p_v = \frac{RT_v}{V_{m,v} - b} - \frac{a\alpha}{V_{m,v}^2 + 2bV_{m,v} - b^2} \quad (10)$$

Where a , b , α , κ are calculated from T_c the critical temperature, p_c the critical pressure, ω the acentric factor and $V_{m,v}$ the molar volume.

The liquid is treated as compressible, so the density changes with pressure and temperature (Nasrifar and Moshfeghian, 1998):

$$\rho_l(T, p) = \frac{\rho_{l,sat}}{1 - \frac{p - p_{sat}(T)}{E}} \quad (11)$$

Where $\rho_{l,sat}$ is the density of the saturated liquid and $p_{sat}(T)$ is the pressure of the saturated vapor at temperature T .

The specific enthalpy and the heat capacity of the fluids were calculated from the NASA polynomials (McBride, Gordon and Reno, 1993) at temperature T Eq. (12) and Eq. (13):

$$\frac{H^0(T)}{RT} = a_1 + a_2 \frac{T}{2} + a_3 \frac{T^2}{3} + a_4 \frac{T^3}{4} + a_5 \frac{T^4}{5} + \frac{b_1}{T} \quad (12)$$

$$\frac{C_p^0(T)}{R} = a_1 + a_2 T + a_3 T^2 + a_4 T^3 + a_5 T^4 \quad (13)$$

3. Computer simulation

The mathematical model was implemented in Simulink by MathWorks and uses the Thermolib Simulink library. Fig. 5 shows the simplified model of the simulation.

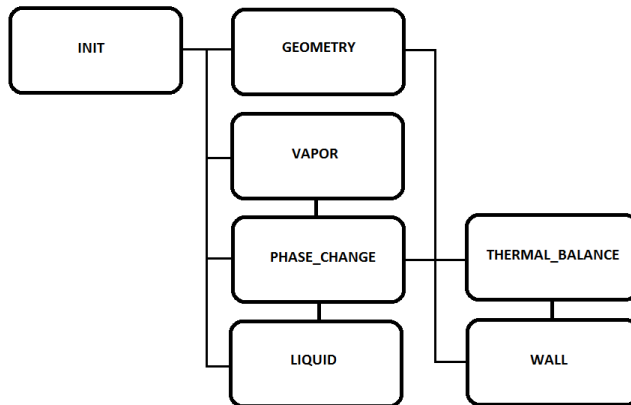


Figure 5. Subsystems of the simulation

The model consists of 7 main subsystems, the Init, Geometry, Vapor, Liquid, Wall, Phase_change and Thermal_balance.

The Init subsystem calculates the initial volume of the phases, the initial pressure in the tank from the ambient temperature, total mass of the fluid in the tank, and the tank volume.

The Geometry subsystem is responsible for calculating the areas of the contacting CVs while the liquid level rises during filling.

The Vapor and the Liquid subsystems model the vapor and the liquid phase: calculates the initial internal energy and the initial amount of substance, it has the implementation of the mass conservation equation and the energy conservation. It also calculates all of the thermodynamic properties of the fluid from the internal energy and the density using Thermolib functions.

The Phase_change subsystem uses the Hertz-Knudsen equation to calculate the rate of evaporation; and calculates the heat of evaporation and the specific enthalpy of the saturated vapor.

The *Thermal_balance* subsystem is responsible for calculating the heat transfer between the phases and to the tank wall. It uses the fluid properties of the vapor and liquid, the convective heat transfer coefficient for the flat plate between the phases and the horizontal cylinder Nusselt number for the wall. Then using Newton's law of cooling outputs the heat transfer rate.

The *Wall* subsystem uses the fluid properties of the air and calculates heat transfer to the environment from the wall. It also calculates the wall temperature from the heat entering and leaving the wall.

Validation

A measurement system was built to validate the model. It consists of four pressure sensor (PI) and six temperature sensor (TI). The sensors were connected to two iLogik remote I/O (moxa). The remote I/O-s were connected by Ethernet cables to a PC which recorded the data from the sensors. The sensors location was chosen to get the needed information like the temperature and pressure of the liquid entering the storage tank. The pressure and temperature of the vapor leaving the tank and the temperature of the tank wall, Fig. 6.

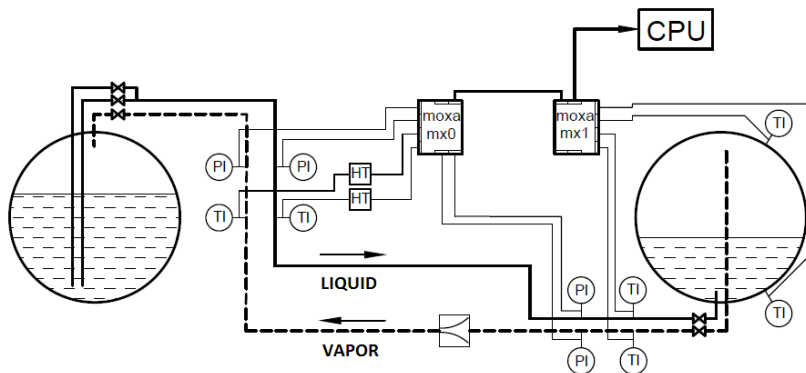


Figure 6. Measurement system

4. Results

Fig. 7 shows the measured and the simulated temperature of the tank wall in contact with the liquid phase. It took 4500 seconds to fill the tank with the equipment. Because of the initial low pressure inside the tank the entering liquid boils off and cools down. Thereafter due to the heat exchange to the environment and the higher entering liquid temperature the wall temperature rises back.

Fig. 8 shows the measured and the simulated pressure inside the tank. In the beginning the tank had a pressure about 4 bars, then when liquid started to enter to

the tank it evaporated quickly, and pressure reached the saturation pressure. The slight rise of the pressure is due to the warming up of the fluid inside the tank.

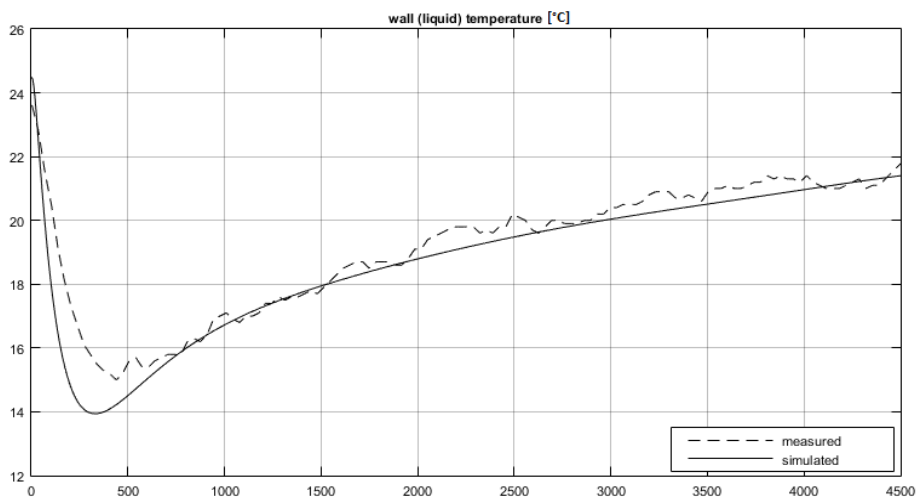


Figure 7. Simulated and measured temperature at the bottom of the tank

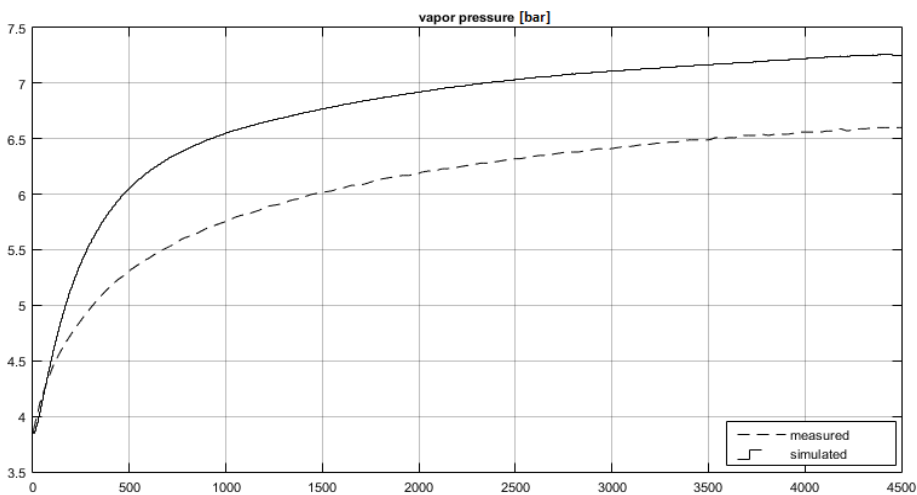


Figure 8. Simulated and measured vapor pressure

Conclusion

The results were evaluated by comparing the data from the simulation and the measurement system by calculating the root-mean-square deviation Eq. (14) of the measured and simulated values:

$$\sigma = \sqrt{\frac{\sum (y_i - f_i)^2}{N}} \quad (14)$$

The root-mean-square deviation for the measured and simulated liquid temperature was $\sigma = 0,7698$ and for the vapor pressure: $\sigma = 0,6969$.

It can be stated that the presented mathematical model and the implemented simulation is acceptable for simulating of the LPG loading into storage tank.

References

- [1] Antoine, C. (1888): Tensions des vapeurs; nouvelle relation entre les tensions et les températures. *Comptes Rendus des Séances de l'Académie des Sciences*, 107, 681–684, 778–780, 836–837.
- [2] Bergman, T. L., Incropera, F. P., DeWitt, D. P., & Lavine, A. S. (2011): *Fundamentals of heat and mass transfer*. John Wiley & Sons.
- [3] Knudsen, M., & Partington, J. R. (1935): The Kinetic. Theory of Gases. Some Modern Aspects. *The Journal of Physical Chemistry*, 39(2), 307-307.
- [4] Lee, K., & Smith, J. L. (1980): Time resolved mass flow measurement for a reciprocating compressor.
- [5] McBride, B. J., Gordon, S., & Reno, M. A. (1993): NASA Technical Memorandum 4513. Coefficients for Calculating Thermodynamic and Transport Properties of Individual Species (Hampton, VA: NASA STI).
- [6] Nasrifar, K., & Moshfeghian, M. (1998): A saturated liquid density equation in conjunction with the Predictive-Soave–Redlich–Kwong equation of state for pure refrigerants and LNG multicomponent systems. *Fluid phase equilibria*, 153(2), 231-242.
- [7] Peng, D. Y., & Robinson, D. B. (1976): A new two-constant equation of state. *Industrial & Engineering Chemistry Fundamentals*, 15(1), 59-64.
- [8] PSG Grand Rapids (2015): *Liquified Gas Handbook*. Retrieved October 22, 2016, from <http://www.psgdover.com/assets/blackmer/myapp/PDF/500-001.pdf>

Development of a solar assisted absorption cooler

Attila SZILÁGYI¹, István FARKAS², István SERES²

¹Department of Vehicle and Agricultural Engineering, University of Nyíregyháza

²Department of Physics and Process Control,
Institute for Environmental Engineering Systems

Abstract

In this paper we are going to show how the solar energy can be used for cooling. This is a very important topic nowadays, because summers are getting hotter and hotter, and numerous air conditioning systems, which are working with electrical energy are used in the summertime. This energy demand would be decreased with solar air conditioning devices, which can reduce the energy consumption and the environmental impact of the heat power plants. The energy demand for cooling can be collected from solar energy (with solar cells or solar collectors), so there is no need for energy storage. For this purpose, a solar collector combined with an absorption cooler can be a proper solution. In this paper the development of the experimental equipment is presented with some measurement results.

Keywords

solar energy utilization, solar cooling, air conditioning, heat exchanger

1. Introduction

The energy from the Sun is indispensable for our life. This energy utilization can assure the comfort for the people environmental friendly way. The incoming solar irradiation is 1.360 kW/m^2 , at the outer border of the Earth's atmosphere. This irradiation reaching the Earth surface in direct or/and indirect form with the maximum value of 1 kW/m^2 . The indirect radiation is caused especially by clouds and fog. The solar energy potential is very different in the different locations of the Earth (Foster et al., 2009). In Hungary this value is 1200-1400 kWh/m^2 per year. This renewable energy source is generally used for electric energy production or for domestic hot water heating, however it can be used for cooling or air conditioning, as well. The advantage of this last mentioned usage is, that the maximum power income is at the same time with the power demand.

2. Solar energy utilization and solar cooling

We can utilize the solar energy with active and passive form. In our case we are using the active form, with solar collectors, which are utilizing the heating effect of the solar energy.

The solar collectors have two main categories (Foster et al., 2009, Kohlenbach and Jacob, 2014):

- concentrated collectors (by solar power plants), and the
- flat collectors.

The flat collectors' two main types are the

- flat plate collector, and the
- vacuum tube collector (Fig. 1).

These collectors are used especially in households. This installation is very simple, it can be used for hot fluid production, which can be used for heating and cooling. The typical heat transfer fluids are: water, water and propylene glycol, thermal oil.



Figure 1. Vacuum tube collector
(Department of Physics and Process Control, SZIU)

The cooling systems have two main forms: active and passive. Passive cooling systems work without energy sources, for example these are e.g. shading, semi-transparent glass covers, solar driven ventilation effects, etc. The passive cooling is depend on the building's structure and its heat resistance. Active cooling systems work with electrical energy or with heat energy.

We can use the solar energy for cooling different ways, as follows:

- solar collectors with absorption system,
- solar collectors with adsorption system,
- solar collectors with Stirling engine and compressing cooler,
- photovoltaic modules with Peltier converters,
- photovoltaic modules with absorption system (heating with electrical energy),
- photovoltaic modules with compression cooler.

The first solar cooler was showed in 1878. in Paris. This was a demonstration absorption system yet, which worked with ammonium and water. In the 1970's the first commercial solar coolers and air-conditioning systems were available in the USA and in Europe (Kohlenbach and Jacob, 2014).

3. Absorption cooling

The absorption cooling systems can work with heat energy or electrical energy, this equipment cools by a chemical process. The system is a closed cycle it is based on fluid sorption. This technology was invented by Edmund Carré and Ferdinand Carré in 1850s. This technology developed by H. Geppert in 1890s and the final form made by two Swedish engineers, Baltzar von Platen and Carl Munters in 1922. Their device operated without pump, used a neutral gas (hydrogen) and air cooling (Komondy and Halász, 1970).

The absorption cooler is quiet, has no moving parts, and works continuously. Its working fluid is ammonium and water (cooling temperature is between -30 and 20 °C, COP = 0.5-0.7, (COP is the coefficient of performance) or lithium-bromid and water (cooling temperature is between 6 and 20 °C, COP = 0.6-1.8) (Kohlenbach and Jacob, 2014).

An experimental absorption cooler is shown in Fig. 2.

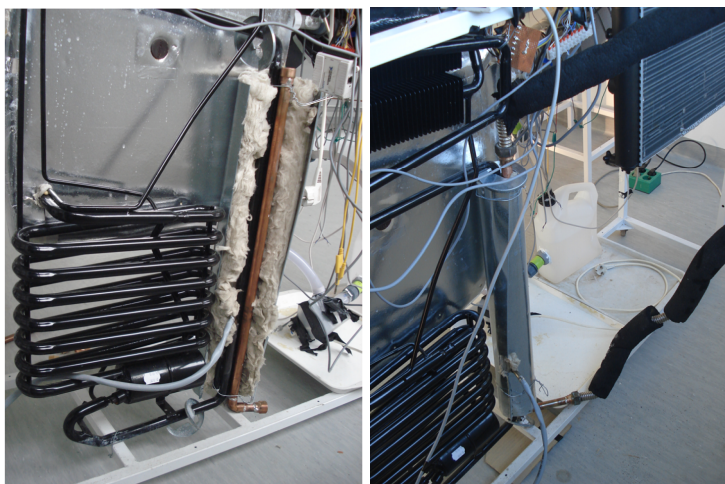


Figure 2. Absorption cooler
(Department of Physics and Process Control, SZIU)

4. Measuring unit and results

We have measured a vacuum tube collector operated by the way shown schematically in Fig. 3. The collector useful surface is 1.485 m², the solar energy was utilized as heat through a heat exchanger, and the heat transfer fluid was water.

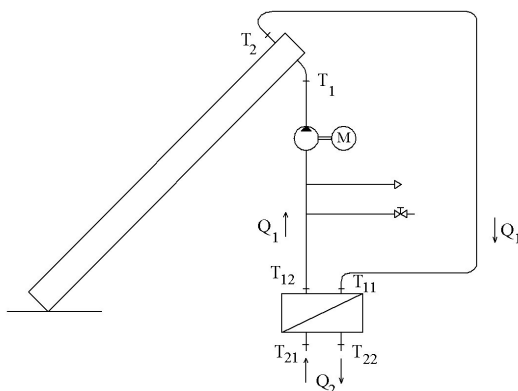


Figure 3. The scheme of the used equipments during the measurement – Solar energy utilization

In Fig. 3. the T_1 and T_2 are the inlet and outlet temperatures of the collector, T_{11} , T_{12} the inlet and outlet temperatures of the of the primer and T_{21} and T_{22} the inlet and outlet temperatures of the secondary side of the heat exchanger. Q_1 and Q_2 are the mass currents of the collector loop and the cooler loop.

Three heat exchangers are used in our experimental setup, one of them to provide the heat for the operation of the absorption cooler unit, the other one is used to cool down to the air of the investigated space by the cold liquid and the third is ensuring with a fan the cold air for the experimental insulated box (Fig. 4).

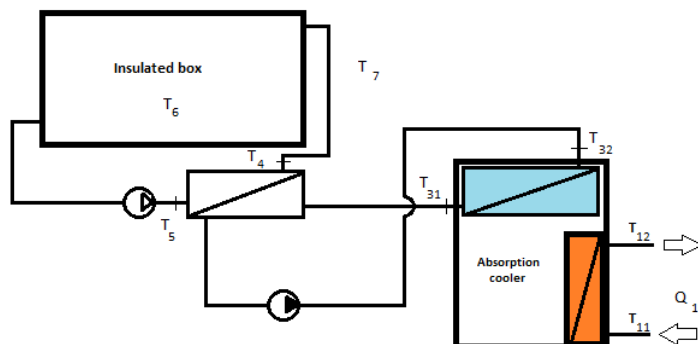


Figure 4. The scheme of the equipment used during the measurement – Absorption cooler utilization for air conditioning

As it was shown during the system description, a liquid-liquid heat exchanger was planned to be used in the heating point of the absorption cooler. For the normal apparatus, it is generally heated by an electric heater, or with direct flame of gas, but as in our case the heat is originated from a solar collector, from there it can be transported to the cooler unit by solar liquid. As the pre prepared cooler unit had a vertical heating tube, with pre fitted electric heater on it, we had to use that construction for our aim. However for the heat transfer other geometry and position – e.g. horizontal – would be more advantageous, the vertical tube position had to be kept as the cooler is using the gravitational flow for its operation. Another disadvantage was, that we could not made a welded connection between the two tubes, because of the fulfilled system and the different materials (iron and copper). Finally the thermal conduction between the two parts was solved by making metallic connection, with some soldering and the usage of heat transfer pasta (thermal conduction glue) between the two parts.

Our measurement showed, that the improvement of the thermal connection was successful, as the temperature drop in the heating liquid went up to about 10 degree Celsius from the three in the heat exchanger part of the input side.

The cool side of the absorption cooler can go down to the temperature of -20 degree without load, which provide a fairly enough temperature difference to cool down the air of the investigated volume. For the first solution an liquid to air heat exchanger was used, which was originally used as a cooler heat exchanger of a passenger car's engine (Fig. 5).

The temperatures were measured at eight point with PT1000 sensors, as Fig. 4. shows these inlet and outlet measurement points. The other main parameter was the fluid flow rate, which we could change in the primer and in the secondary cycle. The actual, daily solar radiation values were recorded by a pyranometer.



Figure 5. Engine's heat exchanger in the experimental unit
(Department of Physics and Process Control, SZIU)

This solution (Fig. 5) was not successful because of the high power of the electric fan (built in fan with 15 W power), and the different tube diameters in the two sides. To solve this problem an own heat exchanger was built from flexible metal tube (diameter of 10 cm) with the help of a low power fan, used for computer power supply units (Fig. 6.). This modification reduced the side effects, as the heating effect of the fan, and the energy loss because of the different diameters.

As the power of the experimental cooler unit is not enough to cool down a complete room (the laboratory), a heat insulated box was created where the cooling of the air can be checked separately. The picture of the modified experimental setup can be seen in Fig. 6.

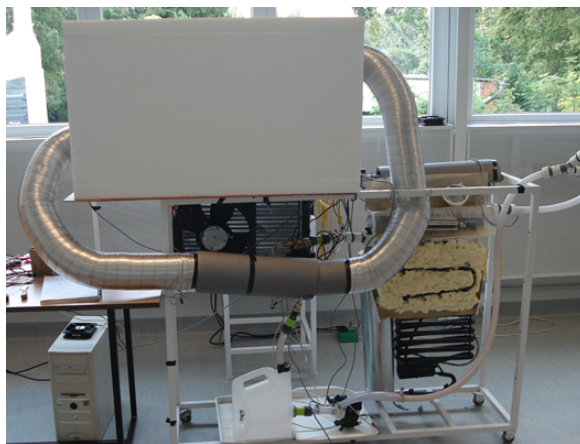


Figure 6. The developed experimental setup (SZIU, Department of Physics and Process Control)

Fig. 7. and Fig. 8. show typical temperature difference between the input and output of the first and as well as the second (modified) experimental systems used for air conditioning.

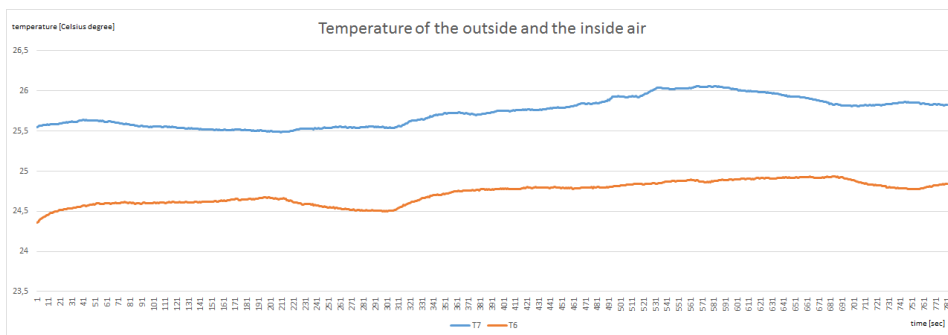


Figure 7. Typical temperature difference (between input and output) in the liquid-air heat exchanger in the input side, before the modification

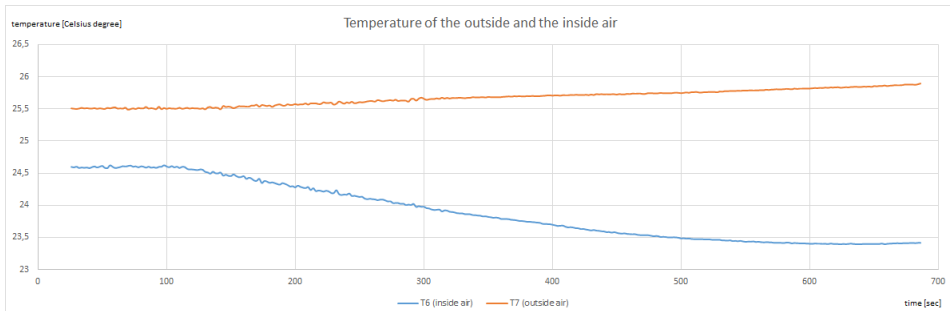


Figure 8. Typical temperature difference (between input and output) in the liquid-air heat exchanger in the input side, after the modification

Conclusion

The incoming solar radiation was converted with about 50% efficiency to heat by the vacuum tube collector. From the heat exchanger, about 300 W heat power was utilized (which is about 25% of the incoming radiation), so the heat exchanger had the thermal efficiency of 50%. The reason of this high loss is due to the experimental setup, no insulation was used on the heat exchanger. It was recognized that the efficiency of the heat conversion depends on the fluid flow. By the first setup the fan was heating the air to cooling, opposite this by the second setup the less power fan was not heating the air, so this setup can solve the cooling.

The power demand of the planned experimental cooling system can be fulfilled with the introduced system by using of the optimal setting point. The next planned step of the research is that during the springtime the developed heat exchanger system will be connected to the vacuum tube collector, to do measurements under the real conditions about the system efficiency.

References

- [1] https://en.wikipedia.org/wiki/Ferdinand_Carr%C3%A9, downloaded December 2, 2016
- [2] Kohlenbach, P., Jakob, U. (2014): Solar cooling, The Earthscan expert guide to solar cooling systems, Routledge
- [3] Komondy, Z., Halász, L. (1970): Hűtőgépek, Tankönyvkiadó, Budapest (in Hungarian)
- [4] M.J. Moran, H.N., Shapiro (2007): Fundamentals of engineering Thermodynamics, Wiley, ISBN: 978-0471787358
- [5] R. Foster, M. Ghassemi, A. Cota (2009): Solar energy: Renewable energy and the environment, CRC Press, ISBN 9781420075663

Institute for Mathematics and Informatics



Professor Dr. Sándor MOLNÁR
Director of the Institute

Dear Reader,

Allow me to briefly introduce our institute. The Institute of Mathematics and Informatics consists of the following distinguished departments: **the Department of Mathematics** (head: Dr. László Székely) and the **Department of Informatics** (head: Prof. Dr. Sándor Molnár). The **External Department of Applied Informatics** (head: Prof. Dr. Andras Edelmayer) is located at the Computer and Automation Research Institute of the Hungarian Academy of Sciences (MTA SZTAKI). Our research activities in 2016 were as follows.

Department of Mathematics

In 2016, based on our already established international cooperation, papers were published on topics of dynamic models of populations (namely biological pest control involving agents with cannibalism, and the development of a change-point method applied to describe seafloor bacterial mat coverage) and on the evaluation of a reform of the Italian pay-as-you-go pension system. As a result of recent years' ongoing research, new results were achieved in the field of modeling solar heating systems and in game theory (Stackelberg games). Furthermore, papers were published on renewable energy resources and sustainable development.

Department of Informatics

The Department has focused its research efforts primarily on linear systems theory. Energy and environment modeling remains a field of interest, sustainability in macroeconomic models remains one of the topics under investigation. A D. Sc. thesis was submitted in the topic of a special class of hierarchical systems in mathematical systems theory. A PhD thesis being finalised on the application of artificial neural networks in geostatistical processes, with a paper submitted in a referred, reviewed journal.

The other relevant focus of activities is applied research in the fields of embedded measurement, control and communication systems, signal processing, detecting and control algorithms. Data mining and analysis is a relevant new field with papers submitted on market based forecasts of share price movements.

External Department of Applied Informatics

The Department focuses on system and control theory application, fault detection, distributed networking, advanced filtering methods, signals and

systems theory. Another field of research is intelligent metering and transportation vehicle fleet guidance under traffic conditions. Some additional topics are the representations of signals and systems using orthogonal rational bases. A current research topic is the mean-value engine model including pathway modeling of the air path of diesel engines, using LTI-modelling, and various fault detection and isolation techniques.

Multiple linear regression based models for solar collectors

Richárd KICSINY

Department of Mathematics,
Institute for Mathematics and Informatics

Abstract

Mathematical modelling is the theoretically established tool to investigate and develop solar thermal collectors as environmentally friendly technological heat producers. In the present survey, recent multiple linear regression (MLR) based collector models are presented and compared with one another and with a physically-based model, used successfully in many applications, by means of measured data. The MLR-based models, called *MLR model*, *SMLR model* and *IMLR model*, prove to be rather precise with a modelling error of 4.6%, 8.0% and 4.1%, respectively, which means that all MLR-based models are more or nearly the same accurate as the well-tried physically-based model. The SMLR model is the most, while the IMLR model is the least easy-to-apply MLR-based model with the lowest and the highest computational demand, respectively. Nevertheless, all MLR-based models have lower computational demand than the physically-based model. Accordingly, the MLR-based models are suggested for fast but accurate collector modelling.

Nomenclature

- A : collector surface area, m^2 ;
 c : specific heat capacity of the collector fluid, $\text{J}/(\text{kgK})$;
 I : global solar irradiance on the collector surface, W/m^2 ;
 t : time, s ;
 T_a : ambient temperature of the collector, $^{\circ}\text{C}$;
 T_{in} : inlet collector (fluid) temperature, $^{\circ}\text{C}$;
 T_{out} : outlet collector temperature (assumed to be the same as the homogeneous collector temperature in case of the physically-based model), $^{\circ}\text{C}$;
 U_L : overall heat loss coefficient of the collector, $\text{W}/(\text{m}^2\text{K})$;
 v : (constant) flow rate inside the collector, m^3/s ;
 V : volume of the collector, m^3 ;
 η_0 : optical efficiency of the collector, - ;
 ρ : collector fluid density, kg/m^3 ;

- τ_A : time delay before *Case A* or *A3*, s;
- τ_B : time delay before *Case B*, s;
- τ_1 : time of flowing inside the collector from the inlet to the outlet when the pump is switched on permanently, s;
- τ_2 : length of time between successive measurements on the collector, s.

1. Introduction

Mathematical modelling is the most widely used and theoretically established tool to investigate and develop solar thermal collectors as environmentally friendly technological heat producers. The two main categories of mathematical models for collectors are physically-based models, which represent exact physical laws (based on theory), and black-box models, which describe empirical correlations (based on experiences or measurements).

Among the most important physically-based models, the Hottel-Whillier-Bliss model (Duffie and Beckman, 2006) may be the earliest, which is frequently used to date. This model determines the collector temperature as a function of time and space. Buzás et al. (1998) proposed a simpler model assuming that the collector temperature is homogeneous in space. This model is a linear ordinary differential equation (ODE) validated in (Kicsiny, 2014) and is likely the simplest physically-based model used in the practice (see e.g. (Kumar and Rosen, 2010; Buzás and Kicsiny, 2014)), but can still describe the transient collector processes with an appropriate accuracy. This model will be called *physically-based model* in short below.

The greatest advantage of black-box models is that it is not needed to know the physical laws of a collector precisely in order to create a model. Nevertheless, the model may be rather precise even if it is simple as in the case of (Kicsiny, 2014). The most frequent black-box model type is perhaps the artificial neural network (ANN) in the field of collectors. Generally, ANNs are accurate but rather troublesome to apply because of the so-called training process. The convergence of the algorithm indicating the end of a training session may be also time-consuming. According to Fischer et al. (2012), a conveniently usable algorithm ensuring a reliable and fast determination of an appropriate ANN for a collector is still missing.

Because of these problems, a simple and general but still accurate black-box model, which can be applied easily and fast for a wide range of solar collectors, has been recently worked out in (Kicsiny, 2014). The model is based on the well-known methods of mathematical statistics, more precisely, the multiple linear regression (MLR). Based on the literature, MLR is a rare black-box modelling technique in the field of collectors despite of its simplicity. Considering the high precision (with a modelling error of 4.6%), simple usability and low computational demand of the mentioned MLR-based model (*MLR model* in short),

it was worth trying to simplify further the MLR model. Such a simplified model, called *SMLR model* (with a modelling error of 8.0%), has been worked out in (Kicsiny, 2015). On the other hand, it was also worth improving the MLR model to try to maximize the precision. Such an improved model, called *IMLR model* (with an error of 4.1%), has been worked out in (Kicsiny, 2016), where it has been empirically shown that the accuracy cannot be significantly improved any more if the regression equations are all linear in terms of the input variables.

In the present survey, as a summary of former works, the above MLR-based models are presented and compared with one another and with the physically-based model by means of measured data.

2. Physically-based and MLR-based models

For the Reader's convenience, the physically-based model, and the MLR-based models are recalled in this section. The scheme of the studied solar collector can be seen in Fig. 1.

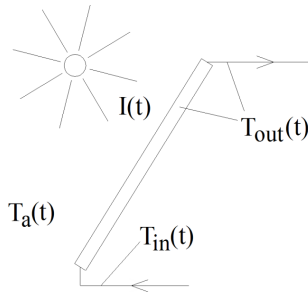


Figure 1. Scheme of the solar collector

2.1. Physically-based model

The physically-based model is the ODE of Eq. (1).

$$\frac{dT_{out}(t)}{dt} = \frac{A\eta_0}{\rho c V} I(t) + \frac{U_L A}{\rho c V} (T_a(t) - T_{out}(t)) + \frac{v}{V} (T_{in}(t) - T_{out}(t)) \quad (1)$$

2.2. MLR model

The inputs of the MLR model are from appropriately chosen values of T_{in} , I , T_a and T_{out} . The output is from appropriately chosen values of T_{out} . The flow rate value v is a fixed positive constant or 0.

Because of the boundedness of the flow rate, $T_{in}(t - \tau_1)$ can play a role as an input in the MLR model if $T_{out}(t)$ is the output, where the positive constant τ_1 is a time delay (more precisely, the time of flowing inside the collector from the inlet

to the outlet when the pump is switched on permanently). Similar considerations hold for I and T_a as well because of the bounded propagation speed of their effects, so former $I(t-\tau_2)$ and $T_a(t-\tau_2)$ values can play roles as inputs in forming the output $T_{out}(t)$. (The time delays of I and T_a are assumed to be the same (τ_2) for the sake of simplicity.) Naturally, appropriate former value of T_{out} also affects the value of $T_{out}(t)$ and participates as the initial value of the MLR model at time $(t-\tau_2)$ in essence. Considering the collector as a black-box, distinct sub-models as parts of the MLR model have been identified for significantly different operating conditions. For example, the collector behaves different if the pump is on ($v>0$) or off ($v=0$) permanently. Even, the effect of T_m is neglected in permanently switched off case, since there is no flow between the collector inlet and outlet.

Considering a typical day, when the temperature increase of T_{out} is significant, three different, main operating cases are distinguished according to Fig. 2.

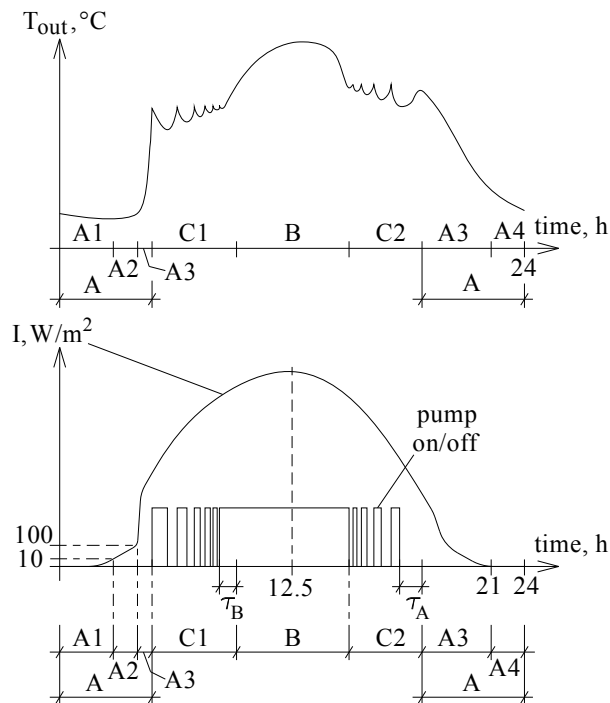


Figure 2. Outlet temperature, solar irradiance and pump operation on a typical day

Case A corresponds to permanently switched off pump, more precisely, Case A contains the term started at the beginning of the day and finished, when the pump is first switched on. All the terms, which begin at a time when the pump is

permanently off for exactly τ_A time and finish at the next switch-on or at the end of the day, also belong to this case. (τ_A is the time, which is generally enough for T_{out} to become not fluctuating but permanently monotone, since, intentionally, frequent fluctuations are characteristics of Cases C1 and C2.) Case B corresponds to permanently switched on pump, more precisely, Case B contains all the terms, which begin at a time when the pump is permanently on for exactly τ_B time and finish at the next switch-off. (τ_B is the time, which is generally enough for T_{out} to become not fluctuating but permanently monotone.) Case C corresponds to frequent switch-ons and -offs. It can be seen that there are two further significantly different operating cases within Case C: T_{out} basically increases before the solar noon and basically decreases after the solar noon, so Case C is divided into Cases C1 and C2.

The MLR model is composed of the linear equations (2a)-(2d), which describe the corresponding sub-model of each operating case.

Case A:

$$T_{out,mod}(t) = c_{I,A}I(t - \tau_2) + c_{a,A}T_a(t - \tau_2) + c_{out,A}T_{out}(t - \tau_2) + c_A \quad (2a)$$

Case B:

$$T_{out,mod}(t) = c_{in,B}T_{in}(t - \tau_1) + c_{I,B}I(t - \tau_2) + c_{a,B}T_a(t - \tau_2) + c_{out,B}T_{out}(t - \tau_2) + c_B \quad (2b)$$

Case C1:

$$T_{out,mod}(t) = c_{in,C1}T_{in}(t - \tau_1) + c_{I,C1}I(t - \tau_2) + c_{a,C1}T_a(t - \tau_2) + c_{out,C1}T_{out}(t - \tau_2) + c_{C1} \quad (2c)$$

Case C2:

$$T_{out,mod}(t) = c_{in,C2}T_{in}(t - \tau_1) + c_{I,C2}I(t - \tau_2) + c_{a,C2}T_a(t - \tau_2) + c_{out,C2}T_{out}(t - \tau_2) + c_{C2} \quad (2d)$$

$c_{I,A}$, $c_{a,A}$, $c_{out,A}$, c_A , $c_{in,B}$, $c_{I,B}$, $c_{a,B}$, $c_{out,B}$, c_B , $c_{in,C1}$, $c_{I,C1}$, $c_{a,C1}$, $c_{out,C1}$, c_{C1} , $c_{in,C2}$, $c_{I,C2}$, $c_{a,C2}$, $c_{out,C2}$, c_{C2} are constant parameters. According to the definition of τ_2 , the measurements take place at times $t = 0, \tau_2, 2\tau_2, 3\tau_2, \dots$. The modelled value of T_{out} (that is $T_{out,mod}$) is determined at times $t = \tau_2, 2\tau_2, 3\tau_2, \dots$

from the measured values of $I(t-\tau_2)$, $T_a(t-\tau_2)$, $T_{out}(t-\tau_2)$ and $T_{in}(t-\tau_1)$ based on Eqs. (2a)-(2d). See (Kicsiny, 2014) for more details.

2.3. SMLR model

The MLR model is simplified to the SMLR model in the way of merging *Cases A, B, C1 and C2*. Thus there is only one operating case with one mathematical relation (see Eq. (3)) here.

$$T_{out,mod}(t) = c_{in}T_{in}(t-\tau_1) + c_I I(t-\tau_2) + c_a T_a(t-\tau_2) + c_{out} T_{out}(t-\tau_2) + c \quad (3)$$

c_{in} , c_I , c_a , c_{out} and c are constant parameters. See (Kicsiny, 2015) for more details.

2.4. IMLR model

The IMLR model is similar to the MLR model. The main differences are the following (see also Fig. 2):

1. The (largest) operating case *Case A* is divided into four sub-cases, *Cases A1, A2, A3 and A4*, as follows: *Case A1* consists of the time period from the beginning of the day to the time when the solar irradiance is first greater than 10 W/m². This case practically belongs to the term of no irradiance in the first half of the day. *Case A2* consists of the time period from the end of *Case A1* to the time when the solar irradiance is first greater than 100 W/m². Usually, this time is followed by a very intensive increase in the irradiance, so this is apparently the time of sunrise, when the irradiance changes from (mostly) diffuse to (mostly) direct. *Case A3* consists of the time periods besides *Cases A1, A2 and A4* (see below) within *Case A*. *Case A4* contains the last three hours of the day. In essence, the term after *Case C2* corresponds to the free cooling of the collector from a relatively high temperature. Based on experiments, this section cannot be modelled well with a single relation, so it should be divided into sub-sections. Empirically, the problem can be solved well with only two sub-parts if the last three hours are separated.

2. The coefficients of the zeroth-order members (cf. c_A , c_B , c_{C1} and c_{C2} in Eqs. (2a)-(2d) in the MLR model) are set zero in Eqs. (4a)-(4g) below. This set is in line with the physical phenomenon that the collector (outlet) temperature must be zero if all the inputs T_{in} , I , T_a and the previous collector temperature are zero. Based on experiments, this natural constraint results in a bit lower precision in the identification but higher precision in the validation, that is the modelling error decreases.

The linear equations (4a)-(4g) correspond to the operating cases of the IMLR model.

Case A1:

$$T_{out,mod}(t) = c_{a,A1} T_a(t-\tau_2) + c_{out,A1} T_{out}(t-\tau_2) \quad (4a)$$

Case A2:

$$T_{out,mod}(t) = c_{I,A2}I(t - \tau_2) + c_{a,A2}T_a(t - \tau_2) + c_{out,A2}T_{out}(t - \tau_2) \quad (4b)$$

Case A3:

$$T_{out,mod}(t) = c_{I,A3}I(t - \tau_2) + c_{a,A3}T_a(t - \tau_2) + c_{out,A3}T_{out}(t - \tau_2) \quad (4c)$$

Case A4:

$$T_{out,mod}(t) = c_{a,A4}T_a(t - \tau_2) + c_{out,A4}T_{out}(t - \tau_2) \quad (4d)$$

Case B:

$$T_{out,mod}(t) = c_{in,B}T_{in}(t - \tau_1) + c_{I,B}I(t - \tau_2) + c_{a,B}T_a(t - \tau_2) + c_{out,B}T_{out}(t - \tau_2) \quad (4e)$$

Case C1:

$$T_{out,mod}(t) = c_{in,C1}T_{in}(t - \tau_1) + c_{I,C1}I(t - \tau_2) + c_{a,C1}T_a(t - \tau_2) + c_{out,C1}T_{out}(t - \tau_2) \quad (4f)$$

Case C2:

$$T_{out,mod}(t) = c_{in,C2}T_{in}(t - \tau_1) + c_{I,C2}I(t - \tau_2) + c_{a,C2}T_a(t - \tau_2) + c_{out,C2}T_{out}(t - \tau_2) \quad (4g)$$

$c_{a,A1}$, $c_{out,A1}$, $c_{I,A2}$, $c_{a,A2}$, $c_{out,A2}$, $c_{I,A3}$, $c_{a,A3}$, $c_{out,A3}$, $c_{a,A4}$, $c_{out,A4}$, $c_{in,B}$, $c_{I,B}$, $c_{a,B}$, $c_{out,B}$, $c_{in,C1}$, $c_{I,C1}$, $c_{a,C1}$, $c_{out,C1}$, $c_{in,C2}$, $c_{I,C2}$, $c_{a,C2}$, $c_{out,C2}$ are constant parameters. τ_1 and τ_2 are the same as in the MLR model. See (Kicsiny, 2016) for more details.

3. Comparison

The below results of the models used in this comparison are from (Kicsiny, 2014; 2015 and 2016). The identification and the validation of the models are based on the same days. The used real flat plate collector field of 33.3 m² (Farkas et al., 2000) at the Szent István University (SZIU) in Gödöllő, Hungary (SZIU collector in short) is also the same. T_{out} , T_{in} , I , T_a and v are measured

once in every minute at the SZIU collector. The measured value of T_{out} serves only for identification and comparison purposes, the measured value $T_{out}(0)$ is fed into the models as initial condition.

Identification

Four measured days (2nd July 2012, 24th June 2012, 28th June 2012 and 8th June 2012) have been selected for the identification in such a way that they cover a wide range of possible operating conditions of a selected season (summer). The constant U_L is identified in case of the physically-based model in such a way that the time average of the absolute difference between the modelled and measured outlet temperatures that is the average of absolute error is minimal with respect to the whole identification period. The constants $c_{I,A}$, $c_{a,A}$, $c_{out,A}$, c_A , $c_{in,B}$, $c_{I,B}$, $c_{a,B}$, $c_{out,B}$, c_B , $c_{in,C1}$, $c_{I,C1}$, $c_{a,C1}$, $c_{out,C1}$, c_{C1} , $c_{in,C2}$, $c_{I,C2}$, $c_{a,C2}$, $c_{out,C2}$, c_{C2} are identified in the MLR model, the constants c_{in} , c_I , c_a , c_{out} , c are identified in the SMLR model and the constants $c_{a,A1}$, $c_{out,A1}$, $c_{I,A2}$, $c_{a,A2}$, $c_{out,A2}$, $c_{I,A3}$, $c_{a,A3}$, $c_{out,A3}$, $c_{a,A4}$, $c_{out,A4}$, $c_{in,B}$, $c_{I,B}$, $c_{a,B}$, $c_{out,B}$, $c_{in,C1}$, $c_{I,C1}$, $c_{a,C1}$, $c_{out,C1}$, $c_{in,C2}$, $c_{I,C2}$, $c_{a,C2}$, $c_{out,C2}$ are identified in the IMLR model. Independent standard MLR routines have been applied based on the measured data of each separate operating case for the identification of the three MLR-based models. The standard MLR routine (based on least squares method) is well-known and available in most statistical and spreadsheet programs (SPSS, Excel, etc.).

Table 1 contains the average of error (time average of the difference between the modelled and measured outlet temperatures) and the average of absolute error (time average of the absolute difference between the modelled and measured outlet temperatures) values for two days (2nd July 2012, 28th June 2012) of the identification of all models. The average of absolute error values are presented in proportion to the difference between the daily maximal and minimal measured outlet temperature values as well, in %. The mean of these values with respect to all of the four days of the identification is also presented in Table 1 (7.8 % for the physically-based, 4.7 % for the MLR, 6.6 % for the SMLR and 3.2 % for the IMLR model).

Validation

In the validation, all identified models are applied with the corresponding measured inputs of the remaining two summer months. The outlet temperature is modelled in the validation (not measured, as in the identification). The modelled days are from 3rd July to 31st August 2012, which are 56 days according to minor technical interruptions.

Table 1 contains the average of error and the average of absolute error values for two days (3rd August 2012, 5th August 2012) of the validation of all models. The average of absolute error values are presented in proportion to the difference between the daily maximal and minimal measured outlet temperature values as well, in %. The mean of these values with respect to all of the 56 days of the validation is also presented in Table 1 (7.8 % for the physically-based, 4.6 % for the MLR, 8.0 % for the SMLR and 4.1 % for the IMLR model).

Table 1. Average of error and average of absolute error values with the models

			Physically-based model	MLR model	SMLR model	IMLR model
Identification	2 nd July (smooth operation)	Average of error	-1.86 °C	-0.47 °C	1.43 °C	-0.53 °C
		Average of absolute error	4.33 °C; 7.0%	2.79 °C; 4.6%	3.88 °C; 6.3%	1.64 °C; 2.7%
	28 th June (intermittent operation)	Average of error	-1.26 °C	-0.23 °C	-2.87 °C	-0.80 °C
		Average of absolute error	4.35 °C; 7.5%	3.01 °C; 5.2%	3.39 °C; 5.8%	1.84 °C; 3.2%
	Mean % value for the whole identification (four days)	Average of absolute error	7.8%	4.7%	6.6%	3.2%
Validation	3 rd August (smooth operation)	Average of error	-1.38 °C	-1.31 °C	-0.12 °C	-1.18 °C
		Average of absolute error	4.70 °C; 7.4%	2.85 °C; 4.5%	3.71 °C; 5.8%	1.92 °C; 3.0%
	5 th August (intermittent operation)	Average of error	-2.57 °C	-1.58 °C	-1.00 °C	-1.90 °C
		Average of absolute error	4.66 °C; 8.0%	3.07 °C; 5.2%	3.95 °C; 6.7%	2.30 °C; 3.9%
	Mean % value for the whole validation (3 rd July – 31 st August)	Average of absolute error	7.8%	4.6%	8.0%	4.1%

As examples of the comparison, Figs. 3, 4 show the modelled and measured outlet temperatures in case of the physically-based and MLR models and in case of the MLR and IMLR models, respectively, for the same day of the validation. The operating state (on/off) of the pump is also shown in the figures.

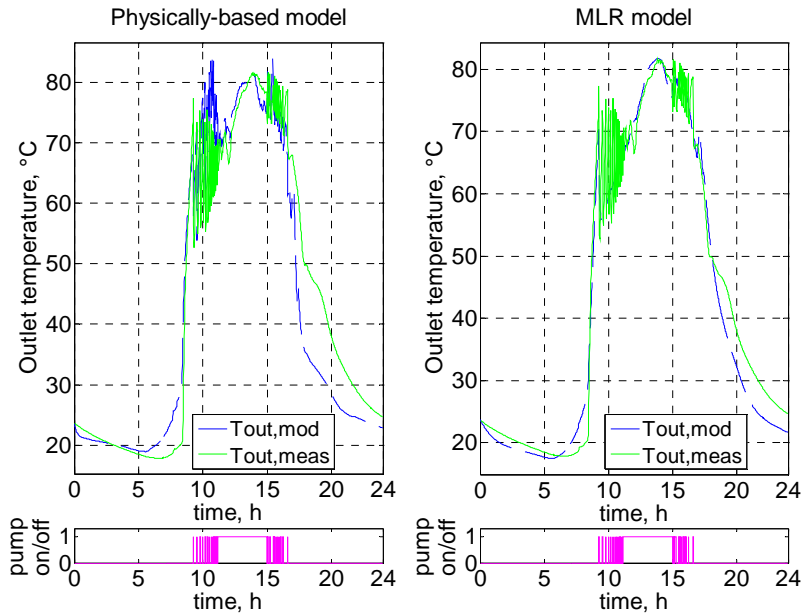


Figure 3. Modelled $T_{out,mod}$ and measured $T_{out,meas}$ collector temperatures on 3rd August 2012 in case of the physically-based and MLR models

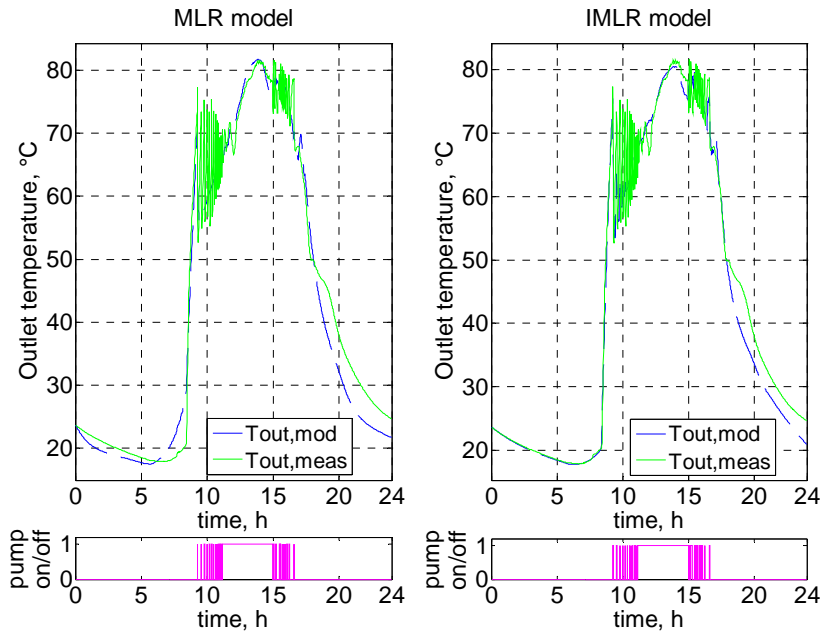


Figure 4. Modelled $T_{out,mod}$ and measured $T_{out,meas}$ collector temperatures on 3rd August 2012 in case of the MLR and IMLR models

Based on Eqs. (1), (2a)-(2d), (3) and (4a)-(4g), it is not difficult to see that the SMLR model is the most, while the IMLR model is the least easy-to-apply MLR model with the lowest and the highest computational demand, respectively. Nevertheless, all MLR-based models with simple linear algebraic equations have lower computational demand than the physically-based model realized with an ODE.

Conclusion

In the present survey, three recent MLR-based models, called *MLR model*, *SMLR model* and *IMLR model*, have been presented and compared with one another and with a well-trying physically-based model by means of measured data. According to the results, all the MLR, SMLR and IMLR models have proved to be rather precise with a modelling error of 4.6%, 8.0% and 4.1%, respectively, which means that all MLR-based models are more or nearly the same accurate as the physically-based model with an error of 7.8%.

The SMLR model is the most, while the IMLR model is the least easy-to-apply MLR model with the lowest and the highest computational demand, respectively. Nevertheless, all the MLR-based models applying simple linear algebraic equations have lower computational demand than the physically-based model realized with an ODE. Accordingly, the MLR-based models can be suggested for fast but accurate collector modelling.

Acknowledgement

The author thanks his colleagues in the Department of Mathematics in the Faculty of Mechanical Engineering (Szent István University) for their support.

This paper was supported by the János Bolyai Research Scholarship of the Hungarian Academy of Sciences.

References

- [1] Buzás, J., Farkas, I., Biró, A., Németh, R. (1998), Modelling and simulation of a solar thermal system, *Mathematics and Computers in Simulation*, Vol. 48, pp. 33-46.
- [2] Buzás, J., Kicsiny, R. (2014), Transfer functions of solar collectors for dynamical analysis and control design, *Renewable Energy*, Vol. 68, pp. 146-155.
- [3] Duffie, J.A., Beckman, W.A. (2006), *Solar engineering of thermal processes*, 3rd ed., John Wiley and Sons, New York.
- [4] Farkas, I., Buzás, J., Lágymányosi, A., Kalmár, I., Kaboldy, E., Nagy, L. (2000), A combined solar hot water system for the use of swimming pool and

- kindergarten operation, Energy and the environment, Vol. I. /ed. by B. Frankovic/, Croatian Solar Energy Association, Opatija, 2000., pp. 81-88.
- [5] Fischer, S., Frey, P., Drück, H. (2012), A comparison between state-of-the-art and neural network modelling of solar collectors, Solar Energy, Vol. 86, pp. 3268-3277.
- [6] Kicsiny, R. (2014), Multiple linear regression based model for solar collectors, Solar Energy, Vol. 110, pp. 496-506.
- [7] Kicsiny, R. (2015), Simplified multiple linear regression based model for solar collectors, Hungarian Agricultural Engineering, Vol. 28, pp. 11-14.
- [8] Kicsiny, R. (2016), Improved multiple linear regression based models for solar collectors, Renewable Energy, Vol. 91, pp. 224-232.
- [9] Kumar, R., Rosen, M.A. (2010), Thermal performance of integrated collector storage solar water heater with corrugated absorber surface, Applied Thermal Engineering, Vol. 30, pp. 1764-1768.

Economic indicators and market prosperity - a new approach for the estimation of market uncertainty

Márk MOLNÁR¹, Tamás TIMÁR², Zsuzsa TÓTH-NAÁR¹

¹Department of Macroeconomics, Institute of Economics

²Department of Informatics,

Institute of Mathematics and Informatics

Abstract

Uncertainty in market has several implications on the actions, decisions and relationships of market actors. Primarily, actors have an *ex ante* intention to deal with uncertainty, namely to analyse it, assess its range and sources, forecast its possible values, predict its implications, and ultimately to reduce its impacts. A typical answer is increased information search which enables actors to develop better founded decisions or to reduce risk. In this paper we focus on regulatory uncertainty in taxation regimes and how it affects market actors in increased information acquirement aimed at establishing better business decisions.

Key words

economic development, uncertainty, tax, stock prices, BUX

1. Introduction

The drawbacks of frequent changes in the regulation of economic affairs (rules of taxation, exemptions, legislative background, etc.) are quite straightforward. The erratic (and perhaps frequent) changes in taxation bring a high level of uncertainty to business planning, and through the increased risk creates a higher required rate of return for projects to be realised [Lemieux et al., 2011].

2. Addressing uncertainty

Furthermore abrupt tax changes create a lucrative environment for lobbying for tax exemptions, thus incentivising rent seeking games. Companies spend resources and time on influencing policymakers in order to get beneficial tax rates, reduced timespan for tax payment or even imposing a painful tax burden on competitors.

Political motives might also find their way into regulative activities, companies or regions with the „proper” background can enjoy an undisturbed environment while other, non-friendly institutions, regions, corporate sectors will be burdened or even punished.

These few exemplary effects well illustrate the severe impact of a volatile regulatory environment on corporate activities. We could further include competitiveness issues in our list as companies operating in such environments clearly face a disadvantage from companies operating in a stable, well defined scene of economic policy. We would like to stress that the absolute tax burden (e.g. the effective tax rate) has little or no consequence on the issues discussed in this paper.

3. Relevance in Hungary

Hungary has dynamic and continuous changes in corporate taxation. Special or surcharge taxes were levied on several economic sectors and industries as extra tax burden, by the end of 2015 around 15 such taxes are in force. Such taxes include but are not limited to the following titles:

- Energy tax. Tax levied on energy producing industries.
- Financial institutions (savings institutions, bank, Insurance companies), financial transactions tax was levied on all financial transactions including bank transfers, wire payments, or debit card purchases.
- Energy service providers’ tax („Robin Hood tax”) levied on energy service provider companies.
- Telecommunication tax (phone tax) levied on phone subscriptions
- Public utilities tax levied on public service providing companies.
- Advertisement tax levied on advertising industries.
- Healthcare contribution of tobacco enterprises levied as a lump sum.
- Taxes on the pharmaceutical industry.
- Product tax for public health („chips-tax“, „hamburger-tax“),
- Accident tax levied on insurances.

The following chart shows the tendency and trend of special taxes in Hungary in million forints.

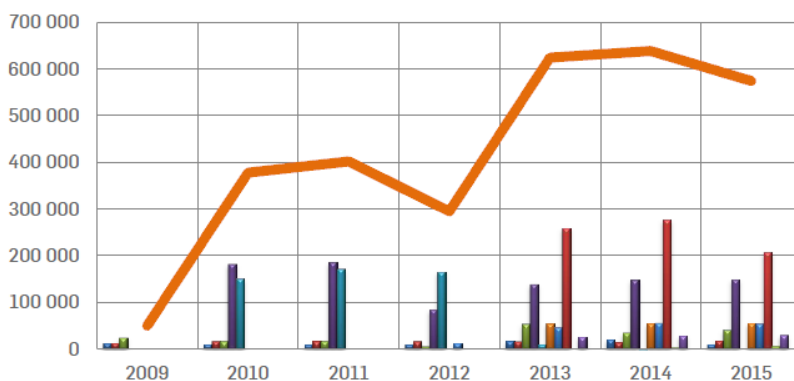


Figure 1. Tendency and trend of special taxes in Hungary [in Hungary in million forints] (Siklós – Mladonyczki, 2016)

Without specific explanation it is well visible that income of the central budget, and thus the tax burden from these taxes has shown a tremendous growth in the last four years reaching 2.5% of the GDP in 2015. Although the Hungarian government has vowed to gradually phase out these taxes, this is still not undertaken [Constantinovits, 2014].

A further problem with these special taxes is that there is a constant tendency from the government institutions to change tax rate and tax basis, give exemptions or beneficial rates, or „punish”. In several cases taxes were introduced for a single year, but charged for multiple years. Despite government efforts the laws of microeconomics are not subject to regulative force and industries involved transfer part of the tax burden to consumers.

The low level of procedural appointment also characterises legislation, notably the reduced time span (only one month) typical for the legislative preparatory phase. Coupled with a complete lack of *ex ante* impact assessment this undoubtedly becomes a challenge for local companies.

Scope of analysis

In the followings we try to model adaptation of market actors to increased uncertainty from the regulatory environment. We assume that abrupt changes in legislation increase market risk for market actors, who react to the perceived increased risk by increasing their information acquirement, market research and market intelligence activities [Ratchford, 1982].

The current state-of-the-art measure search method is Internet based search. It can take various forms and include sophisticated data analysis and data mining methods but the primary information source is the Internet and its news portals, data agencies, and dedicated analyses on specific subjects. As there is only limited means and availability on corporate intelligence and market analysis the only reasonable way for our analysis to proceed is to accept that a typical agent increases its Internet based search activity, either to improve its understanding by gaining new information or to find credible sources of information if faced with a higher uncertainty [Dzielinski, 2012]. Thus, we conclude that the intensity of search for specific topics is a good measure of uncertainty, even if this seems to be a basic approach at first glance.

Concerning market confidence there are good indicators developed by leading agencies in the market to measure actors trust and good faith in the short term future progress, typically in terms of planned purchases, consumption, investment, and so forth. It is also well known that these indicators have a direct relationship with perceived market risk or uncertainty, be it from economic or regulatory shocks.

It also seems quite straightforward to assume that the stock exchange reacts to increased market risk, as market actors, buyers and sellers try to establish better positions as the perceived risk of their assets or liabilities changes. The implied reaction can be a change in turnover of specific assets, the increased volatility of

prices, or perhaps the changes in specific returns though this can be quite awkward to precisely represent or measure.

Applied methods

To analyse market actors exhibited behaviour we turned to potential data sources on Internet search. All throughout its evolution, Google always provided access for researchers to its search database in an aggregated format without any fees or charge. We used Google Trends which provides data in intensity values, namely Search Volume Indices (SVI) to map search interest to specific interests explained as the number of queries for a given keyword projected on total Google search queries. This is a very useful tool if the keyword is selected appropriately. Search interest expressed this way is both indexed and normalised.

An even better source of data would be Keyword Planner (which is intended for identifying optimal keywords for a developer) but data from this source is available only to a limited extent, time series available were deemed to short for a reasonable analytical framework and conclusions could not be drawn with a sufficient degree of reliability. Nevertheless, Keyword Planner is very useful for suggestions, we relied on this to identify the following keywords: economy, law, legislative change, stock index (all in Hungarian) when identifying links between market uncertainty and increased search activity.

The examined period encompasses 2010-2016, in line with the new establishment in economic policymaking. Data was available in a monthly format. Research focuses on the Hungarian bourse and search terms enlisted beneath are in Hungarian.

Figure 1 shows how the search for terms 'economy' and 'BUX' (Budapest Stock Exchange) changed over the previous month. It is well visible that the most volatile periods were in 2010, 2013 and 2014 with respect to changes in search activity. A significant decay is visible in 2015 which is followed by a surge in early 2016.

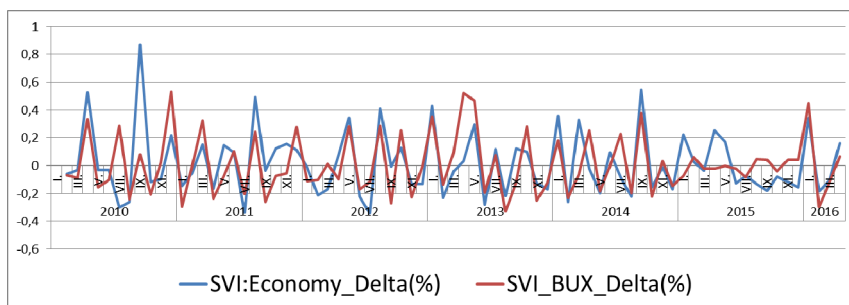


Figure 1. Change in SVI for the terms economy and BUX (Budapest Stock Exchange) over the previous period (Google Trends, own editions)

Figure 2 shows the same data series for 'law' and 'change in legislation' these terms showed more volatility in searches from 2012 onwards. The first two years show a relatively smaller interest, but this has risen since 2012. This might be justified by the increasing frequency of legislative changes.

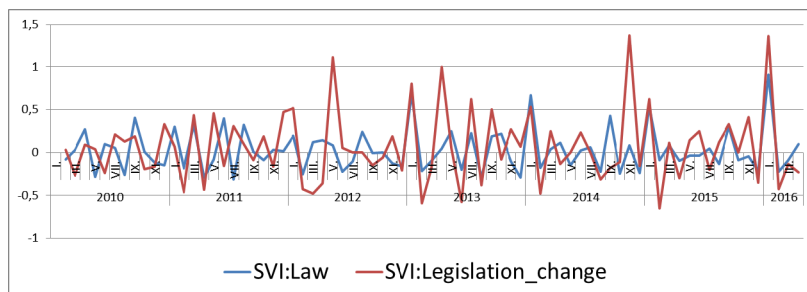


Figure 2. Change in SVI for the terms economy and BUX (Budapest Stock Exchange) month over month (Google Trends, own edition)

Some of the major confidence indices are depicted in Figure 3 where business confidence, consumer confidence and prosperity indices are presented, all three coming from one of the leading Hungarian consultancies, GKI.

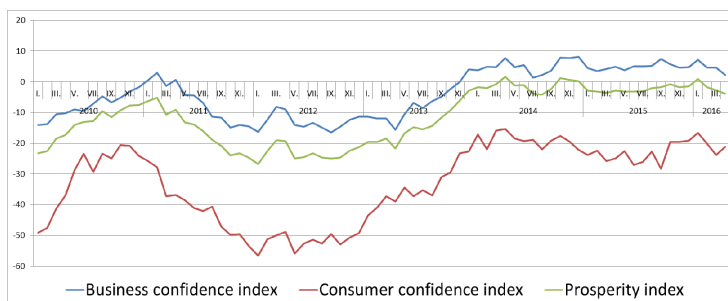


Figure 3. Change in confidence in the Hungarian economy and prosperity month over month (source: GKI)

These indices well illustrate the constant negative tendency of consumer confidence, and that businesses confidence only changed from 2014. The prosperity index is a benchmark developed for macroeconomic trends and shows a similar movement to the confidence indices.

Data used – stock exchange volume and prices

For the purposes of our analysis, time series data was retrieved on stock exchange turnover volumes (turnover), number of transaction (trades) and average prices (BUX), all the data was logarithmised in order to show relative

changes. Figure 4 shows the average daily values of the stock exchange price index, trades negotiated and turnover.

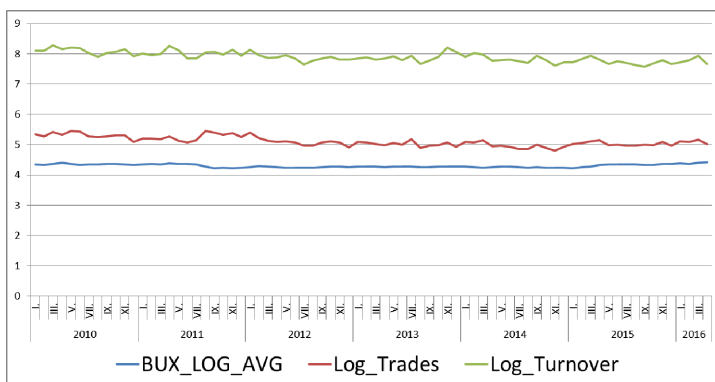


Figure 3. Change in confidence in the Hungarian economy and prosperity month over month (GKI)

Results

We estimated possible vector-autoregression and standalone ARMA models specified using both variables and percentage changes in variables. We used a maximum lag period of 3, this was a reasonable assumption for a reaction time of actors: they should be able to react to changes in legislation with increasing their search activity almost instantly and should not delay this beyond 3 months. Results show that the stock exchange price index can not be modelled with the (lagged) changes in search volume indices for searches on legislative change.

On the other hand the changes in the volume of daily trades do have a strong relationship with the (lagged) changes in search volume indices for searches on legislative change for two lag periods. This means that internet searches do have a slowly decaying impact on daily stock exchange turnover.

We found that search terms based on ‘economy’ show significance in explaining stock market turnover and trade volumes ($\Delta\%/\Delta\%$)

From the analysis we could also draw the conclusion that search terms based on ‘legislative change’ have significant explanatory force in explaining market confidence ($\Delta\%/\Delta\%$), thus is a good measure for uncertainty and has a lagged relationship with turnover and trade volumes.

We also found that there is no significant link between search terms and absolute values of economic development or stock prices.

Sources

[1] Dzielinski M., 2012, Measuring economic uncertainty and its impact on the stock market. Finance Research Letters 9, 167–175

- [2] Lemieux J., Peterson A. R., 2011, Purchase deadline as a moderator of the effects of price uncertainty on search duration. *Journal of Economic Psychology* 32, 33–44
- [3] Ratchford T. B., 1982, Cost-Benefit Models for Explaining Consumer Choice and Information Seeking Behavior. *Management Science* 28(2):197-212. <http://dx.doi.org/10.1287/mnsc.28.2.197> Access on: 14.06.2016.
- [4] Constantinovits M.: The Hungarian economic policy in the light of the EU accession (2004–2013). in: Novák Zsuzsanna (ed.) *Conference on Hungarian-Polish friendship - history, economy and culture. Magyar Fiatalok Határok Nélkül Alapítvány, 2014. pp. 75-78.*

Appendix

Eviews results on VAR estimations

Dependent Variable: TRADES_DELTA

Method: Least Squares

Date: 06/15/16 Time: 19:03

Sample (adjusted): 4 76

Included observations: 73 after adjustments

Variable	Coefficient	Std. Error	t-Statistic	Prob.
SVI_TORV_VALT	0.031441	0.074716	0.420801	0.6753
SVI_TORV_VALT(-1)	0.121198	0.073708	1.644297	0.1049
SVI_GAZD_DELTA	0.072564	0.152620	0.475453	0.6360
SVI_GAZD_DELTA(-1)	-0.059968	0.152337	-0.393651	0.6951
SVI_JOGSZABALY_DELTA	0.602162	0.168070	3.582801	0.0006
SVI_JOGSZABALY_DELTA(-1)	0.378792	0.178547	2.121524	0.0376
SVI_JOGSZABALY_DELTA(-2)	0.437279	0.132895	3.290398	0.0016
R-squared	0.336647	Mean dependent var		0.017621
Adjusted R-squared	0.276342	S.D. dependent var		0.256962
S.E. of regression	0.218592	Akaike info criterion		-0.112240
Sum squared resid	3.153654	Schwarz criterion		0.107393
Log likelihood	11.09675	Hannan-Quinn criter.		-0.024712
Durbin-Watson stat	2.473683			

Dependent Variable: KONJ_DELTA

Method: Least Squares

Date: 06/15/16 Time: 18:52

Sample (adjusted): 5 76

Included observations: 72 after adjustments

Variable	Coefficient	Std. Error	t-Statistic	Prob.
SVI_TORV_VALT	-1.084019	0.695112	-1.559488	0.1241
SVI_TORV_VALT(-1)	-1.108233	0.689368	-1.607607	0.1132
SVI_TORV_VALT(-2)	-2.520797	0.747502	-3.372297	0.0013
SVI_TORV_VALT(-3)	-0.783377	0.762235	-1.027737	0.3082
SVI_GAZD_DELTA	-0.741625	1.501327	-0.493980	0.6231
SVI_GAZD_DELTA(-1)	-0.461612	1.482795	-0.311312	0.7566
SVI_GAZD_DELTA(-2)	-0.676540	1.437636	-0.470592	0.6396
SVI_GAZD_DELTA(-3)	0.506556	1.417931	0.357250	0.7222
SVI_JOGSZABALY_DELTA	-0.628438	1.766646	-0.355724	0.7233
SVI_JOGSZABALY_DELTA(-1)	-0.239942	2.017039	-0.118958	0.9057
SVI_JOGSZABALY_DELTA(-2)	1.826804	1.782939	1.024602	0.3097
SVI_JOGSZABALY_DELTA(-3)	-0.247190	1.631786	-0.151485	0.8801
R-squared	0.217383	Mean dependent var		-0.359344
Adjusted R-squared	0.073903	S.D. dependent var		1.962104
S.E. of regression	1.888210	Akaike info criterion		4.260147
Sum squared resid	213.9201	Schwarz criterion		4.639591
Log likelihood	-141.3653	Hannan-Quinn criter.		4.411205
Durbin-Watson stat	2.047975			

A new approach for the estimation of non-linear switching-type systems

Sándor MOLNÁR¹, Márk MOLNÁR²

¹Department of Informatics, Institute for Mathematics and Informatics

²Department of Macroeconomics,
Institute of Economics

Abstract

A common problem in systems and control theory is to provide an approximation to non-linear systems. We provide a novel approach as a general solution to this problem originally conceived by Gamkrelidze. We consider and solve a general approximation problem which provides the fundamentals for various switching-type systems thus encompassing a wide range of systems theory problems.

Keywords

non-linear system theory, switching type systems, optimal control, approximation

1. Introduction

Vertical integration is one of the key elements of modern industrial production [1,2]. We witness the widespread penetration of industrial sensors and monitoring devices embedded in the production chain resulting in a vast amount of digital data on plant level activity. This, together with the control and system theory provides a unique chance to implement a decentralised automated production system resulting in improved efficiency and higher output as production optimisation requires optimal systems. In the following we provide an important element in optimal system control applicable to a wide range of state-of-the-art systems.

Optimising linear control systems shows similarities with linear programming as it was noticed by Pontryagin and others. Starting with the qualitative analysis of optimal control, Gamkrelidze [3] considered the

$$\dot{x}(t) = A(t)x(t) + B(t)u(t), \quad x(0) = \xi,$$

linear, time varying (LTV) system for controls over the $u(t) \in \times_1^k [0,1]$ cube. He

proved that if $u : [0, T] \rightarrow \times_1^k [0,1] = U$ is piecewise continuous, then for every $\varepsilon > 0$

there exists a $v : [0, T] \rightarrow U$ piecewise continuous control, which directs the system to the vertices of the cube and the solution

$$\dot{y}(t) = A(t)y(t) + B(t)v(t), \quad y(0) = \xi$$

satisfies the condition

$$\|x(t) - y(t)\| < \varepsilon.$$

Thus, even though the $u(t)$ and $v(t)$ controls might show significant pointwise differences, the respective trajectories will still remain uniformly close.

We will use a simple application in the following sections to demonstrate the novel approach presented in the approximation theorems. This application is a simple Buck-Boost converter and is widely applied [4,5].

2. Problem formulation

We will demonstrate the proposed approximation problem through a well-known engineering application. Let's consider the so called Buck-Boost converter circuit:

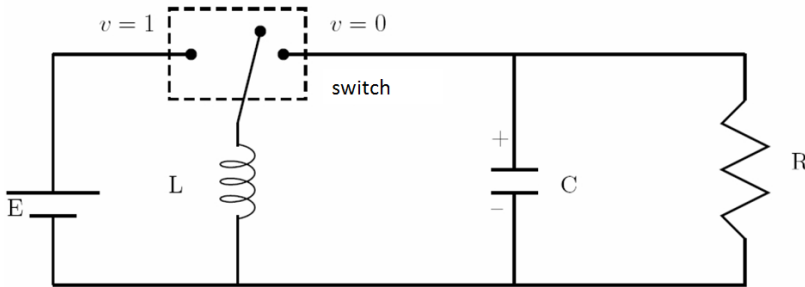


Figure 1. A Buck-Boost converter circuit

The function $v(t)$ describes the state of the switch and can take discrete values $\{0, 1\}$, as it is visible on Figure 1. The ideal behaviour can be characterised by a piecewise continuous function $u : [0, T] \rightarrow [0, 1]$ which is described by the following system of differential equations

$$\begin{aligned} L\dot{x}_1 &= (1-u)x_2 + uE \\ C\dot{x}_2 &= -(1-u)x_1 - \frac{x_2}{R} \end{aligned} \tag{3}$$

where x_1 denotes current flowing through the coil and x_2 the voltage drop on the capacitor.

Function u which describes the ideal behaviour can not be generated by turning the switch on and off, only a good approximation can be achieved. For example, for a given precision $\varepsilon > 0$ a function $v(t)$ can be assigned describing a set of switchings,

$$\begin{aligned} L\dot{y}_1 &= (1-v)y_2 + vE \\ C\dot{y}_2 &= -1(1-v)y_1 - \frac{y_2}{R} \end{aligned} \quad (4)$$

where the resulting y_1 and y_2 fulfill the conditions

$$|x_1(t) - y_1(t)| < \varepsilon, |x_2(t) - y_2(t)| < \varepsilon.$$

It is visible that our simple example is nonlinear, does not have any connection with the optimal control, and is a typical problem in systems theory. Mathematically, however it is of a very similar nature as the approximation problem considered by Gamkrelidze.

3. Problem formulation

Herewith we consider and solve a general approximation problem which provides the fundamentals for further switching-type systems encompassing a wide range of systems theory problems. The Buck-Boost converter is considered as the paradigm of switching systems.

The system is non-linear, thus it can not be fitted in the framework of the Gamkrelidze approximation theorem. Instead of linearising we introduce a parameter to replace the $\begin{pmatrix} x_1 \\ x_2 \end{pmatrix}$ state making the system formally linear. After dividing by the physical constants L and C , (3) can be rewritten as

$$\begin{aligned} \dot{x}_1 &= \frac{1}{L}x_2 + \left(\frac{E}{L} - p_2 \frac{1}{L}\right)u, \\ \dot{x}_2 &= -\frac{1}{C}x_1 - \frac{1}{RC}x_2 + \frac{1}{C}p_1u, \end{aligned} \quad (5)$$

or in matrix form,

$$\begin{pmatrix} \dot{x}_1 \\ \dot{x}_2 \end{pmatrix} = \begin{pmatrix} 0 & \frac{1}{L} \\ -\frac{1}{C} & \frac{1}{RC} \end{pmatrix} \begin{pmatrix} x_1 \\ x_2 \end{pmatrix} + \begin{pmatrix} \frac{1}{L} p_2 \\ \frac{1}{C} p_1 \end{pmatrix} u. \tag{6}$$

Considering the $\begin{pmatrix} p_1 \\ p_2 \end{pmatrix}$ parameter vector as the $\begin{pmatrix} x_1 \\ x_2 \end{pmatrix}$ state variable, we arrive

to the non-linear system in (4). We can immediately raise the problem of adopting a Gamkrelidze-type approximation theorem to LPV or LPTV systems, while in the same time giving a generalisation.

It is well visible that the outlined problem is purely of system theory and not of optimisation theory. We will call the approximating systems which will be piecewise continuous constant parametric linear systems, similarly to the Buck-Boost switches switching systems.

Let $U \subset \mathbb{R}^{k_1}$ convex polyhedron and $P \subset \mathbb{R}^{k_1}$ a compact set. We assume that

$$A : P \times [0, T] \rightarrow \mathbb{R}^{n \times n}$$

$$B : P \times [0, T] \rightarrow \mathbb{R}^{n \times k_1}$$

are satisfying the uniform Lipschitz-condition in t with L_1 and L_2 parameters, respectively.

We substitute the p parameter of the

$$\dot{x} = A(p, t)x + B(p, t)u \tag{7}$$

LPTV system with a state-time-dependent variable. For this consider an open set $D \subset \mathbb{R}^n \times [0, T]$, and the $p : D \rightarrow P$ parameter-function. We assume that function p is uniformly Lipschitz-continuous with an L_3 Lipschitz-constant. To have an easy picture of the structure of such a set D , consider the following figure:

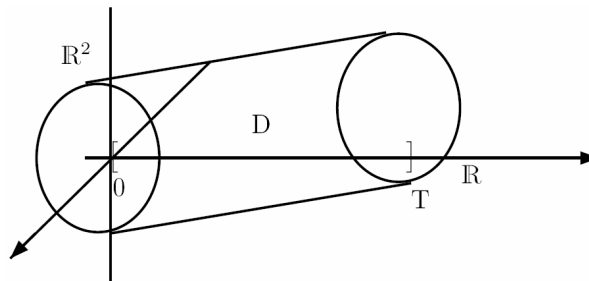


Figure 2. The structure of set D .

The basis and top shape of the cylinder-like object belongs to the D -domain, but the constituents of the cylinder do not, due to the openness in $\mathbb{R}^2 \times [0, T]$

4. Approximation Theorems

In the followings we outline two approximation theorems. In the case of the first theorem the approximation of control u can contain large discrete-point errors, since the approximating v control considers the vertices of the U convex polyhedron, but the respective trajectories are uniformly close. The second theorem states significantly more. Not just that the above mentioned statement holds, but also parameter function q (which is used for approximating parameter function p) considers values of the vertices of the P convex polyhedron and despite this, the approximation of the trajectories is uniform.

Approximation Theorem I. Assume that for a piecewise continuous $u : [0, T] \rightarrow U$ control, and for a $p : D \rightarrow P$ uniformly global Lipschitz-continuous state-time-dependent parameter function in t , and for a $\xi \in \mathbb{R}^n$ initial condition there is a solution for the

$$\begin{aligned} \dot{x}(t) &= A(p(x(t), t), t)x(t) + B(p(x(t), t), t)u(t), \\ x(0) &= \xi \end{aligned} \tag{8}$$

initial value problem. Then, there is a $\varepsilon_0 > 0$ for which for every $0 < \varepsilon < \varepsilon_0$ the following exist:

- 1) $\delta > 0$,
 - 2) a piecewise constant $v : [0, T] \rightarrow U$ which takes the values of the vertices of the U convex polyhedron,
 - 3) $q : D \rightarrow P$ piecewise constant state-time-dependent parameter function,
- that for all $\eta \in \mathbb{R}^n$ initial conditions satisfying $\|\xi - \eta\| < \delta$ the solution of the initial value problem of

$$\begin{aligned} \dot{y}(t) &= A(q(y(t), t), t)y(t) + B(q(y(t), t), t)v(t), \\ y(0) &= \eta \end{aligned} \tag{9}$$

has the whole $[0, T]$ interval as a domain, and there $\|x(t) - y(t)\| < \varepsilon$ holds.

For the next interpolation theorem let's assume that $P \subset \mathbb{R}^{k_2}$ is also a convex polyhedron. We assume that functions $A : P \rightarrow \mathbb{R}^{n \times n}$ és a $B : P \rightarrow \mathbb{R}^{n \times k_1}$ are linear in p , that is, functions $p \rightarrow A(p, t)$ and $p \rightarrow B(p, t)$ are linear for all t .

From this, for a fixed t the Lipschitz-condition holds, thus we need only assume continuity and uniformity in t . With these additional assumptions we can improve our previous theorem.

Approximation theorem II. Assume that for a piecewise continuous control $u : [0, T] \rightarrow \mathbf{U}$ and for a time-state-dependent function $p : D \rightarrow \mathbf{P}$ satisfying the uniform global Lipschitz-condition in t , and for an initial state $\xi \in \mathbb{R}^n$ there is a solution $x : [0, T] \rightarrow \mathbb{R}^n$ for the initial value problem on the whole $[0, T]$ domain. Then there exists $\varepsilon_0 > 0$ so that for all $0 < \varepsilon < \varepsilon_0$ the followings exist:

- 1) $\delta > 0$,
- 2) a piecewise constant $v : [0, T] \rightarrow \mathbf{U}$, which takes its values from the vertices of the \mathbf{U} convex polyhedron,
- 3) a $q : D \rightarrow \mathbf{P}$ piecewise constant state-time parameter function which takes its values from the \mathbf{P} convex polyhedron, so that for all $\eta \in \mathbb{R}^n$, for which $\|\xi - \eta\| < \delta$, if the initial value condition $y(0) = \eta$ is satisfied the solution of the initial value problem is available on the whole domain $[0, T]$, and there

$$\|x(t) - y(t)\| < \varepsilon$$

holds.

While the Gamkrelidze-type of optimisation can not be applied to the Buck-Boost switch, our approximation theorems are applicable. As we discuss a system which is linear in parameters we can endeavour to apply the second theorem. For this we have to ensure that at least on the finite $[0, T]$ interval we can keep the

$p = \begin{pmatrix} p_1 \\ p_2 \end{pmatrix}$ parameters in a convex polyhedron if $p = \mathbf{x}$. Let's consider Equation

(3) and integrate on the interval $[0, t] \subset [0, T]$. Consider the following system of equations

$$\begin{aligned} x_1(t) &= \xi_1 + \frac{E}{L} \int_0^t u(\tau) d\tau + \frac{1}{L} \int_0^t (1 - u(\tau)) x_2(\tau) d\tau \\ x_2(t) &= \xi_2 + \frac{1}{C} \int_0^t (u(\tau) - 1) x_1(\tau) d\tau - \frac{1}{RC} \int_0^t x_2(\tau) d\tau \end{aligned} \quad (10)$$

and substitute $x_1(t)$ from the first equation into the second and from this equation substitute $x_2(t)$ to get:

$$\begin{aligned}
 x_2(t) &= \xi_2 + \frac{1}{C} \int_0^t (u(\tau_1) - 1) \left[\xi_1 + \frac{E}{L} \int_0^{\tau_1} u(\tau_2) d\tau_2 + \frac{1}{L} \int_0^{\tau_1} (1 - u(\tau_2)) x_2(\tau_2) d\tau_2 \right] d\tau_1 - \\
 &- \frac{1}{RC} \int_0^t x_2(\tau) d\tau = \frac{1}{C} \int_0^t (u(\tau_1) - 1) d\tau_1 \xi_1 + \xi_2 + \frac{E}{LC} \int_0^t (u_1(\tau_1) - 1) \int_0^{\tau_1} u(\tau_2) d\tau_2 d\tau_1 + \\
 &+ \frac{1}{LC} \int_0^t \left((u(\tau_1) - 1) \int_0^{\tau_1} (1 - u(\tau_2)) x_2(\tau_2) d\tau_2 \right) d\tau_1 - \frac{1}{RC} \int_0^t x_2(\tau) d\tau = \\
 &= \frac{1}{C} \int_0^t (u(\tau_1) - 1) d\tau_1 \xi_1 + \xi_2 + \frac{E}{LC} \int_0^t (u_1(\tau_1) - 1) \int_0^{\tau_1} u(\tau_2) d\tau_2 d\tau_1 + \\
 &+ \int_0^t \left[\frac{1}{LC} (1 - u(\tau_1)) \int_{\tau_1}^t (u(\tau_2) - 1) d\tau_2 - \frac{1}{RC} \right] x_2(\tau_1) d\tau_1.
 \end{aligned}$$

Let's introduce the following notations

$$\begin{aligned}
 \phi_1(t) &= \frac{1}{C} \int_0^t (u(\tau_1) - 1) d\tau_1, \\
 \phi_2(t) &= \frac{E}{LC} \int_0^t (u_1 \tau_{-1}) \int_0^{\tau_2} u(\tau_2) d\tau_2 d\tau_1, \quad \text{és} \\
 \phi_3(\tau_1) &= \frac{1}{LC} (1 - u(\tau_1)) \int_{\tau_1}^t (u(\tau_2) - 1) d\tau_2 - \frac{1}{RC}.
 \end{aligned}$$

Then

$$x_2(t) = \phi(t) \xi_1 + \xi_2 + \phi_2(t) + \int_0^t \phi_3(\tau) x_2(\tau) d\tau.$$

We can estimate a $P \subset \mathbb{R}^2$ polyhedron (in our case a square $\mathbf{P} = [-M, M] \times [-M, M]$) using the physical constants, the definitions of ϕ_1, ϕ_2, ϕ_3 , and the condition $0 \leq u(t) \leq 1$, which will contain the $p = \mathbf{x}$ parameter function all along the interval $[0, T]$. Our second theorem guarantees an interesting but physically not implemented circuit approximation model for the Buck-Boost converter.

Instead of the model in (3) we can use models defined over discrete sections where in the bilinear element we put $\pm M$ instead of x_1 as the current in the coil, and $\pm M$ instead of x_2 for the potential in the capacitor.

$$\begin{aligned}
 L\dot{x}_1 &= x_2 + (E \pm M)u, \\
 C\dot{x}_2 &= -x_1 - \frac{1}{R}x_2 \pm Mu.
 \end{aligned} \tag{13}$$

This means that the sectionwise switching of the four linear system models corresponding to the four vertices of the square will be the „linearisation” of the bilinear system, nonetheless having not too many common features with conventional linearisation.

The proofs of the above theorems are omitted from this paper due to size limitations. Additionally an approximation lemma is stated hereby which will replace matrix-norm estimations during the proofs of the theorems. This lemma is also not proved.

Approximation lemma. Let $U \subset \mathbb{R}^{k_1}$ be a convex finite polyhedron, $u : [0, T] \rightarrow \mathbf{U}$ a piecewise continuous function, and $\mathbf{B} : [0, T] \rightarrow \mathbb{R}^{n \times k_1}$ a piecewise continuous matrix function. Then for any $\bar{\varepsilon} > 0$ there exists a $v : [0, T] \rightarrow \mathbf{U}$ piecewise continuous approximation function, which takes values in the vertices of \mathbf{U} , and

$$\left\| \int_0^t B(\tau)(u(\tau) - v(\tau)) d\tau \right\| < \bar{\varepsilon} \quad (14)$$

Conclusions

Let us now notice that although we required that the A and B matrix functions to be linearly dependent from the parameter, we can, for all $(x, t) \rightarrow A(x(t), t)$, $(x, t) \rightarrow B(x(t), t)$, satisfying the smoothness condition transform the

$$\dot{x} = A(x, t)x + B(x, t)u$$

system to an LPV system. For this consider the following

$$A(x, t) = \left(a_{ij}(x, t) \right)_{i,j=1}^n, \quad B(x, t) = \left(b_{ij}(x, t) \right)_{i=1, j=1}^{n, k_1}$$

matrices. Replace $a_{ij}(x, t)$ with the p_{ij} parameters, and $b_{ij}(x, t)$ with the q_{ij} parameters. Thus, we defined the $A(p)$ and $B(q)$ parameter-variable matrices, which are obviously linear in p, q parameters, which is nothing else but the linearity of matrix addition. With this we get the

$$\dot{x} = A(p)x + B(q)u$$

LPV system. Using the substitutions $p_{ij} = a_{ij}(x, t)$ and $q_{ij} = b_{ij}(x, t)$ trivially the original system is recovered. Obviously, not too much is gained with this LPV-

ification, under such general circumstances the system will not show any interesting qualities.

Our example with the converter well illustrates the range of applicability of our approximation theorems specific to real life applications [7],[8].

In systems theory analysis these theorems are also quite promising, e.g. in stability, controllability and observability [6],[9], especially Theorem 2, where we can approximate arbitrary system qualities by switching constant parametric linear systems assigned to the vertices of the P convex polyhedron.

References

- [1] Molnár S., Szigeti F.: “On “Verticum”-Type Linear Systems with Time-Dependent Linkage”, *Applied Mathematics and Computation* , Vol. 60., pp. 89-102., 1994.
- [2] Molnár S.: A Special Decomposition of Linear Systems, *Belgian Journal of Operations Research, Statistics and Computer Science*, Vol. 29. No. 4, pp. 1-19, 1989.
- [3] Gamkrelidze, R V: Principles of optimal control theory. (Mathematical concepts and methods in science and engineering) Translation of Osnovy optimal'nogo upravleniia. Based on lectures presented in 1974 at Tbilisi State University., 1978 Plenum Press, New York
- [4] Sira-Ramírez H: Sliding Mode Control, Birkhauser Verlag Gmbh, p. 258, 2015.
- [5] Sira-Ramírez H, Agrawal S.K.: Differentially Flat Systems (Automation and Control Engineering), Marcel Dekker Inc., New York, Basel, p. 450, 2004.
- [6] L. S. Pontryagin, V. G. Boltyanskii, R. V. Gamkrelidze, E. F. Mishchenko, *The Mathematical Theory of Optimal Processes*, J. Wiley, New York, 1962.
- [7] H. Hermes, J. P. Lasalle, *Functional Analysis and Time-Optimal Control*, Academic Press, New York, 1969
- [8] L. D. Berkovitz, *Optimal Control Theory (Applied Mathematical Sciences, Vol. 12)*, Springer-Verlag, New York, 1974.
- [9] J. Warga, *Optimal Control of Differential and Functional Equations*, Academic Press, New York, 1972

Institute for Mechanical Engineering Technology



Professor Dr. Gábor KALÁCSKA
Director of the Institute

Dear Reader,

The Institute for Mechanical Engineering Technology (including Department of Material and Engineering Technology, Department of Maintenance of Machinery, Department of Mechatronics) focused on more research topics during 2016 connected to PhD programs, however the cold atmospheric plasma (DBD) treated polymer surfaces - sponsored by OTKA found - was the core research field. Beside that the positioning and control problems of pneumatic cylinders, composite machining and management tools of production technologies were also investigated. The obtained results partly were already published and some brief highlights of the topics will appear at present issue of MEL.

- DBD cold plasma treated polymer surfaces: dielectric barrier discharge (DBD) method was applied to modify the polymer surfaces (UHMW-PE, PP, PTFE, PA6, POM C, PETP, PEEK). The change of chemical composition, surface energy, 3D surface topography, adhesion capability and tribological behaviour of those were investigated. Present article gives a short review about the adhesion behaviour of the DBD treated polymer surfaces compared to the virgin ones. For those different gluing materials were selected and shear strength of overlap joints were measured using polymer/polymer and polymer/steel bonded pairs.
- Control of servo-pneumatic drive from the point of air consumption: Evaluating a positioned servo-pneumatic drive not only the control quality indicators should be taken into account, but also the air consumption is an important parameter. As compressed air applications have high energy costs, each air-consumption reducing solution must be considered. In position controlled servo-pneumatic systems there is an opportunity to reduce the air consumption without constructional modifications by the tuning method of the controller. The attached article shows optimizing methods.
- Management tools in production technologies: The article analyses the results and the adaptation possibility of the International Manufacturing Strategy Survey (IMSS) in the maize pickers industry. The analysis is based on our survey in 2012. After the examination the IMSS was developed with new questions in the 8 original units and we made a new unit for the examination of the lean management.

Methodological development of the International Manufacturing Strategy Survey based on the case of the Hungarian maize pickers' manufacturer sector

Adrienn GODA¹, Viktor MEDINA¹,
László ZSIDAI²

¹Institute for Engineering Management

²Institute for Mechanical Engineering Technology

Abstract

The present paper analyses the results and the adaptation possibility of the International Manufacturing Strategy Survey (IMSS) in the maize pickers industry. The analysis is based on our survey in 2012. After our examination we developed the IMSS with new questions in the 8 original units and we made a new unit for the examination of the lean management. On the basis of the developed questioner we can receive more detailed and exacter overview about the maize pickers' manufacturer sector. We can see better the presence of losses in the sector to be able to make more profit by correcting the errors and building up a lean management.

Keywords

lean management, IMSS, manufacturing strategy, manufacturing planning

1. Introduction

The basis of our research is the International Manufacturing Strategy Survey (IMSS) which examines the questions of the manufacturing strategy with a focus to the machine industry (Matyusz-Demeter, 2011). The IMSS was established in 1992. The goal of the survey was examination of the international manufacturing strategies, their introduction and results in the manufacturing process and the connected fields (supply chain management, new product development etc. (Demeter-Matyus, 2009). The data was collected in Europe, America and Asia. The whole survey consisted 562 companies' answers in 2009. The Hungarian research added 71 new enterprises' answers (Matyusz-Demeter, 2011). Then we made our research in the maize picker manufacturing sector in Hungary and after the analysis of its efficiency we formulated our proposals to develop the questions of the IMSS.

2. International and Hungarian surveys in the manufacturing

The surveys about the manufacturing strategy play an increasing role in the research of manufacturing management. We collected these surveys and summarized in the table 1. An overview about the researches is very important to be able to make proposals to develop the IMSS.

Table 1. International surveys about manufacturing strategy

SURVEY	SECTOR	SUBJECT
International manufacturing research group	Small machine tools	Efficiency, sales, forecast, manufacturing planning
International manufacturing strategy	Machine manufacturers	Business, strategies, manufacturing programs, manufacturing efficiency, plans for the future
International research of the production's future	America, Europe, Japan	Production strategy
World level manufacturing project	Electronics, vehicles, machines (America, Japan, Germany, Italy, UK)	Organisation factors, human resources, technology, infrastructure, quality management, partner relations, efficiency
Research of competitiveness	International	The whole process of the functioning (business, efficiency, relationships etc.)
Lean management	International	Introduction of the lean management
Other related research	International	Competitiveness of the countries

[Demeter (2011), Flynn et. all (1997), Holweg (2007), Laugen et al., (2005), Miller et.all (1990), Phillips et.al. (1983) Schonberger, (2007), Voss, (1995, 2005)]

3. Development of the IMSS

The original IMSS is a result of an international research (Matyus-Demeter, 2011). The survey focused on different fields like the efficiency, the manufacturing strategy, the organisation, the human resource, the supply chain management, the logistics etc. We developed the original survey based on

- the cognition of the manufacturers with deep interviews,
- development of questions about the maize picking industry,
- pilot questioners in the examined sector,
- correction of the questions based on the pilot research,
- personal interviews with the management of the manufacturers,
- collection of the problems and weaknesses of the manufacturing process.

With the development of the original survey we expanded the questioner with new questions and with a new topic. The developed structure is presented in the table 2.

Table 2. The new structure of the developed questioner

N.	TOPIC	N. OF SUBTOPICS	N. OF QUESTIONS
1	Efficiency of the production	11	58
2	Production strategy and goals	8	37
3	Production program and its investments	5	26
4	Production and information technology	4	49
5	Organisation and human resource	10	18
6	Sales forecast and production planning	6	16
7	Globalization, investment and outsourcing	3	8
8	Supply chain and logistics	7	59
9	<i>Lean management</i>	4	54
	TOTAL	58	325

Efficiency of the production

One key of the success is the production. We have to know how the manufacturing supports and influences the corporate strategy (Bitici, 1994).

Examination of the characteristics of the production strategy

The production strategy plays an important role in the success of the business activity. We have to observe how the manufacturing strategy can increase the profitability (Matyusz-Demeter, 2011).

Production program

The main goal of the production program is to set up the quantity and the list of the manufactured products. Its result is a production plan which is real and calculates with all existing conditions. This plan specify the deadlines and how many and which products must be manufactured.

Production and information technology

The technological process plays role in the manufacturing with changing the parameters (physical, mechanical, chemical, geometrical etc. condition) of the subject of the production (parts, structural units, product etc.). In the production and information technology we have to choose the most profitable way with the examination of many possible technical solutions (Dudás, 2001).

Organisation and human resource

The organisation is a formation established by the common activity of people. The organisation has to mobilize all available tools and human resources to reach its goals.

Sales forecast and production planning

We need exact information about the future demand to be able to organize successfully the manufacturing processes. The goal of the product planning is to make a comprehensive conception for the time and material management. The starting point of the production planning is the market and the customer demand.

For this reason during the production planning we have to focus how to satisfy better the customer needs (Matyusz-Demeter, 2011).

Globalisation, investment and outsourcing

The outsourcing helps to make more rational the functioning and uses more effective the own resources. We can allocate some tasks to other specialized companies and on this way we can increase the profit (Kuhár, Jacob, 1999). The spread of the globalisation was stimulated by the demolition of international barriers and the development of logistics and transport. The goal of the globalisation is to increase the competitiveness and efficiency (Trembecky, 2007).

Supply chain and logistics

The supply chain management is based on the logistics. The chain consist the whole process from the raw material exploitation to the transport of finished product to the end user. It includes also all services related to the product (Trembecky, 2007).

Lean management

Nowadays the lean management flourishes second time (Holweg, 2007 and Schonberger, 2007). There are international researches verifying and validating that the lean management based on the customer needs is a key factor of the competitiveness (Laguen et al, 2005). The lean improves the competitiveness (Voss, 1995, 2005). All companies have to use as few resources as they can to be more competitive. The advantages of the lean management: decreasing of the production cycles, decreasing of the switching time, decreasing of the stocks, increasing manufacturing space, increasing product quality, increasing efficiency, increasing production (Shah, Ward, 2003). For these reasons we thought it is very important to expand the IMSS with questions about the lean management. We added 4 subtopics and altogether 54 questions (Table 3).

The first subtopic focuses to the losses of the production. We defined 11 questions to discover the 7 kind of losses (over production, waste, surplus, not adequate operation, unnecessary transport, unnecessary waiting time, unnecessary movement). The questions help to find the highest loss points.

The lean keeps in mind the improvements of the processes, it uses a number of tools to make the processes even more perfect and to increase the product quality from the point of view of the customers. The losses can be removed by the lean tools, so we can reduce the costs, increase the incomes because of the better quality and higher competitiveness. We need less working capital because we need less inventory, production equipment and space. It has also a positive effect to the efficiency of the work.

We examine in the second subtopic in the professional literature most commonly referred tools of the manufacturing process. We would like to have a good overview about which tool are used and for what extent.

The 13 questions of the third subtopic research the factories and their production from the point of view of the lean management. We would like to

know which companies use and how the lean management. One of the key principles of lean the continuous and balanced production process and the process approach. The demarcation of some areas seems to be optimal, but it doesn't necessarily lead to the optimum. If we look the processes from the perspective of production, we see a lot of stops. In these stops there are a lot of saving possibilities from the perspective of lean management which affect the whole value stream. If these stops could be identified and eliminated and we could harmonize the production process, then we could arrange a flexible manufacturing with taking into account the customer needs. The companies where there is process development, machine productivity improvement, quality improvement, process orientation, they are enterprises having lean management.

The examination of the implementation of lean management is important because the traditional companies focus only to decrease the production costs. In contrast, the lean management has the goal to decrease the costs with increasing the product value for the customer.

We studies the way of thinking of lean on several criteria in the 4th subtopic. The lean concept recognizes the workforce is a very important building block which connects the thought and action, so highly skilled workforce is needed. In case of low-skilled human resource the thinking and action would separate and the managers have to think, employers have to act, and there would be losses in the working process which would result higher costs.

The implementation of lean thinking is reflected in the handling of challenges. In the case of traditional companies the treatment is symptomatic while the enterprises using lean management always research the root of the problems. With this way of thinking the errors can be corrected at the point of beginning and this results cost savings.

In the lean management the innovation drives the organisation to the ideal state. The continuous development is ensured by the involvement of the full range of employees. Not an isolated person is responsible for development, but all workers are involved in it.

This way of thinking has an effect not only inside but also outside of the organisation, such as a supplier is an ally not an enemy, based on the lean thinking. The information from the production is appropriate to share with the suppliers, because it can improve the quality of the delivered product. The lean takes into account the production with the suppliers to satisfy the customer need on a higher level and to maximize the profit. From the answers we can see the areas where the traditional concept maintained his role. Then we have to focus on these areas when we want to introduce the lean management.

Finally all questions about lean can give an overview about the maize picker industry from an interesting point of view.

The majority of the questions in our questionnaire are closed questions, mainly with scale and predefined answers. We took care of the symmetry of scales, and we have same size scales on the positive and negative side. The number of degrees of the scale is generally unmatched. If there is no middle of the scale, the responders must make a decision to give a positive or negative answer. It can't be neutral. It is more difficult to answer. It is also harder to answer when the number of scale grades is higher. The most common scale is the 1-5 scale (Scipione,

1999). The “1” represents the worst evaluation, “3” means neutral or indifferent, “5” is the best value (Laugen-Boer, 2011).

Table 3. Subtopics of lean management

N.	SUBTOPIC	N. OF QUESTIONS
09_01	Losses during the production	11
09_02	Level of use of lean tools	17
09_03	Lean management in the factory and in the manufacturing	13
09_04	Way of thinking and lean	13
09	LEAN MANAGEMENT	54

A survey always is fraught with many risks and difficulties like representativeness, subjectivity, understanding etc. Not only the questionnaires have disadvantages but all kind of methods of the empirical analysis have various difficulties. There isn't any perfect methodology for analysing a sector, but we think our developed questioner gives a good answer to this.

Conclusion

Our research focuses to the maize picker manufacturing industry and to develop a research methodology for examining the sector. We reviewed many national and international researches and we found only few surveys about lean management. We found the questionnaire of the IMSS useful, but we concluded it must develop. The questions of IMSS about efficiency of the production, organisation, human resources, sales forecast, supply chain, logistics, production strategy, program and planning were detailed and we had to widen them only with some questions, but there was no questions about the lean management. Based our review of the professional literature the lean plays an increasing role in the manufacturing. For this reason we decided to add a new topic to our developed IMSS questionnaire. The questions about lean management we grouped in 4 subtopics. We examine losses during the production, the level of use of lean tools, the lean management in the factory and in the manufacturing and finally the thinking on a way of lean. This survey can give us more useful results about the development and the actual situation of the manufacturing. We can see the fields where improvements needed. We can find the tools how to develop the manufacturing, how to decrease the losses and how to increase the profit. Finally we can have a good visibility to the examined sector and we can forecast better the future with our developed questionnaire presented in this paper.

References

- [1] Bitici, U.S. (1994): Measuring your way to profit, *Management Decision* Vol.32. No.6.pp. 16-24.

- [2] Demeter K., Matyusz Zs. (2009). A „külső tényezők és adottságok hatása a vállalatok teljesítményére az értékteremtés szűrőjén keresztül” projekt záró tanulmánya. 54.sz Műhelytanulmány, 19.o.
- [3] Demeter K. – Jenei I. – Losonczi D. (2011): A lean menedzsment és a versenyképesség kapcsolata
- [4] Dudás I. (2001): Gépgyártástechnológia II., Forgácsolás elmélet, technológiai tervezés alapjai. Miskolc: Egyetemi Kiadó 157-225.
- [5] Flynn et. all 1997. 671old. // Flynn, B., Schroeder, R. G., Flynn, E. J., Sakakibara, S. and Bates, K. A. [1997]: World- class manufacturing project: overview and selected results, International Journal of Operations and Production Management, Vol. 17., No. 7, pp. 671-685
- [6] Holweg, M. (2007): The geneology of lean production. Journal of Operations Management, 25: p. 420–437.
- [7] Kuhár P. – Jacob, H. R. (1999): Tevékenység-kiszervezés (outsourcing) Bankszemle, 1999. 43 évf. 5-6. szám pp. 85-93., Hajós, S. (2003): Régi és új menedzsmentirányzat, Vezetéstudomány 2003 7-8. pp. 71-75.
- [8] Laugen, B.T. and Borer, H., Cinet Research Series (2011): The International Manufacturing Strategy Survey, Serial Number: 20011-7. pp.16-17. ISBN 978-90-77360-14-09
- [9] Laugen, B.T. – Acur, N. – Boer, H. – Frick, J. (2005): Best manufacturing practices. What do the best-performing companies do? International Journal of Operations & Production Management 25(2): p. 131–150.
- [10] Matyusz Zs., Demeter K. (2010). A termelési stratégia és termelési gyakorlat kutatás eredményei 2009-2010. 121. sz. Műhelytanulmány, Budapest, 22. o.
- [11] Matyusz Zs., Demeter K. (2011). A termelési stratégia és termelési gyakorlat kutatás részletes eredményei 2009-2010. 145.sz. Műhelytanulmány, Budapest, 21-23.o. HU ISSN 1786-3031
- [12] Miller et.all 1990, 34.oldal // Miller, J. G. and Roth, A. [1994]: A taxonomy of manufacturing strategies, Management Science, Vol. 40 No. 3, March, pp. 285 304
- [13] Paul A. Scipione (1999): A piackutatás gyakorlata, Budapest, Springer-Hungária Kiadó, 151-162.o.
- [14] Schonberger, R.J. (2007): Japanese production management. Journal of Operations Management 25: p. 403–419.
- [15] Shah, R. - Ward, P. T. (2003): Lean manufacturing: context, practice bundles, and performance. Journal of Operations Management, Vol. 21 pp. 129-149 ISSN 1741-038X
- [16] Voss, C.A. (1995): Alternative paradigms for manufacturing strategy. International Journal of Operations & Production Management 15(4): p. 5–16.
- [17] Voss, C.A. (2005): Alternative paradigms for manufacturing strategy. International Journal of Operations & Production Management 25(12): p. 1211–1222.

Shear strength of polypropylene bonded joints using pristine and DBD plasma treated surfaces

Al-Maliki HAYDER¹, Zoltán SZAKÁL², Róbert KERESZTES³,
Gábor KALÁCSKA³

¹PhD student

²Department of Material and Engineering Technology

³Department of Maintenance of Machinery

Institute for Mechanical Engineering Technology

Abstract

Among numerous engineering polymers polypropylene (PP) surfaces were treated by atmospheric cold plasma (DBD method – dielectric barrier discharge) to modify the surface properties. Beside the change of chemical composition, surface topography and surface energy the bonding adhesion were tested applying different gluing materials. On tensile machine the shear strength values of the bonded joints were measured. It was found that the plasma treatment could enhance the adhesive bonding capability due to the increased surface energy and modified surface topography.

Keywords

polypropylene, cold plasma treatment, surface energy, shear strength, bonded joints

1. Introduction

Polypropylene is one of the most known polymer, which is successfully used in different areas of engineering activities due to its good mechanical property/price ratio [1,2]. Typical areas of use: machine parts exposed to a smaller degree of mechanical wear, such as for example bearings, gearwheels, instrument housings, reservoirs, parts used in electroplating technology; electrically insulating parts; tanks, reservoirs used in the chemical industry, equipment, instruments used in the entertainment and advertising industry; elements of material handling systems. [3]

Reinforced, composite versions exist to satisfy special requirements, but characteristically not in semi-finished product use but in the mass production (injection molding) of special parts, such as for example in auto industry [4].

Very often adhesive bonding is needed for a complex form or part [5], units made of PP. PP formerly was considered as hardly be bonded material, thus, heavily loaded joints were not designed and manufactured from PP. Present research introduce a method (cold atmospheric plasma treatment) and results of bonding tests carried out with different adhesive materials.

2. Plan of experiments

Table 1. shows the used materials and glues for the experiments.

Table 1. Bonding plan of experiment

Bonded materials	Glue	Primary / Activator
PP / PP	Superglue: Loctite 406	Primary: Loctite 770
	Structural adhesive: Loctite 3035	-
PP / S235 steel	Superglue: Loctite 406	Loctite 770 only for PP
	Structural adhesive: Loctite 3035	-

3. Method and materials

3.1. Shear tests on tensile machine

According to the plan of the experiment, the shear of 2 mm thick PP plates overlap adhesive bonding was carried out on a tensile machine with pulling (Figure 1.). The tensile test were carried out in accordance with DIN EN 1465 standard.

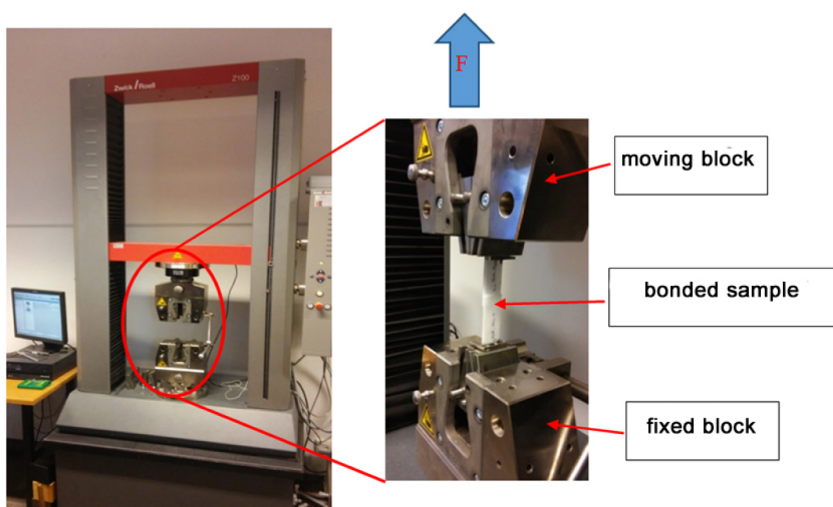


Figure 1. Shear test of overlap bonds on tensile Zwick Roell Z100 machine

3.2. The specimen

The specimens used for bonding were cut out from 2mm thick extruded plates with a disc saw. The dimensions of the specimen are shown in Figure 2. The overlap of the joint is 12,7 mm according to DIN EN 1465 standard.

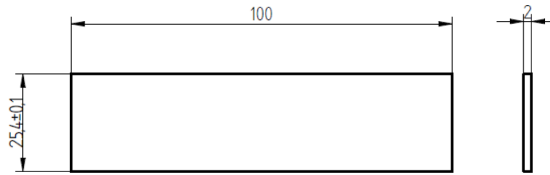


Figure 2. Dimensions of the specimen

The requirements for bonding of the specimen:

- 5 repeated bonding at the same time with a given materials
- overlapping has to be 12.5 ± 0.1 mm
- The same normal force (5 N) applied during curing,
- Stick-free bonding-jig to prepare the bonds

3.3. The procedure of bonding

The experiments were carried out according to the glue producer's (Henkel Loctite) recommendations (detailed technological steps specified to each glue are not mentioned below but available in Technical Data Sheet - TDS - of Loctite).

- Rough cleaning with water.
- Degreasing of the surfaces with Loctite SF 7063.
- Creating the bonds in jig.

Reference measurements were carried out with untreated polymer surfaces.

Furthermore DBD atmospheric cold plasma treatment was applied on the extruded polymer surfaces to modify them for bonding tests.

3.4 Dielectric barrier discharge treatment (cold plasma)

The atmospheric pressure ambient air plasma was generated by DCSBD plasma source. The principle of DCSBD plasma is based on a coplanar DBD where comb-shape electrodes are embedded in a dielectric [6]. The diffuse plasma is generated in thin 0.3 mm thick flat layer on alumina ceramic which designates the DCSBD to be used especially for treatment of flat surfaces. The DCSBD electrode system was powered by AC HV source of frequency approx. 14 kHz and voltage approx. 20 kV peak-to-peak and the total power in plasma during the experiments was 400 W. The area of generated plasma of DCSBD is 170 cm², thus the surface energy density and volume energy density at power of 400 W are approximately 2 W cm² and 80 W cm³, respectively. The DCSBD plasma is described in detail [7]. The plasma treatment was performed in dynamic treatment mode and the distance between the treated polymer surface and DCSBD ceramic was 0.3 mm.

3.4. The used materials

Structural steel (S 235 JR N)

This is one of the most common type of the general-purpose, non-alloy steels with low carbon content, (0.17 % (C)). in general its $R_m = 400-500 \text{ N/mm}^2$. (Ferroglobus Ltd, Hungary)

Polypropylene (PP)

Commercial grade of not reinforced and filled version of semi-finished PP plate was used for testing. (QuattroplastLtd. Hungary). Its tensile strength in average is 30 MPa. Further other properties of the material are freely available at the distributor's database.

Loctite 406 adhesive

Cyanoacrylate instant adhesives with low viscosity, it is in particular recommended to plastics and rubber bonding. Its advantage is that to 120°C to withstand the temperature, it allows the polymers and elastomers fast the bonding. Before bonding the Loctite 770 polyolefin primary increases the bonding strength in the difficult cases by polymers. The recording time is 2-10 seconds. It is colourless, limpid material. In principle available shear strength is with the bonded 15 MPa.

Loctite 3035

This is an acrylic based, two components adhesive, mixture ratio of product is 1:1 which mingles on the surface by its formation of tube during the application. It is offered for low surface energy of materials without surface treatment. Its setting time is at most 15 minutes. It is adaptable to bonding of steel and polymers. In principle available shear strength is 14 MPa by the adhesive bonding.

Loctite 770 primary

This is a polyolefin primer, which allows the most polyolefins, including polyethylene, polypropylene, thermoplastic caoutchoucs and other difficult-to-bond plastic materials to together, or to other materials. It is a single component material which dries very quickly, this allows the cyanoacrylate bonding of the low surface energy materials.

3.5. The marking system of bonded specimens

The different combination of specimens must be distinguished, therefore the following identification has been introduced.

PP example:

0_PP_PP_406_11_1

1. marking: It indicates the condition of surface (0-natural surface without plasma treatment, 1-with cold plasma (DBD) treated surface)
- 2.-3. marking: refers to the conjugate materials.
4. marking: refers to the type of adhesive
5. marking: use of activator. 11-both, 00 not one of them, 10, 01 - only one
6. marking: refers to the serial numbers of specimen in the bonding device (from 1 to 5).

4. Results and discussion

The Figure 3 shows the measured force values (average of 5 measurements), as well as the figure 4 shows the calculated shear strength. Figure 5 is about the tested samples.

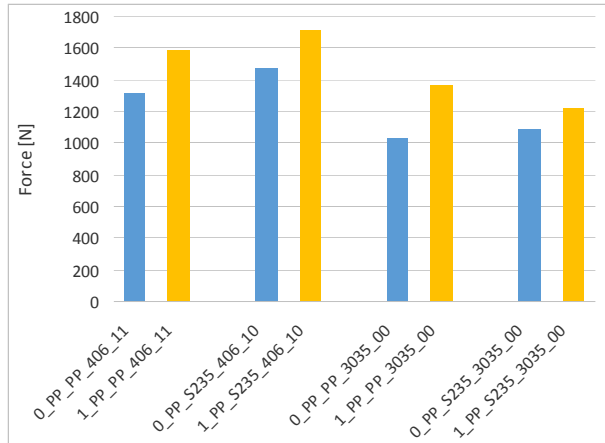


Figure 3. The results of the tensile force of PP adhesive bonding (Loctite 406 + primary, Loctite 3035)

- The adhesive bonding is difficult in the case of polypropylene specimens because the surface energy of polypropylene specimen is low so its adhesive ability is weak. The surfaces must be treated with primer during the experiment, so, the primer can modify the surface energy and wettability of the glue. It can be stated that the shear strength of PP-PP overlap bond with Loctite 406 and primer can reach almost 18-20% of the material's tensile strength. That happened with the repeated measurements. The shear strength of adhesive bonding increases in case of PP-S235 JR N material couple.
- The shear strength of the bonds with Loctite 3035 structural adhesive between PP surfaces is around 5-7% of PP's tensile strength of base material.

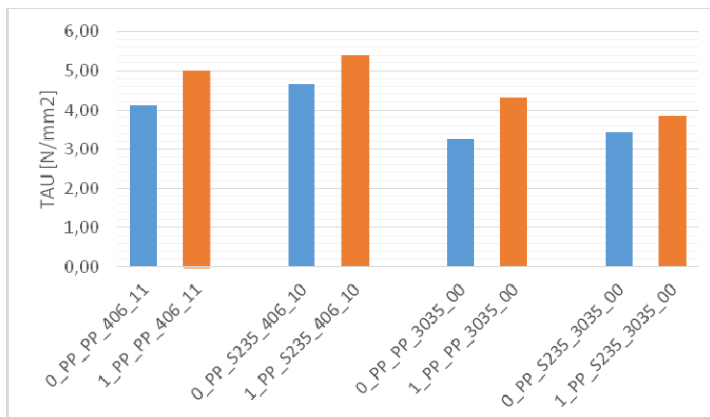


Figure 4. The shear strengt of PP/PP and PP/steel adhesive bonding (Loctite 604 + primary, Loctite 3035) in natural and clasma treated condition.

- The DBD treatment of PP surfaces caused increase of the shear strength in all tested cases. The shear strength of the joints was better with both applied Loctite glues. The adhesive bonding of PP-PP and PP-S235 material couple were stronger than the base material. The strength of joints increase with 20-30 % in case of Loctite 3035.

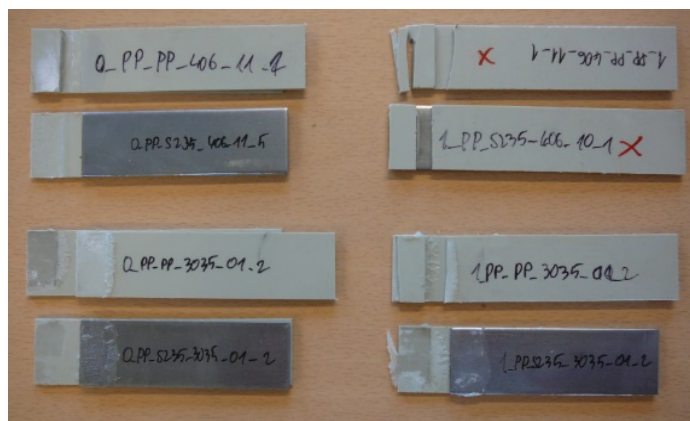


Figure 5. Specimens after shear test of PP adhesive bondings

Conclusion

- Good and reliable bonding can be created with DBD cold plasma treated PP surfaces with Loctite 406 and Loctite 3035. Both types of gluing materials performed even adhesion. During the test the failure occurred in the base material next to the bonded surface. The adhesive detached from the metal surface in case of 3035.
- In absolute values the Loctite 406 with primer offered a bit higher (10-15%) shear strength comparing to Loctite 3035 data.
- Alltogether the PP is still hardly be bonding polymer instead of DBD improved surfaces concerning the max.20% of the base material strength reached by the tests.

Acknowledgement

The present research is part of the broad OTKA K113039 supporting project.

References

- [1] Kalácska - Keresztes - Kozma- Zsidai (2007): Műszaki polimerek és kompozitok a gépészmérnöki gyakorlatban. 3C-Grafika Kft. 2007. p. 1-315. ISBN-10: 963-06-1566-5, ISBN 13: 978-963-06-1566-2

- [2] Czvikovszky – Nagy - Gaál (2006): A polimertechnika alapjai. Műegyetemi kiadó. ISBN 963-420-621-2
- [3] www.quattroplast.hu. Download available January, 2017
- [4] Kalácska Gábor: Műszaki műanyag féltermékek ragasztása. Műszaki ismerető sorozat I. rész. Quattroplast – Q print Kft. 2005. ISBN 963 871 132 9
- [5] Farkas – F. Farkas F.J. (1997): A ragasztás kézikönyve. (Handbook of adhesive bonding). Műszaki könyvkiadó. ISBN 963-16-1380-1
- [6] Z. Károly – Sz. Klébert - H. Al-Maliki – T. Pataki (2016): Comparison of NPIII and DBD plasma treatment in terms of wettability of PTFE and PA6. The 11th International Conference Of The Carpathian Euro-Region Specialists In Industrial Systems. Ceursis 2016, 2 - 4 June, 2016, Baia Mare, Romania. pp 85 – 89.
- [7]. M. Cernák, L. Cernáková, I. Hudec, D. Kovácik, A. Zahoranová, (2009). European Physical Journal: Applied Physics vol.47 ISSN 1286-0042 p.1–6.

Reduction of air consumption of positioned pneumatic drive by the optimization criteria of GA

Eszter SÁRKÖZI

Department of Mechatronics,
Institute for Mechanical Engineering Technology

Abstract

Evaluating a positioned servopneumatic drive not only the control quality indicators should be taken into account, but also the air consumption is an important parameter. As compressed air applications have high energy costs, every air consumption reducing solution must be considered. In position controlled servopneumatic systems there is an opportunity to reduce the air consumption without constructional modifications by the tuning method of the controller. In this paper this optimizing method is presented and evaluated.

Keywords

Servopneumatic drive, Position control, Status controller, Genetic algorithm, Optimization criteria, Air consumption

1. Introduction

In order to achieve linear motion, pneumatic, electromagnetic and hydraulic actuators are typically used. Due to their advantageous characteristics in position controlled applications the latter two are more widespread, but also pneumatic actuators have several advantages: they are fast, cheap, have an outstanding power-to-weight ratio, are easily maintainable and they do not contaminate the work piece. The challenge to the use of pneumatic drives is that due to piston friction and the characteristics of compressed gas flow their behaviour is non-linear. As a result their typical industrial use is such applications which require linear motions between end positions.

In the last decade such industrial controllers became available which have adequate computing capacity for real-time usage. With the use of them servopneumatic systems are also capable for positioning purposes. Evaluating the positioning result of servopneumatic system, the achieved accuracy, the settling time and the speed are the main viewpoints, but also the air consumption is an important consideration. As the pressured air is one of the most expensive energy form used in the industry, reducing the air consumption during the positioning has great importance.

2. Objectives

In this article my main objective was to examine the potential of air consumption reduction by a new optimization criteria of the tuning method of control algorithm. Null hypothesis was that if the air consumption is taken into consideration as a part of the optimization criteria, then the air consumption will decrease during positioning, but other control parameters will deteriorate. To prove the hypothesis the following steps were implemented:

- selection and assembling of examined servopneumatic system,
- selection and applying of the used control method,
- mathematical modelling of the examined system,
- identification of the model,
- selection of optimization method,
- designation of applied optimization criteria,
- implementation of controller optimization (tuning),
- evaluation of behavior of tuned systems.

3. Experimental apparatus

As an actuator a Festo DGPL-25-450-PPV-A-KF-B double acting rodless pneumatic cylinder of 450mm stroke length was applied. A Festo MLO-POT-0450-TLF analogue displacement encoder was attached to the cylinder, which has a 0,01 mm travel resolution. The applied encoder is a potentiometer which provides a voltage signal in proportion to the displacement. The used way-valve was an MPYE-5-1/8-LF-010-B 5/3 proportional valve (Fig. 1).

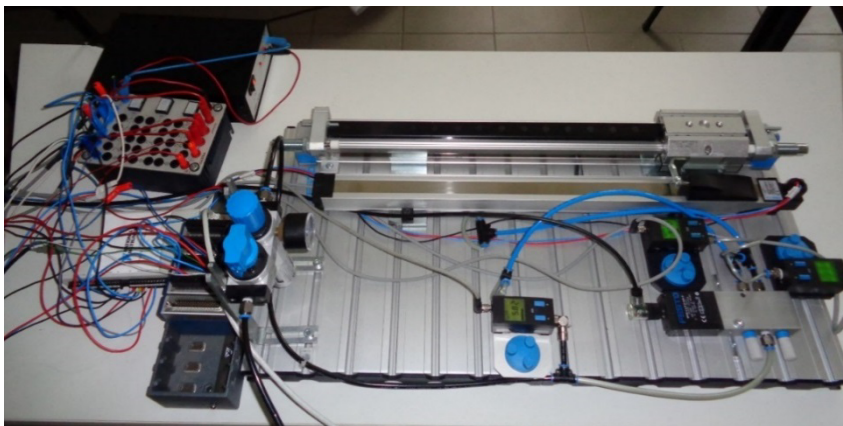


Figure 1. The experimental apparatus

The major elements of the electronic system are a 0-24 V direct current power supply (NI PS-15), an electronic instrument board (Festo), a NI CompactRIO™ (cRIO 9073) programmable automation controller and the already mentioned

electro-pneumatic elements (displacement encoder, pressure sensors and proportional solenoid valve). The applied NI CompactRIO™ programmable automation controller is a modular system; out of its modules we used the analogue-to-digital converter (NI 9201). The proportional solenoid valve was controlled with the help of the analog output module (NI 9472). The communication between the CompactRIO™ and the computer was ensured by an Ethernet connection. The circuit diagram of the pneumatic positioning system is presented on Figure 2.

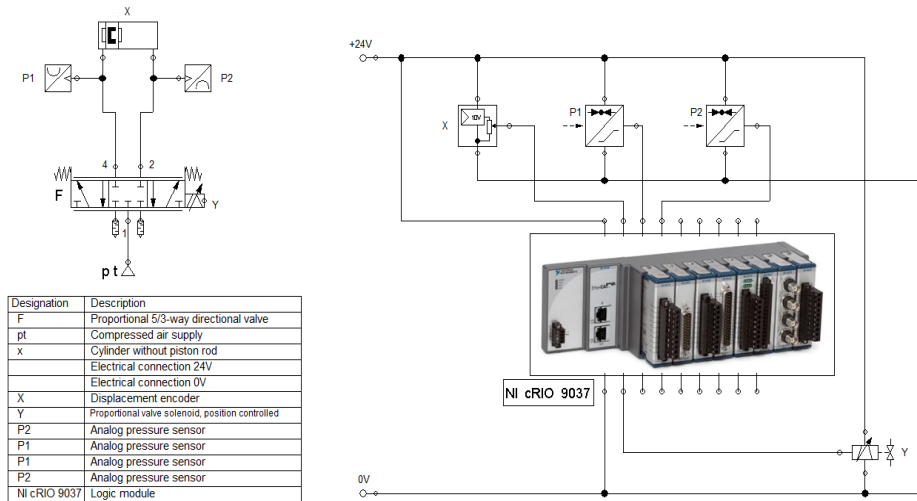


Figure 2. The pneumatic and electric circuit diagram

4. Mathematical model of pneumatic linear drive system

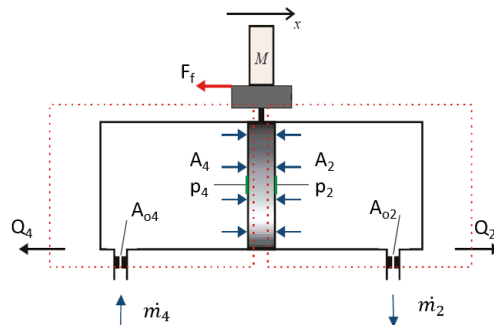


Figure 3. Outline of the cylinder

The mathematical model of pneumatic linear drive system contains the model of the used cylinder and the proportional valve. To create mathematical model of

double-acting pneumatic cylinder three main mathematical formulas have to be declared: the descriptive equation of the flow mass rate flowing through an orifice, the force equation and a vessel filling equation. During the deduction, the conservation laws (energy and mass), the ideal gas law and Newton 2nd law of motion were used. After some simplification, as we consider the flowing gas as ideal gas, and neglecting the effect of the temperature change, the following equation was used (Figure 3).

The mass flow rate through an orifice due to the pressure difference is:

$$\dot{m} = A_o \cdot p_u \cdot \sqrt{\frac{2 \cdot \kappa}{(\kappa - 1) \cdot R \cdot T} \cdot \left(\left(\frac{P_d}{P_u} \right)^{\frac{2}{\kappa}} - \left(\frac{P_d}{P_u} \right)^{\frac{\kappa+1}{\kappa}} \right)} \quad (1)$$

The mass flow rate in function of p_d/p_u has a maximum value at $\frac{p_d}{p_u} = \left(\frac{2}{\kappa + 1} \right)^{\frac{\kappa}{\kappa+1}} = 0.528$, so this pressure ratio is called critical pressure ratio. Below the critical pressure ratio the velocity of flow is maximal, and this velocity is the speed of the sound at exhausting temperature. Above the critical pressure ratio the velocity of flow is lower than the speed of sound, the value of it depends on the actual pressure ratio.

The force equation of the cylinder:

$$m \cdot \ddot{x} = A_4 \cdot p_4 - A_2 \cdot p_2 - F_f - F_l \quad (2)$$

The container filling equation:

$$R \cdot T \cdot \dot{m} = V \cdot \dot{p} + \dot{V} \cdot p \quad (3)$$

In the Eq. 2, the friction force is defined with the use of Stribeck friction as follows:

$$F_f = \begin{cases} F_{str}, & v \geq 0,001m/s \\ \min(F_b, |\sum F_i|) \cdot \text{sign}F_i, & v < 0,001m/s \end{cases} \quad (4)$$

Where

$F_i = p_4 \cdot A_4 - p_2 \cdot A_2 - F_l$, and the Stribeck friction is:

$$F_{str} = (F_C + (F_{br} - F_C) \cdot \exp(-c_v \cdot |v|)) \cdot \text{sign}(v) + f \cdot v \quad (5)$$

The proportional directional control valve is the element that makes contact through pneumatics and electronic control. The spool of the proportional valve can move into any position within its stroke proportionally to the control signal. So the opened cross-section of the valve is proportional with the input control signal, which is the setpoint (input) voltage (or current) signal (U_v) of the actuating electromagnet. With this solution not only a precise positioning can be solved, but also the flow control function in order to vary the speed of the cylinder.

Examining the physical construction of 5/3 proportional valve it can be stated that the inlet and the outlet mass flow rates of the valve can be interpreted by the application of four orifices, which are the followings:

- orifice (A_{1_4}) between the supply port (1) and the left side working port (4),
- orifice (A_{4_5}) between the left side working port (4) and the exhaust port (5),
- orifice (A_{1_2}) between the supply port (1) and the right side working port (2),
- and orifice (A_{2_3}) between the right side working port (2) and the right side exhaust port (3).

The mass flow through these orifices can be determined with use of Equation 1 and the proportional valve flow rate (q [%]) – setpoint voltage (U [V]) characteristics (Sárközi, Földi, 2016).

5. Applied control method: status controller

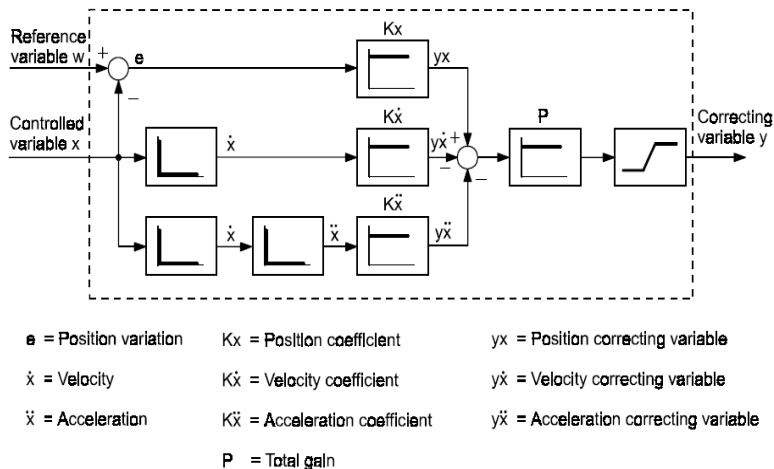


Figure 4. Block diagram of status controller

The status controller is based on the classic proportion controller with the addition that it takes into account the first and second derivative of the feedback signal. Typical field of application of the status controller is the positioning of pneumatic linear drives. In this case the controlled variable is the position. The

first derivative is the velocity, the second derivative is the acceleration. So the status controller takes into consideration the motion parameters. In the block diagram (Fig. 3.) it can be also seen that the velocity and the acceleration have negative impact, so they are a dampings proportionally to the velocity and the acceleration.

The gain proportional to the position error:

$$y_x = Kx \cdot e \quad (6)$$

Damping proportional to the velocity:

$$y_{\dot{x}} = K\dot{x} \cdot \dot{x} \quad (7)$$

Damping proportional to the acceleration:

$$y_{\ddot{x}} = K\ddot{x} \cdot \ddot{x} \quad (8)$$

6. Tuning of the controller

Proper tuning of the controller is an optimization task. For status controller there is an experimental method for tuning the controller based on the transient response of the system (Gerhartz, Scholz, 2001), but in this case, as the viewpoints of the tuning are more complex, this method can not be used. The selected tuning method is optimizing the control parameters by genetic algorithm combined with a gradient fminsearch method. Both algorithms perform large number of settings, so the optimization was implemented on the identified system model by MATLAB r2015 software Optimization Toolbox Genetic Algorithm Solver and fminsearch solver.

These solvers need a criterion for the optimization. The first used one is the Integral of Time multiply by Absolute Error (ITAE) criterion (Equation 9).

$$ITAE = \int_0^{\infty} t |e(t)| dt \quad (9)$$

These ITAE criterion takes into consideration the control error (e) - which is the difference between the set point (in case of positioning this is the target position) and the present value (the present position)- and the elapsed time (t).

In this paper I have examined the effect of an expanded ITEA criterion which contains an additional part next to the ITAE. This additional part is proportional to the air consumption, as the nominal air consumption (V_n) is weighted by an air consumption coefficient (AC), so the new optimization criterion is:

$$Cr_{AC} = AC \cdot V_n + \int_0^{\infty} t |e(t)| dt \quad (10)$$

Due to the Equation 10, as AC coefficient increases, the weight of the air consumption is increasing in the conditions of optimization. It can be presumed

that the total air consumption will be decreasing during the positioning, as AC is increasing, but in the other hand the other control results as accuracy and settling time will increasing as well.

The positioning task was the following during the optimization: from start position (0 mm) the piston should move to 360 mm. The simulation time was 5 s. 10 AC values were applied from 0 to 2, with each 10-10 optimization process was run. From the 10-10 results of the optimization the best 5-5 controller tunings were chosen and evaluated.

Results

The air consumption coefficient value- air consumption, -steady-state error and – settling time characteristics is shown in the Figure 4, 5 and 6.

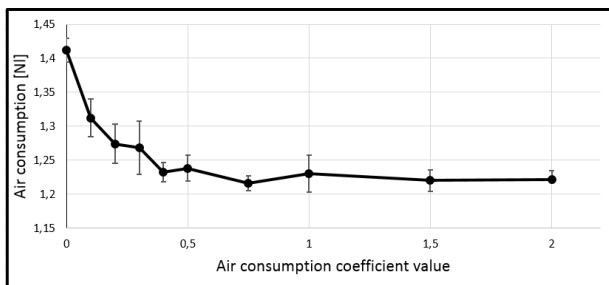


Figure 4. Air consumption coefficient value - air consumption characteristics

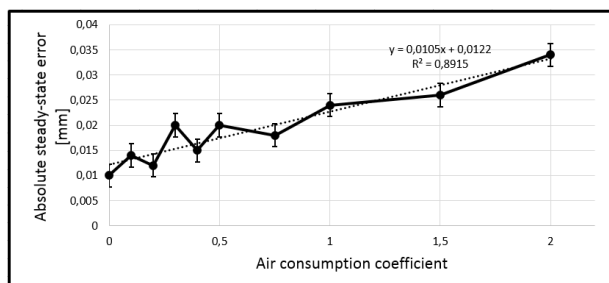


Figure 5. Air consumption coefficient value – absolute steady-state error characteristics

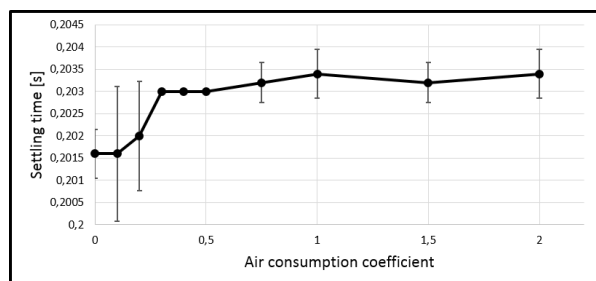


Figure 6. Air consumption coefficient value – settling time characteristics

Based on the characteristics it can be declared that the null hypothesis was right, as increasing of air consumption coefficient value causes decreasing of nominal air consumption and increasing steady-state error and settling time during the positioning. The decreasing of air consumption has limitation, because the movement during the positioning needs compressed air. With the use of these diagrams, that controller tuning can be applied which results the lowest air consumption besides considering the technical requirements, such as accuracy and settling time.

Summary

In position controlled servopneumatic applications such parameters are used to be considered as accuracy, overshoot, settling time, but also the energy consumption is an important parameter, as the compressed air is one of the most expansive energy form. The objective of this work was to examine the potential of air consumption reduction by a new optimization criteria of the tuning method of the applied controller.

In the implementation status controller was applied, which takes into consideration the moving parameters, such as velocity and acceleration, so it works properly in servopneumatic positioning. Behaviour of the controlled system is determined by not only the used algorithm but also the tuning method of the controller. The applied optimization method was genetic algorithm combined with *fminsearch*, and the objective function of the optimization was an ITAE criterion with an additional part, which is proportional to the air consumption, as it contains the nominal air consumption multiplied by a weight factor, the air consumption coefficient. Based on the results it can be declared that the air consumption can be reduced by the used optimization criterion without any structural modification.

Nomenclature

U_v	– control signal (voltage)
A_o	– area of an orifice
A_2 or A_4	– surface of the piston (2 or 4 side)
p_2 or p_4	– pressure in cylinder chamber
M	– mass, moved by the cylinder
x	– displacement
\dot{m}	– mass flow rate
V	– volume
w	– velocity
p_u	– upstream pressure
p_d	– downstream pressure
ρ	– density
κ	– heat capacity ratio
R	– universal gas constant
T	– temperature

Ff	– friction force
FStr	– Stribeck friction
Fc	– Coulomb friction
Fbr	– Breakaway friction (static friction)
cv	– coefficient
v	– relative velocity of the surfaces
f	– viscous friction coefficient
Fl	– external load force
K_x	– position coefficient
$K_{\dot{x}}$	– velocity coefficient
$K_{\ddot{x}}$	– acceleration coefficient
E	– error
T	– time
Vn	– air consumption [NI]
AC	– air consumption coefficient

References

- [1] Czmerk, A. (2015). Pneumatikus rendszerek dimanikájának és beállási pontosságának a javítása. *PhD Thesis*. BME Budapest
- [2] FESTO. (2015). Proportional directional control valves MPYE. *Product catalog*.
- [3] Hamiti, K; Voda-Besançon, A.; Roux-Buisson H. (1996): Position control of a pneumatic actuator under the influence of stiction, *Control Engineering Practice*, Vol. 4. pp. 1079-1088
- [4] Sárközi E.- Földi L. (2016) The effect of the leakages on the behavior of 5/3 pneumatic proportional directional control valve, 11th International Conference of the Carpathian Euro-Region Specialists in Industrial Systems (CEurSIS 2016) 2-4 June, BAIA MARE, ROMANIA
- [5] Messina, A., A., G. N., & Gentile, A. (2005). Experimenting and modelling the dynamics of pneumatic actuators controlled by the pulse width modulation (PWM) technique. *Mechatronics*, Vol. 15. pp. 859–881.
- [6] Metwally M., E.-A. A. (2013). Effect of spool side chambers on dynamic response of contactless electro-operated pneumatic directional control valve, *Computres & Fluids*, Vol. 86. pp. 125-132.
- [7] Rahmat, M. F. (2011). Review on modeling and controller design in pneumatic actuator control system. Vol. 4., Nr. 4.
- [8] Gerhartz J., Scholz D. (2001) Closed-loop pneumatics, FESTO, Denkendorf
- [9] Takashi Miyajima, T. F. (2007). Development of a digital control system for high-performance pneumatic servo valve. *Precision Engineering*, Vol. 31. pp. 156-161.
- [10] Xiang, F., & W. J. (2004). Block-oriented approximate feedback linearization for control of pneumatic actuator system. *Control Engineering Practice*, pp. 387–399.

- [11] Yi-Chang Tsai, A.-C. H. (2008). Multiple-surface sliding controller design for pneumatic servo systems. *Mechatronics*, Vol. 18. pp. 506–512.
- [12] Laskawski M., Wcislik M. (2016) Sampling Rate Impact on the Tuning of PID Controller Parameters, *International Journal of Electronics and Telecommunicators*, 2016, Vol. 62, No. 1, PP. 43–48

Institute for Process Engineering



Professor Dr. Péter KISS
Director of the Institute

Dear Reader,

The Institute of Process Engineering - as a dominant education and research division at the Faculty of Mechanical Engineering - integrates three very important professional fields of engineering. These are: (1) engine- and vehicle technology, (2) energetics and energy transfer and (3) electronics and measurement system.

During our educational and scientific work, we paid special attention to the following topics:

- Basic technical knowledge in aspects of engineering approach,
- Engineering thermodynamics, electrical engineering and electronics,
- Basic and applied knowledge of energy conversion, energy utilization and energy economy,
- Special technical knowledge for development of environmental industry and utilization of alternative energy sources,
- Basic and applied knowledge of engine technology, automotive and off-road techniques and technologies,
- Land locomotion and soil mechanics,
- Disciplines of measurement technology applied in different engineering processes,

According to our tradition, the Institute for Process Engineering is eager to present some of its scientific activities concerning the year of 2016.

Last year we focused on the following scientific topics:

Influence of Energy and Mass Transport on Microwave Drying Process of Vegetables: This study shows the effects of morphological characteristics of the drying material to the efficiency of energy and mass transfer as well as other parameters of the drying process. As a result of our investigation it can be stated that during the microwave treatment the groups of vegetables with similar morphological properties behave similarly which provides sufficient information for a special classification

Development of Earth-Air Heat Exchanger Based Cooling System for Building in Subtropical Conditions: This paper aims to study the possibility of using the geothermal energy through an earth-air exchanger for cooling and heating premises for living function.

Determination of Rolling Losses of a Towed Vehicle: This article deals with rolling and additional losses of a vehicle during moving on terrain. The power loss

of an off-road vehicle consists of gear loss, slip loss and rolling loss. Off-road operations are important in many fields. Vehicle performance is affected by the tyre-terrain interaction. This article discusses how the coefficients of rolling resistances can be determined.

I hope that these papers interest you and if you need more information do not hesitate to contact us.

Professor Dr. Péter KISS
Director

Influence of energy and mass transport on microwave drying process of vegetables

Zoltán KURJÁK, Kornél BESSENYEI, János BEKE

Department of Energetics, Institute for Process Engineering

Abstract

Efficiency of the energy transfer during microwave drying strongly depends on the morphological properties of the drying product. In order to determine these properties, we had carried out experiences on a few vegetables e.g. potato, carrot, tomato, onion and parsley. The results of these measurements were published. Completion of this investigation required the examination of additional vegetables (celery, parsnip, eggplant) and energy levels. In order to compare the results of measurements some special specific energetic parameters were introduced and calculated. This study shows the effects of morphological characteristics of the drying material to the efficiency of energy and mass transfer as well as other parameters of the drying process. As a result of our investigation it can be stated that during the microwave treatment the groups of vegetables with similar morphological properties behave similarly which provides sufficient information for a special classification. Based on the measurement data the parameters of similarity can be calculated.

Keywords

microwave drying, vegetables, energy consumption, morphological effects

1. Introduction

Drying is one of the largest energy consuming processes. In agriculture, the major part of energy demand comes from drying. Moreover, drying in agriculture is a much more complex procedure than in industry, because in parallel with reducing the water content of the living material, physiological and morphological changes occur. It is important, therefore, to select the parameters of the drying process on a scientific basis in order to prevent structural damage of the product and to optimize the drying process energetically [Mujumdar and Beke 2002].

Most of the agricultural dryers operate by convective method. As a possible non-convective drying technology – especially for the drying of materials with high initial moisture content – microwave drying can be taken into consideration.

However, the agricultural products are not homogenous dielectric materials, thus their specific characteristics largely influence their behaviour in microwave

fields and make processes more difficult to recognize/identify [Ludányi and Beke 2002]. We investigated such plant groups (Solanaceae and Umbelliferae) from agricultural products, which have high initial moisture content, but their morphological structures are noticeably different.

The Solanaceae are the third most important plant taxon economically and the most valuable in terms of vegetable crops, and are the most variable of crops species in terms of agricultural utility, as it includes the tuber-bearing potato, several fruit-bearing vegetables (Tomato, Eggplant). Another important genus, Capsicum, produces both chili peppers and bell peppers. [Jagatheeswari 2014]

The Umbelliferae (or Apiaceae), commonly known as carrot or parsley family, is a group of mostly aromatic plants with hollow stems. For example: anise, carrot, celery, coriander, cumin, dill, fennel, lovage, parsley, parsnip, sea holly. Umbelliferae is a large, important, successful family of herbs, sharing easily identifiable common characteristics, their famous upside down ‘Umbrella flowers’ on stalks, which fill our hedgerows and bridle ways with an abundant profusion of summer color. [Mabberley 1987]

2. Theoretical background of microwave drying

If we put moist material in a microwave field (cavity), it causes space perturbation and changes the resonance frequency of the dissipation area as follows [Ludányi and Beke 2000]

$$\frac{\Delta\omega}{\omega_0} = -\frac{1}{W} \int_V \left(\frac{d\varepsilon}{\varepsilon} w_e + \frac{d\mu}{\mu} w_m \right) \frac{dV}{V} \quad (1)$$

Since for biological materials $m=1$ and $dm=0$ using the practical perturbation equation for ε' and ε'' the next two equations can be derived

$$\varepsilon' = \frac{Kf_0}{Kf_0 - 2\Delta f} \quad (2)$$

$$\varepsilon'' = \frac{P_d}{55,6 \cdot 10^{-14} \cdot E^2 \cdot f} \quad (3)$$

In the case of electromagnetic radiation emitted onto a metal surface the Lebedev-type jet-pressure (p_{jp}) is well known, which is based on the law of energy and momentum conservation [Ludányi and Beke 2002]

$$p_{jp} = \frac{C_B}{c_\lambda} S_P \quad (4)$$

By introducing the reflection coefficient ($G=e_r/e_i$) the density of the absorbed energy comes from the following formula

$$e_m = \frac{c_i \cos \Psi_i}{c_m \cos \Psi_m} (1 - \Gamma) \cdot e_i \quad (5)$$

The microwave energy of magnetron is forced through a funnel-shaped antenna and to prevent the bypass radiation wave traps are applied.

The electromagnetic energy is reflected to the sample surface with the help of special plates, which is adjusted to the Brewster-angle (Ψ) calculated as follows. In this case $G=0$. [Kurják et al. 2012]

$$\Psi = \arctg \sqrt{\frac{\rho_m^2 - \varepsilon_m \rho_i^2}{\rho_i^2 (\varepsilon_m - 1)}} \quad (6)$$

In the case of usual measuring systems, the instruments show detected performance (P_{det}) and the real performance can be calculated by using the so-called coupling coefficient (C_{dB}) as follows

$$P = 10^{\frac{C_{dB}}{10}} \cdot P_{det} \quad [W] \quad (7)$$

It is an essential problem that usually in biological materials there is no homogenous internal moisture and temperature distribution, because these types of materials are living tissues with complex composition and their biochemical processes still continue during a significant part of the treatment [Obermayer et al. 2009]. Based on previous scientific findings, it can be assumed that besides the usual microwave field parameters and the physical properties of the material placed in microwave zone – depending on the equipment setup – the applied microwave performance and the residence time also have a significant influence on the drying process.

3. Materials and methods

Measuring instrumentation

For the analysis of the microwave drying process special laboratory equipment was developed (Figure 1).

The magnetron works at 2.45 GHz and a microwave power can be continuously adjusted, using a toroid transformer (1) between 100 and 700 W. The dissipated performance was calculated as the difference of transformed and reflected power.

During the drying the transmitted and reflected energy of the magnetron was measured by the power sensors (8). To protect the power meters, the signals of power sensors were lead through an attenuator (7). The temperature and moisture

content of the entering and outgoing air of the drying chamber were also measured. Change of the sample's mass was measured in every minute by a scale (12) under the sample holder (11). To prevent precipitation of the moisture evaporating from the samples, the drying chamber was ventilated with a fan.

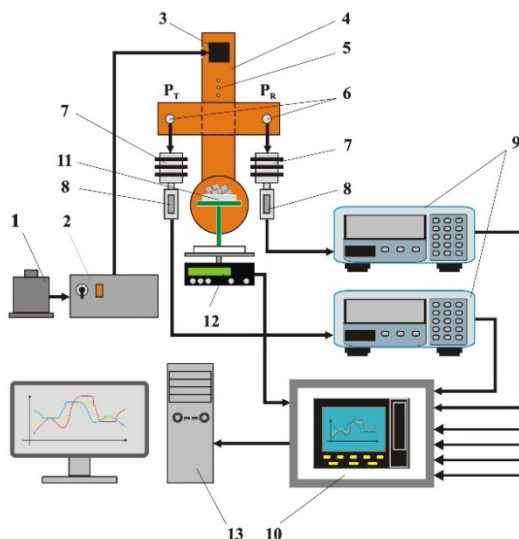


Figure 1. Microwave drying and measuring equipment
 1-toroid transformer, 2-transformer and switch unit, 3-magnetron, 4-waveguide,
 5-tuner probe, 6-measuring probes, 7-attenuators, 8-sensors for transmitted and
 reflected energy, 9-power meters, 10-data recorder, 11-sample holder,
 12-scale, 13-PC.

Sample preparation

Drying experiences were performed using materials from two morphologic groups with different characteristics. The Solenaceae group contains 4 vegetables (potato, eggplant, pepper and tomato). The Umbelliferae group contains 4 other plants (parsnip, parsley, carrot and celery). To ensure the same initial parameters, sample preparation for the produces was done in the same way. Materials were cut into 10 mm cubes and 80 grams of them were put into the drying chamber.

After the microwave drying, the samples were put into a drying oven for 24 hours to determine the entire moisture content, according to the ASAE standards.

Measurements for each produce were performed at 3 different power levels, 456.8 W, 523 W and 554.6 W. One measuring procedure was repeated five times under the same conditions; the results were averaged and drying speed curves were created. For the analysis of the relationship between the moisture content and the energy consumption of the drying process – as a characteristic parameter – the relative energy consumption was created. Similarly, by knowing the dissipated

performance the temporary absorbed microwave energy could be determined. The relative energy consumption was given as the quotient of the temporary and the minimum values of the energy consumption measured during the same experiment.

4. Results and discussion

Examination of the drying process

Data evaluation was carried out in the same way for both plant groups. The process is presented through the Solanaceae group.

From the recorded data, the kinetic curves were constructed at each power level. Due to the different values of initial moisture content, moisture ratio is represented as a function of time (Figure. 2).

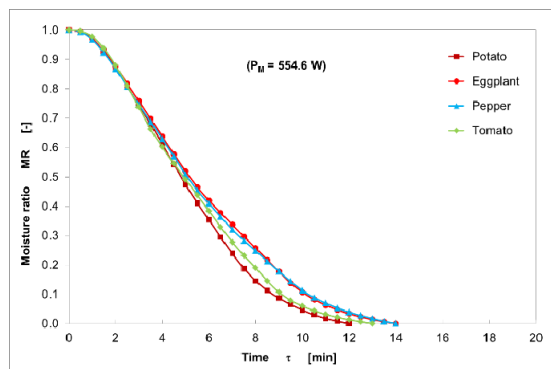


Figure 2. Kinetic curves of Solanaceae drying ($P_M = 554.6 \text{ W}$)

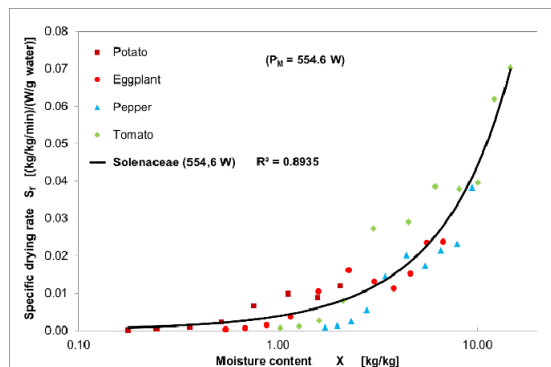


Figure 3. Drying rates of Solanaceae, caused by 1 W/g water incident energy ($P_M = 554.6 \text{ W}$)

After that drying rate and specific drying rate curves were calculated. To calculate this parameter the actual absorbed energy were used. Since in these

experimental settings no segment with a constant drying rate could be identified, the falling rate period was investigated (Figure 3.).

Based on the measurement data, the individual and the overall curves of Solenaceae group can be described with the following quadratic polynomial function:

$$S_f = aX^2 + bX + c \tag{8}$$

The “a”, “b” and “c” factors in Equation (8) were determined by regression analysis. Their final values can be seen in Table 1.

Analyzing the curves at different power levels (Figure 4.a.) it is clear that by increasing the power level the drying rate increases as well.

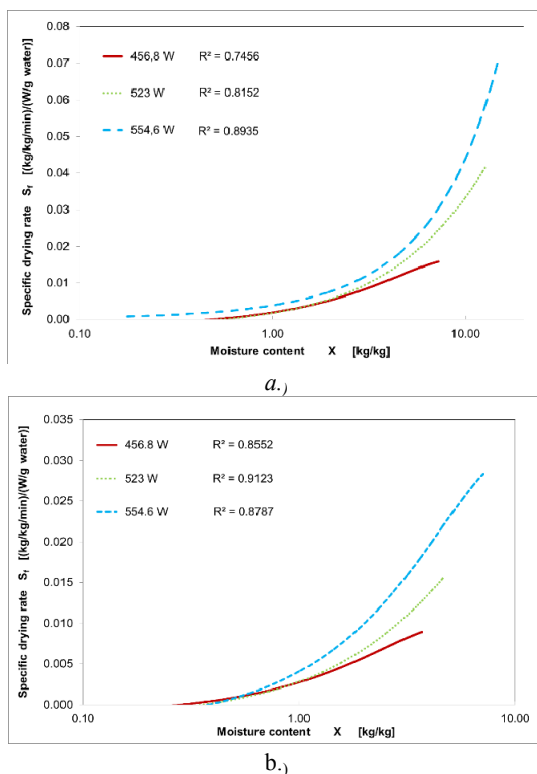


Figure 4. Drying rates caused by 1 W/g water incident energy at 3 different power levels
 a.) Solenaceae, b.) Umbelliferae

Similar phenomena can be observed in the case of Umbelliferae drying (Figure 4.b.). Curves of the Umbelliferae group can be formally described with the same equations as the Solenaceae group (8), however with different factors. (Table 1.)

Table 1. Values of constants in Equation (8)

Drying material		a	b	c	R ²
Solenaceae	456.8 W	-0.0002	0.0041	-0.002	0.7456
	523 W	-0,00004	0.004	-0.0022	0.8152
	554.6 W	0.00005	0.0036	0.0002	0.8935
Umbelliferae	456.8 W	-0.0004	0.0043	-0.0012	0.8552
	523 W	-0.0002	0.0046	-0.0016	0.9123
	554.6 W	-0.0004	0.007	-0.0026	0.8787

Energetic analysis

In the falling drying rate period the relative energy consumption was determined for all power levels for each vegetable. Relative energy consumption curves can be created as a function of moisture content (Figure 5).

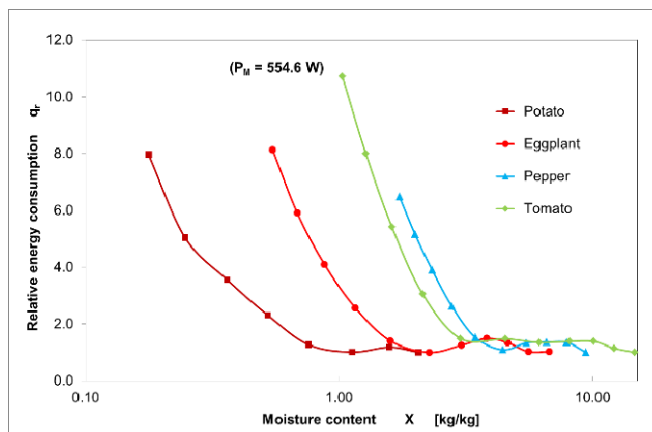


Figure 5. Relative energy consumption of Solenaceae drying as a function of moisture content (PM = 554.6 W)

For each plant the process can be divided into two typical sections. In the first part the moisture content is higher and the energy consumption is constant. After that, where the moisture content is lower, the energy consumption is increasing. However, it can be seen that the starting points of this increase in energy consumption are different for each plant. For proper comparison of these second segments, it is necessary to create a common starting point. In order to determine this point, the relative moisture content was created, similarly to the energy consumption. The resulting curves can be seen in Figure 6.

The segment with an increase in relative energy consumption can be described with the same formula for both morphological groups (9).

This equation expresses the relationship between the relative energy consumption and the moisture content.

$$q_r = a' X_r^{b'} \tag{9}$$

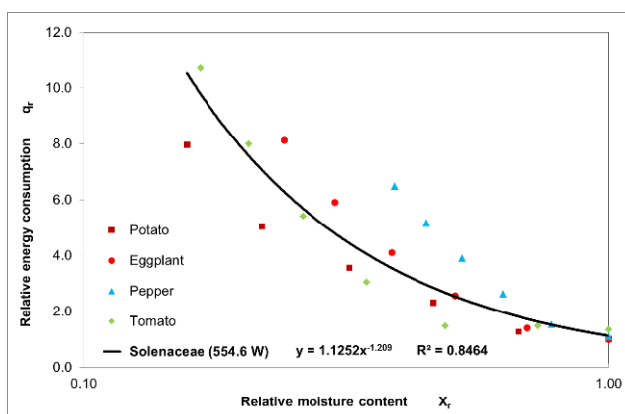


Figure 6. Relative energy consumption of Solenaceae drying as a function of relative moisture content ($P_M = 554.6 \text{ W}$)

The “ a’ and “ b’ ” factors in Equation (9) were determined by regression analysis. Their final values can be seen in Table 2.

Table 2. Values of constants in Equation (9)

Drying material		a'	b'	R ²
Solenaceae	456.8 W	1.2098	-1.266	0.8654
	523 W	1.2551	-1.193	0.8742
	554.6 W	1.1252	-1.209	0.8464
Umbelliferae	456.8 W	0.9028	-1.44	0.9829
	523 W	0.823	-1.388	0.9707
	554.6 W	0.9609	-1.208	0.9012

Looking at the curves at different power levels (Figure 7.a. and 7.b.) it can be observed that with increasing power levels the slope of relative energy consumption is decreasing.

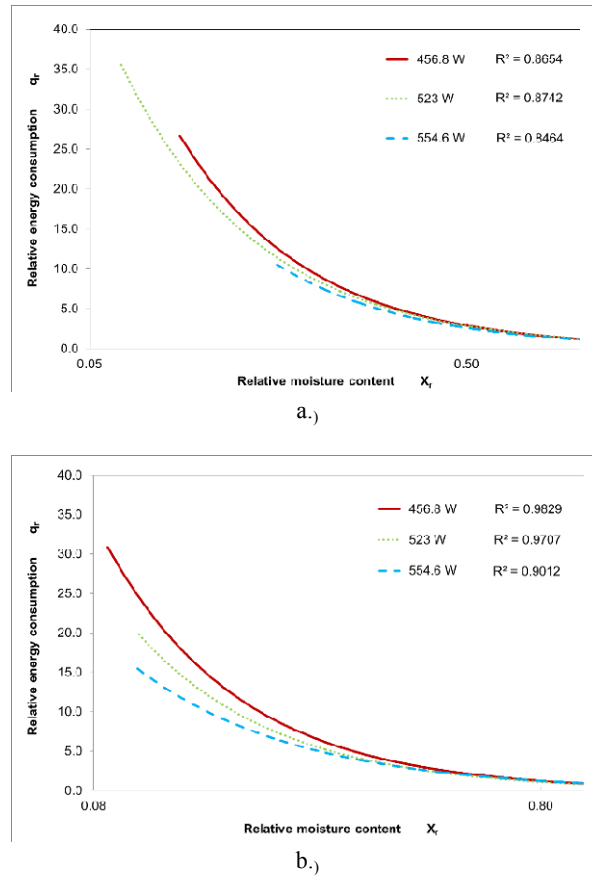


Figure 7. Energy consumption as a function of relative moisture content at 3 different power levels
 a.) Solenaceae, b.) Umbelliferae

Conclusions

During microwave drying, the phase of decreasing drying rate can be divided into two well divisible phases from the point of view of energy consumption. The first phase can be characterized by higher moisture content and constant relative energy requirement. The second phase, which can be characterized by low moisture content, can be described by a progressive function. This division caused by energy requirement can be detected at both plant groups, whose morphological structures are significantly different.

The location of the critical point that separates the two energetic phases is determined by both the applied microwave power level and the morphological structure of the plant group together. Within a certain morphological group, applying higher microwave power shifts the location of the critical point in the direction of higher moisture content.

References

- [1] Mabberley, D. J., *The Plant Book*. Cambridge University Press. 1987. 707 p.
- [2] Mujumdar, A.S., Beke, J. *Industrial Drying* (in Hungarian) Szaktudás Kiadó Ház: Budapest, 2002. 247 p.
- [3] Jagatheeswari D. Morphological studies on flowering plants (Solanaceae). *International Letters of Natural Sciences* 2014, 15, 36-43.
- [4] Kurják Z.; Barhács, A.; Beke J. Energetic analysis of drying biological materials with high moisture content by using microwave energy. *Drying Technology* 2012, 30 (3), 312-319.
- [5] Ludányi, L.; Beke, J. Study of intermittent and continuous microwave drying method. *Hungarian Agricultural Engineering* 2000, 13., 41-43.
- [6] Ludányi, L.; Beke, J. Energetical problems of dissipation heat transfer by microwaves. *Hungarian Agricultural Engineering*. 2002, 15., 50-52.
- [7] Obermayer, D.; Gutmann, B.; Kappe, O.C. Microwave chemistry in silicon carbide reaction vials: separating thermal from nonthermal effects *Angewandte Chemie (International edition in English)* 2009 48., 8321 –8324.

Development of Earth-air heat exchanger based cooling system for building in subtropical conditions

Mohammed HUSSEIN ALI¹, Márta SZABÓ², János BEKE¹

¹Department of Energetics, Institute of Process Engineering,

²Department of of Building Service and Environmental Engineering,
Institute for Environmental Systems,

Abstract

This paper aims to study the possibility of using the geothermal energy through an earth-air exchanger for cooling and heating premises for living function. This system will be designed according to the needed performance for that building after making the necessary cooling and heating loads calculations.

Keywords

Earth-Air Heat Exchanger, thermal conductivity, soil moisture transfer, heat transfer model

1. Introduction

Cooling and heating systems were considered for a long time as of the buildings for different uses and enormous budgets were assigned to their installation, maintenance and operation [1]. The global expenditure is increasing constantly during years due to increasing the world demand. In addition to the problems of the environmental pollution related to the conventional systems, such as the emission of greenhouse gases [2], the overall affinity had prompted to investigate other non-routine types of such frameworks that receive renewable energy sources.

One of those types of renewable energy is the geothermal one, which is used to air-conditioning and other energetic systems. Cooling and heating systems based on the earth-air heat exchanger (EAHE) were of these choices that discovered different applications in Canada, USA and many European countries since it was described for the first time by Lord Kelvin in 1853 and developed by Peter Ritter von Rittinger in 1855 [3]. EAHE is the most accessible ecologically clean solution, its energy is efficient and cost of operation is reasonable, however the cost of investment is rather high according to (the U.S. Environmental Protection Agency (EPA)). Heat pumps had allowed significant emission reductions possible, especially where they were used for both cooling and heating and where electricity was produced via the renewable energy resources [4].

There are a lot of developed countries using this technique in adapting to buildings, but in most developing countries (like Iraq) it is still not widespread.

This paper aims to study the possibility of using the geothermal energy through an earth-air exchanger for cooling and heating premises for living function. This system will be designed according to the needed performance for that building after making the necessary cooling and heating loads calculations. Design of the earth-air heat exchanger system will be done depending on the test results which were completed in 2010 by researcher 'Salam J. Bash Al-Maliky', [5].

In this paper, CLTD/SCL/CLF method and HAP software program are used to estimate the cooling load required for air-conditioning the building. The development of the EAHE system involves the use of basic heat transfer equations and design several cases in order to conduct a comparative analysis in addition to design the earth-air heat exchanger (EAHE). The excel spreadsheet and MATLAB software program are used to solve the equations and draw the necessary charts. The design is based on soil properties of the location and ambient conditions which are around the building.

2. Scientific background

Geothermal energy means literally the heat of the Earth. The majority of the available energy on this planet is heat energy; the six miles of the Earth's crust contain 50000 times as much energy as the fossil fuels oil, coal and gas. Milton(2001), [6].

The temperature underground for few feet around 10-15 °C and it's remains relatively constant. Geothermal systems use the Earth's constant temperature to regulate indoor air temperature across all season using an underground piping system.

Every geothermal heating and cooling systems have three major subsystems: a geothermal heat pump which is able to move heat between the building and the fluid in the earth connection; an earth connection (loops) for transferring heat between its fluid and the earth, and finally a distribution subsystem for delivering heating or cooling. Iowa energy center (2002), [7]. Most geothermal systems are closed-loop systems composed of large areas of underground piping, a heat exchanger and ductwork in the building. The closed loop system is environmentally friendly because water or any other fluid in the loop prevents contamination to the external environment. The least geothermal systems are open-loop systems also composed of large areas of underground piping, but one end of the pipe is inlet of fresh fluid and another one connected with building directly or connected with a heat exchanger and ductwork in the building. The length of loop piping varies depending on ground temperature, soil thermal conductivity, soil moisture, pipe diameter and system design, and the condition whether geothermal heat pump is used or it is not used [8].

The soil thermal properties as heat capacity, thermal diffusivity and thermal conductivity are important in many applications. Soil thermal properties are

largely depending on the volume fraction each of water, solids, and air in the soil, Tyson et al (2001), [9].

Thermal conductivity of soil media is highly affected by mineralogical composition, texture and organic matter content that are inherent in the porous media, and by more variable factors including porosity, water content, and temperature, as well as by water vapor content and gas pressure, [10]. Conduction is the dominant mode of heat transfer under most circumstances. The thermal conductivity is effected largely by the moisture content. For most building locations, the soil moisture content does not vary much except for the top few centimeters of soil, which can change daily or seasonally with atmospheric conditions. Usually, the error associated with using a fixed value of thermal conductivity is small for calculations over a long period if an appropriate value is chosen. For building locations where the moisture content has large variations with the depth or with season, the thermal conductivity can be varied to account for the changing conditions, De Vries (1975), [11].

Soil temperature is an important agrometeorological parameter. Availability of water content causes variation in soil temperatures, Renuka and Tessy (2002), [12].

Many research were related to the effect of evaporation and the heat and moisture content on the ground surface energy balance simulation results. It was observed that the heat losses changed a lot when evaporation or radiation was included in the simulations. The application of the uncoupled or the coupled equations for soil heat moisture transfer leads to notably different basement wall heat losses. Bahnfleth (1989) [13], Shen (1986) [14]

Rees et al. (2001) [15] clearly demonstrated and also Deru (2001) [16] concluded that the effect of that soil moisture transfer has a notable influence on building heat loss via the ground. Mitalas (1987) [20] noted that the heat loss can be significantly affected by ground water, changes in soil thermal conductivity due to moisture and temperature, and variations in ground surface conditions.

Janssen et. Al. (2004) [17] studied the influence of soil moisture transfer on building heat loss via the ground by comparing fully coupled simulations with linear thermal simulations. The observed influences of the coupling were: (1) the larger amplitude of surface temperature, (2) the variation of thermal conductivity with moisture content, and (3) the advection of sensible heat by liquid transfer. In a parameter study, it was shown that these conclusions hold for a variety of climate, soils and foundation constructions. The transfer equations and boundary conditions are solved with a two-dimensional finite element spatial and a fully implicit time stepping scheme.

A detailed ground-coupled heat transfer model, a three-dimensional, finite element-heat transfer computer program developed by Deru et.al. (2003) [18], provides another method of testing and refining the simple models and analyzing complex problems. It was used in conjunction with the "SUNREL" whole-building energy simulation program to analyze ground-coupled heat transfer from buildings.

Saati (2006) [19] used the finite difference scheme to study the effect of horizontal and vertical edge insulations on the heat transfer rate to the cold store through the contact slab with the ground. The results showed almost a negligible change due to increasing the length of the horizontal edge insulation. In addition, increasing the length of the vertical insulation decreases the rate of heat transfer to the cold store. The heat flux to the cold store with the insulation vertical is lower compared with the horizontal edge.

Chuangchid and Krarti (1998) [21] found that three-dimensional foundation heat transfer from either buildings or refrigerated structures (with low indoor air temperatures) is independent of the foundation shape.

The most widely accepted physical model for soil thermal conductivities was derived by De Vries (1966) [22]. For moist soils, he assumed the liquid phase as a continuous medium in which solid grains and small air pockets are uniformly distributed. The thermal conductivity of soil is calculated as the weighted average of the conductivities of various soil components.

Campbell et al. (1994) [23] introduced a simpler version of the most widely method of De Vries. They assumed that the solid phase is uniform, having a single value of thermal conductivity. Also, they introduced an apparent fluid as the continuum of the soil particles. The thermal conductivity of this fluid equals to that value of thermal conductivity of an air at dry conditions, and raises its value to that of thermal conductivity of water at saturation.

Based on terms of heat resistance, Usowicz (1992) [24] made the statistical-physical model. This model allows to estimate the thermal conductivity for any type of soil by comparing the resultant resistance of the system, with consideration of all possible configurations of molecule associations together with a mean thermal resistance of a given join soil volume.

3. Mathematical model

This chapter presents the development of a two-dimensional transient heat transfer model to predict the temperature distribution and the amount of heat rate that may be dissipated to earth. The model is based on the energy conservation law and is solved by fully implicit finite difference method.

Heat is a form of energy transmitting from one region to another due to a temperature gradient. In theory the thermal transmission methods can be established as conduction, convection, and radiation.

Thermal conduction is the procedure of heat transfer from one a part in a body at a higher temperature to another part because of arbitrary molecular movement dispersion. Heat can be conducted through solids, liquids and gases. The heat transfer rate of conduction can be expressed as:

$$Q = -k A \frac{\partial T}{\partial x} \quad (1)$$

Equation (1) is known as Fourier's law of heat conduction, which can be rewritten as:

$$Q = \frac{\Delta T}{R} = \frac{T_1 - T_2}{R} \quad (2)$$

Where R is the thermal resistance = $\frac{L}{KA}$ (°C/W)

Heat exchange by convection happens at the surfaces. In view of the temperature distinction between the fluid and the contact surface, there is a density variety in the fluid. This heat exchange between the fluid and the surface is known as free convection. However, if the motion of the fluid is due to external force, it is known as forced convection.

Newton's law of cooling expresses the overall effect convection as follows:-

$$Q = h A (T_w - T_\infty) \quad (3)$$

Radiation is the heat transfer from a body by property of its temperature. At a different temperature for two bodies and the exchange heat by radiation, heat will be emitted, absorbed and reflected by each body. The radiation exchange between two surfaces (of equal area a) at uniform temperatures can be written as follows, [25]:

$$Q = A \varepsilon_{eff} \sigma (T_1^4 - T_2^4) \quad (4)$$

With: $\varepsilon_{eff} = [1/\varepsilon_1 + 1/\varepsilon_2 - 1]^{-1}$

In case of buildings, external surfaces such as walls and roofs are always exposed to the atmosphere. So, the radiation exchange between the exposed parts of the building and the atmosphere is an important factor and is given by:

$$Q_{\text{radiation}} = A \varepsilon \sigma \cdot (T_s^4 - T_{sky}^4) \quad (5)$$

An ideal thermal radiator or a black body absorbs the entire radiation incident upon it. Thus, it will emit thermal radiation as:

$$Q_{\text{emitted}} = A \sigma T^4 \quad (6)$$

Where :

σ – Proportionality constant (Stefan – Boltzmann) = 5.669×10^{-8} (W/m².K⁴)

Equation (5) is called the Stefan-Boltzmann law of thermal radiation and it applies only to the black bodies. For building applications, usually convective and radiative heat transfer coefficients are combined to define surface heat transfer coefficient.

The radiation exchange between two surfaces depends on some factors as geometry, size of two surfaces and emissivity of the surface. The emissivity itself depends on the surface material.

Soil Heat Transfer Model

The three modes of heat transfer are considered through soil components. However, conduction is the dominant mode of heat transfer under most conditions. The thermal conductivity of soil is usually given as an effective value accounting for conduction, [26].

As it was explained above, thermal conductivity of the soil is strongly affected by temperature distribution and heat flux. A lot of experimental work is done and several simulation models are suggested to determine the value of thermal conductivity. In this work, the most widely accepted physical model for soil thermal conductivity derived by De Vries [22] is used. The overall thermal conductivity of soil is calculated as the weighted average of the conductivities of the various soil components according to the formula:

$$K = \frac{\sum_{i=1}^n k_i x_i \lambda_i}{\sum_{i=1}^n x_i \lambda_i} \quad (7)$$

Where x_i is the volume fraction of each constituent, and (n) is the number of soil constituent.

The weighting factor (λ_i) depends on the shape and the orientation of the granules of the soil constituents, and on the ratio of the conductivities of the constituents. It can be calculated as:

$$\lambda_i = \frac{1}{3} \sum_{j=1}^3 \left[1 + \left(\frac{k_i}{k_o} - 1 \right) g_j \right]^{-1} \quad (8)$$

The subscript zero refers to the continuous fluid surrounding the solid particles (air for dry soil and water for moist soil), $\lambda_o=1$.

Where g_j represents the shape factors for the i-th constituents granules considered as ellipsoids,

$$g_1 + g_2 + g_3 = 1(\text{for each component}), [22] \quad (8a)$$

Assuming (g_1) and (g_2) are equal; only one shape factor must be estimated for each constituent.

The thermal conductivity of water is 0.596 W/m.K at 20°C. The thermal conductivity of the air is 0.025W/m.K at same condition.

The shape factor, (g_1) for the soil solids was taken to be 0.144, [26], For water contents, the value of g_1 is given by:

$$g_1 = 0,333 - \frac{x_a}{1 - x_s} (0,333 - 0,035), [9] \quad (8b)$$

Volumetric heat capacity C_v (KJ/m³·K) was calculated using empirical formula proposed by Vries De [22]:

$$C_v = (2.0 x_m + 2.51 x_o + 4.19 x_w) 10^3 \quad (9)$$

Where; x_m , x_o , x_w (m³/m³) are volumetric contributions of mineral, organic components and water, respectively.

For the purposes of this study, a soil sample is modeled as a mixture of two constituents according to special study for a certain location in Iraq, Baghdad, Alkry'at city. The two constituents are Clay and silt with the characteristics summarized in Table 2. However all this values have a standard deviation, in this calculation the average value has been considered, [5].

Soil temperature fluctuates annually and daily affected mainly by variation in air temperature and soil radiation. The annual variation of daily average soil temperature at different depths can be estimated using the following sinusoidal function [37]:-

$$T(z, t) = T_a + A_o e^{-z/d} \sin \left[\frac{2\pi(t - t_0)}{365} - \frac{z}{d} - \frac{\pi}{2} \right] \quad (10)$$

At the soil surface, $z=0$:

$$T(0, t) = T_a + A_o \sin \left[\frac{2\pi(t - t_0)}{365} \right] \quad (11)$$

Where:

- $T(z,t)$ is the soil temperature at time t (s) and depth z (m)
- T_a is the average surface temperature of the soil (°C).
- Z =depth (m).
- $d = (2 D_h/\omega)^{1/2}$
- $\omega = 2\pi$ times the actual frequency. For diurnal period (24 h or 86400 s).
- $\omega = 7.27 \times 10^{-5}$ rad/s.
- The amplitude of the surface A_o is the soil temperature (the range from maximum or minimum to average temperature).
- The damping depth (d) in (m), is the depth at which temperature amplitude decreases to the value of $1/e=0.37$ for the amplitude at the soil surface A_o .
- t_0 is the time lag from an arbitrary starting date to the occurrence of the minimum temperature.

At any depth (z), the amplitude of temperature fluctuation A_z is smaller than A_0 by a factor $e^{z/d}$ and that there is a time delay of temperature peak equal to z/d . The decrease of amplitude and increase of phase lag with depth lies in the fact that a certain amount of heat is absorbed or rejected when the temperature of the conducting soil increases or decreases.

Methodology of Solution

A mathematical model is developed and applied in order to analyze the thermal behavior of buildings and soil. A lumped approach to model the room air temperature and heat flux is used, while a multi-layer model in two dimensional finite differences for both, the building envelope and the soil, is employed.

The investigation model allows studying the transient air temperature of a room when it is submitted to the weather of the city of Baghdad in Iraq. The room is submitted to loads of solar radiation and convection. However, the other sources of heat like infiltration, internal gains from light, equipment and people, are all not neglected.

Initially the temperature in the control volume was assumed to be at room temperature which is 25 °C.

At $t=0$,

$$T(x,y,t) = 25 = T_{in} \tag{12}$$

On the external side of the room, the wall is exposed to the solar radiation and to convective heat transfer. So, the external boundary condition can be expressed mathematically as follows:-

$$q_{conduction} = q_{convection} + q_{radiation}$$

$$-\left(k \frac{\partial T}{\partial x}\right) = h_o (T_w - T_\infty) + \alpha q_r \tag{13}$$

On the internal side, the room wall is exposed to the inside environment.

$$q_{conduction} = q_{convection}$$

$$-\left(k \frac{\partial T}{\partial x}\right) = h_i (T_w - T_\infty) \tag{14}$$

Heat Gain through the Opaque Surface

It is possible to calculate the various heat exchanges taking place in the building. The rate of heat conduction (Q_{cond}) through any element, such as roof, wall or soil under any condition can be written as:

$$Q_{\text{cond}} = A U \Delta T \quad (15)$$

U is given by:

$$U = \frac{1}{\sum R_t} \quad (16)$$

$$R_t = \frac{1}{h_i} + \left(\sum_{j=1}^m \frac{L_j}{k_j} \right) + \frac{1}{h_o} \quad (17)$$

h_i and h_o are the inside and outside heat transfer coefficients respectively. In this study, it was assumed that $h_i=9$ (W/m².C) and $h_o=22$ (W/m².C) [27]. (L_j) is the thickness of the jth layer and (k_j) is the thermal conductivity of its material. If the surface is exposed to solar radiation then $\Delta T = T_e - T_i$.

Where T_i is the indoor temperature; T_e is the sol-air temperature, calculated using the following expression [27]:-

$$T_e = T_o + \frac{\alpha I_t}{h_o} - \frac{\varepsilon \Delta R}{h_o} \quad (18)$$

Where (α) is absorptance of the surface for solar radiation. For this study, it was chosen to be $\alpha=0.6$ [28].

ΔR is the difference between the long wavelength radiation on the surface from the sky and the surroundings, and the radiation emitted by a black body at ambient temperature.

For vertical surface, $\Delta R=0$: equation (18) becomes:

$$T_e = T_o + \frac{\alpha I_t}{h_o} \quad (19)$$

The materials used for insulation and those used for construction purposes exhibit similar characteristics. Many walls contain air cells in their constructions.

The purpose of this air gap is to increase the ability of the wall, roof, and atc. for insulating, and, also to reduce the noise coming from outside. For such walls, it is difficult to estimate both, film and air resistances to heat flow.

Finally, the thermal resistance for any composite wall including air gap can be found from the following equation:-

$$R_t = \frac{1}{h_i} + \left(\sum_{j=1}^m \frac{L_j}{k_j} \right) + \frac{1}{c} + \frac{1}{h_o} \quad (20)$$

5. Earth-air heat exchanger (eahe) design

A common situation which facing a lot of engineers is a heat transfer to or from the fluid flowing through the tube. This can occur in the heat exchangers and evaporators, heaters, condensers and a host of equipment to complete this process.

In this part of this chapter, the value of the heat exchange of the air flow inside the tube will be calculated. The tube is made of the polyvinyl chloride (PVC) substance. This pipe is buried at a certain depth to be determined based on information and sources documented.

The desired length of the tube and the area of land required to bury the pipe, can be determined via using the scheme based on the needed performance.

Assumptions

In order to simplify the development of the one dimensional model of the EAHE system the following initial assumptions have been made:

- The temperature of the ground at the depth equal to zero is specified as equal to the ambient air temperature, which equals the temperature of inlet air in the pipe.
- Underground temperature can be taken from the measurements which is done by the author (Salam J. Bash 2010) for the location (Iraq, Baghdad, AlKry`at City) and at a certain depth.
- PVC pipe used in the EAHE is of uniform cross-section along length of pipe and it's equal to D_{pipe} .
- Thermal resistance of pipe material is negligible (the thickness of the pipe used in the EAHE is very small).
- The temperature on the surface of the pipe is uniformly in the axial direction.
- The soil has a medium heat conductivity, this sufficient for the conditions.
- The soil temperature is constant. It's not changed with the time.

Boundary conditions: At the outlet of the EAHE pipe, the relative pressure was equal to zero atm. (Subsonic flow regime). At the inlet of the EAHE pipe, the static temperature of the inlet air, T_{in} (°C), and velocity of air flow value have to be defined. The specific heat capacity, density, thermal conductivity, and dynamic viscosity of air has to be defined at a static temperature of the inlet air (Thermodynamic and transport properties) [29] [30].

The temperature of the pipe surface (wall) was defined as equal to earth's temperature at a specific depth and was uniformly in axial direction. The depth of pipe is specific and depending on the design aim according to earth's temperature distribution.

Mass flow rate of air:

$$\dot{m} = \frac{\frac{\pi}{4} D^2 \rho v_a}{N_p} \quad (21)$$

N_p : number of parallel pipes (-).

ρ : air density (m^3/kg).

v_a : air flow velocity (m/s).

\dot{m} : mass flow rate of air through a pipe (kg/s).

D_{pipe} : The internal of the pipe (m^2).

Heat exchanger design and effectiveness:

The total heat transferred to the air when flowing through a buried pipe is given by:

$$Q_h = \dot{m} C_p (T_{out} - T_{in}) \quad (22)$$

Due to convection between the wall and the air, the transferred heat can also be given by:

$$Q_h = h A_{\text{surf.}} \Delta T_{\text{lm}} \quad (23)$$

Q_h : The total heat transferred to the air when flowing through a buried pipe (W).

C_p : is the specific heat of air ($\text{J}/\text{kg}^\circ\text{K}$).

T_{out} : is the temperature of air at outlet of EAHE pipe ($^\circ\text{C}$).

T_{in} : is the temperature of air at inlet of EAHE pipe ($^\circ\text{C}$).

h : is the convective heat transfer coefficient ($\text{W}/\text{m}^2\text{-K}$).

$A_{\text{surf.}}$: is the internal surface area of the pipe (m^2).

ΔT_{lm} : The logarithmic average temperature difference (-), $T_{\text{wall}}=T_{\text{soil}}$ at a certain depth.

$$\Delta T_{\text{lm}} = \frac{T_{in} - T_{out}}{\ln \frac{T_{in} - T_{wall}}{T_{out} - T_{wall}}} \quad (24)$$

The internal surface area of the pipe is a function to both of diameter (D_{pipe}), and length (L_{pipe}) of EAHE.

$$A_{\text{surf.}} = \pi D_{\text{pipe}} L_{\text{pipe}} \quad (25)$$

The convective heat transfer coefficient (CHTC) during the pipe is characterized by:

$$h = \frac{Nu k}{D} \quad (26)$$

Nu : is Nusselt number.

k : is the thermal conductivity ($\text{W}/\text{m-K}$).

The EAHE system analyzed in this study consists of cylindrical pipes of D_{pipe} inner diameter made up of PVC with a total burial length of L_{pipe} . Assuming that the internal surface of PVC pipes used in the EAHE system is smooth, the Nu correlations given by De and Janssens (2003) can be used to simulate the performance of the system.

$$Nu = \frac{\left(\frac{f}{s}\right)(Re-1000)Pr}{1 + 12,7\sqrt{\frac{f}{s}}\left(Pr^{\frac{2}{3}} - 1\right)} \quad (27)$$

Re: is the Reynolds number.

Pr: is Prandtl number.

f: is the friction factor for smooth pipes.

$$f = (1.82 \log Re - 1.64)^{-2} \quad (28)$$

If $2300 \leq Re < 5 \times 10^6$ and $0.5 < Pr < 10^6$ the Reynolds number is related to the average air velocity and diameter:

$$Re = \frac{\rho v_a D}{\mu} \quad (29)$$

μ : the dynamic viscosity of air (kg/m-s).

The Prandtl number is given by:

$$Pr = \frac{\mu C_p}{k} \quad (30)$$

The pressure drop in a smooth pipe is given by:

$$\Delta p = f \frac{L}{D} \rho \frac{v_a^2}{2} \quad (31)$$

and the EAHE efficiency, η , as:

$$\eta = 1 - e^{-\left(\frac{hA}{mC_p}\right)} = \frac{T_{out} - T_{in}}{T_{wall} - T_{in}} \quad (32)$$

To calculate the pressure drop in the pipe as a result of bends in the pipe:

$$\Delta p_{loss} = C_{loss} \rho \frac{v_a^2}{2} \quad (33)$$

Where C_{loss} is the bend loss coefficient can be gotten from fitting the measured data introduced in the ASHRAE Handbook (ASHRAE 2009) to a quadratic condition. The results are:

$$C_{loss} = 0.09057 - 0.001.139D_{pipe} + 0.001294D_{pipe}^2 \quad (34)$$

Then, the total drop pressure in EAHE system (Δp_T) given by:

$$\Delta p_T = \Delta p + \Delta p_{loss} \quad (35)$$

The air fan power (AFP) required to move the volume of air (m^3/s) over the total pressure drop Δp_T is then computed as:

$$AFP = V_{air} \Delta p_T \quad (36)$$

Table 1. Thermo-physical properties of air at temperature equal to the static temperature of the inlet air, T_{in} ($^{\circ}C$)= 46 $^{\circ}C$, [30].

Density (ρ)(kg/m ³)	Specific heat capacity (C_p) (J/kg-K)	Thermal (k) (W/m.K)	Dynamic viscosity (μ) (kg/m.s)	Kinematic Viscosity(ν) (m ² /s)
1.127	1005	0.0271	1.917224E-05	16.97E-06

Table 2. Soil properties of tested locations at AlKry`at cities, Baghdad, Iraq [27].

Composition	Alkry`at city	
	Average	Standard deviation
Major composition	Clay and silt	
Density (kg/m ³)	1350	7.8
Water content %	56	4.863
Heat conductivity (W/m.K)	2.15	0.225
Soil temperature at (4m) depth ($T_{wall}=T_{soil}$, $^{\circ}C$)	17.518	

Using the above described method 22 different cases were investigated comparing to the local possible conditions. After the obtained data analysis as optimum solution the following system was designed (Figure 1).

Conclusions

The design of the EAHE system is based on required specifications for air-conditioning of the building according to the analysis of design results. The final conclusions can be drawn for this design as following:

1. The EAHE system meets the needs air-conditioning the building; cooling with desired performance, which is equal to 17.809 kW and it's suitable for pre-heating the building.
2. By discussing the twenty-two cases, it was observed the following:
 - The value of the air flow velocity inside the pipes, Reynolds number, Nusselt number, the convective heat transfer coefficient (CHTC), drop pressure, and the air fan power are reverse proportional to the diameter of the EAHE system pipes. That is mean, the increase in diameter leads to decrease the air flow velocity inside the pipes, and thus, increase the Reynolds number, Nusselt number, the convective heat transfer coefficient (CHTC), drop pressure, the air fan power and vice versa.
 - The friction factor and length of pipe are directly proportional to the diameter of the EAHE system pipes. In this case, the investment cost will be higher, but the operation and maintenance costs will be lower as a result of decreasing the drop pressure and thus decreasing the air fan power.
 - The value of the Prandtl number was constant, because it depends on the thermal properties of the air which it's remained constant through the system.
3. More appropriate case design should combine the suitable cost of system investment and least operation and maintenance costs. According to an analysis of the design results for cooling the building, the more appropriate is where the efficiency is the best, the materials which should be used is reasonable, and operation power is more suitable.

The system specifications are mentioned in the Table 3. below and shown in the detailed scheme of the whole system Figure 2.

Table 3. The specifications of the designed cooling system

Capacity (kW)	17.809	Diameter (m)	0.2
Length of pipe (m)	98.915	Drop Pressure (Pa)	461.430
Number of pipes	2	Air fan Power (W/fan)	139.5252

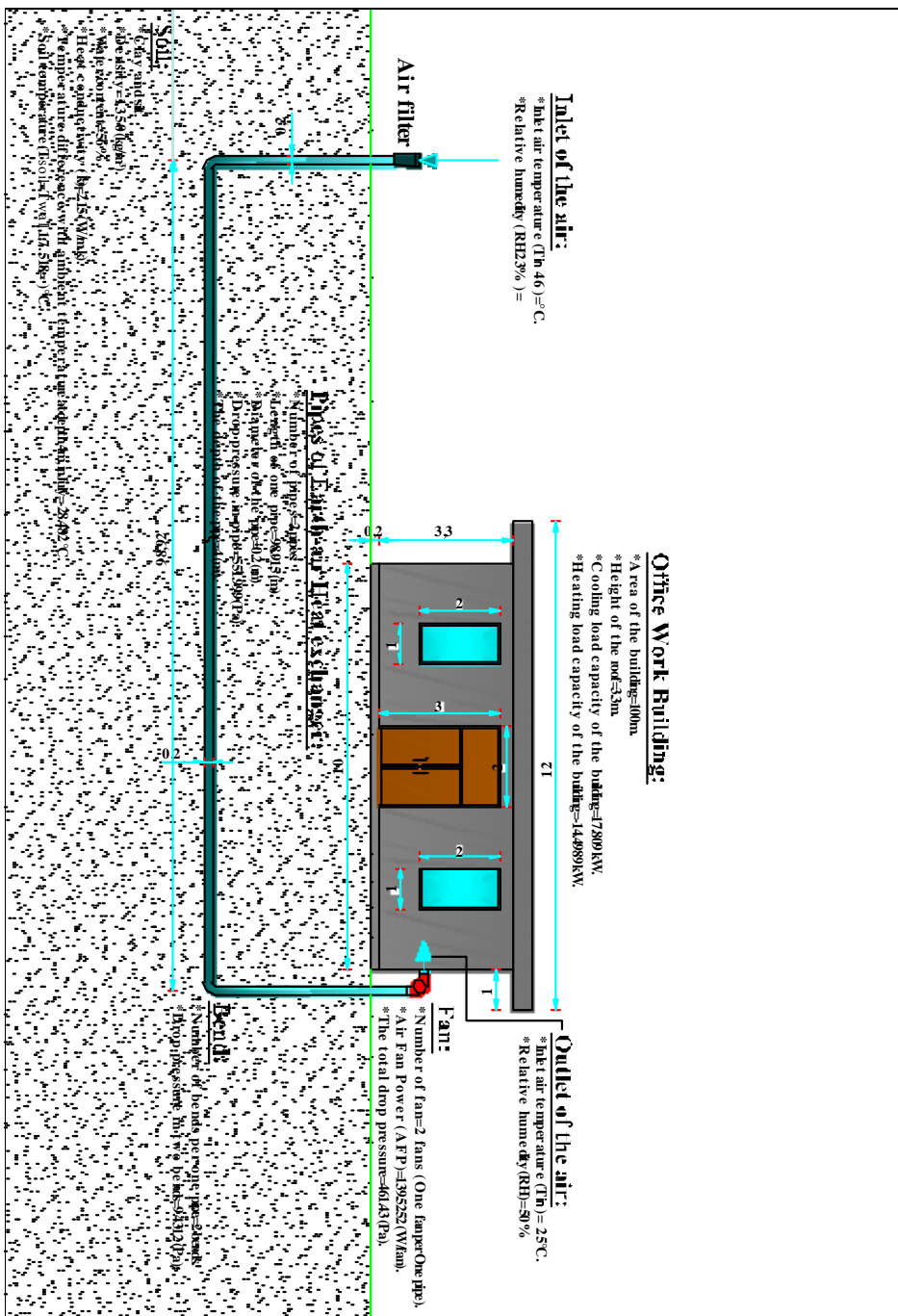


Figure 1. Scheme of the designed earth-air heat exchanger based cooling system

References

- [1] Economist (2010). [Online] Available at www.economist.com (September, 2010).
- [2] Energy Information Administration, US Department of Energy, 2007, "Voluntary Reporting of Greenhouse Gases, Electricity Emission Factors". [Online] Available at: www.eia.doe.gov .
- [3] International Ground Source Heat Pump Association, 2009. [Online] Available at: www.igshpa.okstate.edu (March, 2009).
- [4] Greenhouse Gas Technology Center, (2005). Test and Quality Assurance Plan. Southern Research Institute, NC, USA.
- [6] Milton, K. "Geothermal", the national energy centre, UK, (2001).
- [5] Salam J. Bash Al-Maliky: " Investigation of the Readiness of Ground Soils for the Installation of Ground Heat Exchange Systems in Baghdad City", Geography and Geology, (2011).
- [7] "Iowa Energy Center", <http://www.energy.iastate.edu> , (2002).
- [8] "Geothermal Heat Pump Consortium": www.geoexchange.org and "U.S. Department of Energy ":Energy Efficiency and Renewable Energy, <http://www.energy.gov/geothermal/> .
- [9] Tyson, E., Horton, O. R. And Tusheng, R.: "A new Perspective On Soil Thermal Properties", Soil Sci. Soc. Am J. Vol.65, pp. (1641-1647), (2001).
- [10] Usowicza, B. J., Lipieca, W. and Marczewskib, A.: "Thermal conductivity modeling of terrestrial soil media-A comparative study" Planetary and Space Science, Vol. 54, pp.(1086-1095), (2006).
- [11] De Vries, D. A.: "Heat Transfer in Soils", John Wiley And Sons, New York, (5-28), (1975).
- [12] Tessa, C. And Renuka, G.: "Temperature Mapping, Thermal Diffusivity and Subsoil Heat Flux at Kariavattom Of Kerala", Department of Physics, University of Kerala, Kariavattom, Thiruvananthapuram, pp. (581-695), India, (2002).
- [13] Bahnfleth, W. P.: "Three-Dimensional Modeling Of Heat Transfer From Slab Floors", National Technical Information Service, Springfield, Va, ADA210826, (1989).
- [14] Shen, L. "An Investigation Of Transient, Two-Dimensional Coupled Heat And Moisture Flow In Soils'", Doctoral dissertation, University Of Minnesota, United States, (1986).
- [15] Rees, S., Zhou, Z. And Thomas, H.R.: "The Influence Of Soil Moisture Content Variations On Heat Losses From Earth-Contact Structures: An Initial Assessment", Building And Environment J. Vol.36, pp. (157-165), (2001).
- [16] Deru, M.: "A Model For Ground-Coupled Heat And Moisture Transfer From Buildings", Doctoral Dissertation, Colorado State University, United States, (2001).
- [17] Mitalas, G. P.: "Calculation Of Below-Grade Residential Heat Loss: Low-Rise Residential Building", ASHRAE Transactions, Vol. 93, pp.(743-784), (1987).

- [18] Janssen, H. J., Carmeliet, D. And Hens, H.: "The Influence Of Soil Moisture Transfer On Building Heat Loss Via The Ground", *Building And Environment, J. Vol 39*, Pp. (825-836), (2004).
- [19] Deru, M., Judkoff, R. and Neymark, J.: "Whole-Building Energy Simulation With A Three-Dimensional Ground-Coupled Heat Transfer Model", Chicago, (2003).
- [20] Saati, A. A.: "A Numerical Investigation Of Ground Heat Transfer Effects On Buildings Including Edge Or Composite Slab Insulation" *Umm Al-Qura Univ. J. Sci.Med.Eng.*, Vol. 18, No.1, pp. (73-88), (2006).
- [21] Chuangchid , P. And Krarti, M.: "Comparative Analysis Of Three-Dimensional Foundation Heat Transfer From Slab-On-Grade Floor Slabs". *Proceedings Of Asme Solar Energy Engineering*, pp. (37-44), (1998).
- [22] De Vries, D.A.: "Thermal Properties Of Soils", *Physics Of The Plant Environment*, North-Holland, Amsterdam, (1966).
- [23] Campbell, G. J., Jungbauer, W. and Hungerford, R.: "Predicting The Effect Of Temperature On Soil Thermal Conductivity", *Soil Science J.*, Vol. 158, pp. (307-313), (1994).
- [24] Usowicz, B.: "Statistical- Physical Model Of Thermal Conductivity In Soil", *Pol. J. Soil Sci.*, Vol.1, pp.(25-34), (1992).
- [25] Duffie, J. A.: "Solar Engineering Of Thermal Propcesses", Joun Wiley, (1980).
- [26] Deru, M., Judkoff, R. and Neymark, J.: "Whole-Building Energy Simulation With A Three-Dimensional Ground-Coupled Heat Transfer Model", Chicago, (2003).
- [27] ASHRAE, Handbook: "The American Society Of Heating, Refrigerating And Air-Conditioning Engineers", *Fundamentals*, Ch.29, (1997).
- [28] Bureau of Indian of Standards: "Handbook On Functional Requirements Of Buildings", New Delhi, (1987).
- [29] Ralph T Muehleisen: " Simple Design Tools for Earth-Air Heat Exchangers", *Conference Paper*, DOI: 10.13140/2.1.2854.5607, January (2012). <https://www.researchgate.net/publication/269096337>.
- [30] Trilok Singh Bisoniya: "Design of earth–air heat exchanger system", DOI 10.1186/s40517-015-0036-2, (2015).

Determination of rolling losses of a towed vehicle

László MÁTHÉ, György PILLINGER, Péter KISS

Department of Automotive Technology,
Institute of Process Engineering

Abstract

The power loss of an off-road vehicle consists of gear loss, slip loss and rolling loss. Off-road operations are important in many fields. Vehicle performance is affected by the tyre-terrain interaction. This article discusses how the coefficients of rolling resistances may be determined.

Keywords

Rolling resistance, bulldozing resistance

1. Introduction

1.1. Objectives

In a road run-off accident, the vehicle comes to a halt as its kinetic energy is absorbed on the terrain by rolling resistance, vibrational accelerations and large terrain obstacles. As part of a comprehensive research project, field experiments were conducted to study the effects of rolling resistance, bulldozing resistance (if it occurs), wheel sinkage, tyre contact area, tyre pressure and soil load bearing capacity on vehicle motion. These parameters of the terrain and the vehicle are important for the understanding of run-off accidents.

1.2. Literature Overview

Accidents on terrain pose many problems for forensic scientists (Ridella et al. 2012). In his book on the subject, Hugemann (2007) stated that analysis of terrain accidents with computer simulation at present only provides approximate results. There is a need for the study of soil mechanical parameters to improve the analysis of terrain accidents (Liu and Subramania 2009). Accident analyses must include studies of the soil-tyre interaction and the effects of soil mechanical parameters on vehicle motion. Results obtained by many researchers concerned with vehicles moving on terrain could be useful for analysing terrain accidents.

The mobility of off-road vehicles is determined by the soil surface, the tyre contact area and the pressure distribution in the soil (Bekker 1960; Plackett 1985; Bukkhari et al. 1988; Crolla et al. 1992; Rahman et al. 2004). Ayun (1983) reported tests on the normal loading of vehicles with particular regard to mobility on wet soil. Sánchez-Girón et al. (1998) found that the load-bearing capacity of high clay-content soil is better for normal loads.

Wesson et al. (2007), Cronjé and Els (2010), Fan et al. (2011), Nguyen and Inaba (2011), Liu and Kushwaha (2012) and Ringdahl et al. (2012) studied soil displacement under the wheel, wheel slip, the resulting vibrations and the mobility of the vehicle as a function of tyre inflation pressure, speed of travel and axle loads. Mohsenimanesh and Ward (2010) studied the soil-tyre interaction to determine rut depth and the 3D form of the tyre contact area at different inflation pressures. The results yielded conclusions on the volume of compacted loose loam soil. Shoop (2001) used a finite-element method to analyse the soil-tyre interaction.

Wheel bulldozing also occurs during travel across terrain. It may be caused by soil of loose structure and the use of inappropriate tyres. Because we know little about the phenomenon, the circumstances of an accident in which a vehicle runs off the road and experiences bulldozing on the terrain are difficult to reconstruct so as to determine the run-off speed. Forensic scientists incorporate the phenomenon of bulldozing (Hugemann 2007) firstly via the deformation energy, which can only approximate reality and secondly they consider the change of speed. To obtain the kinematic changes caused by bulldozing, they compare these results with various deceleration values obtained from experience. Knowledge of this phenomenon is important for more than just accident analysis. Bulldozing also occurs during the work of earthmoving machinery. Tsuji et al. (2012) examined it in the case of a bulldozer shovel.

2. Material and Method

The research involved field measurements to determine the rolling resistance on soils of various load bearing capacity (cone index). The bulldozing factor was determined wherever bulldozing was observed. The towing tests made use of a special towing mechanism to prevent the towed vehicle from travelling in the ruts of the tractor. The towing force was measured using a 50 kN load cell fitted to the towing mechanism.

2.1. Measurement Methods

The experimental settings were denoted by a letter and a number (e.g. B1.5). The letter refers to the terrain under study (B=concrete; T=stubble; H=stubble-cultivated; K=cultivator-tilled) and the number to the tyre inflation pressure of the test vehicle (1.5-1.8-2.1-2.4 bar).

The cone index was measured on the terrain on both wheel tracks of the towed vehicle before towing. Another letter was added to the notation for field measurements indicating that the measurement was made on the right (J) or left (B). For example H1,5J denotes a measurement made on stubble-cultivated ground with tyre pressure of 1.5 bar, on the track of the right wheel. This notation was mostly used for cone index measurements but was unnecessarily detailed for pulling force tests.

The pulling tests were carried out at a constant speed of 10 km/h in every case.

2.2. Measurement on Concrete Surface

A vehicle being towed on concrete is a case of deforming wheel on rigid surface, where the rolling resistance is due to deformation of the tyre. The aim of the measurement was to determine rolling resistance factors at different tyre pressures. Comparison of the results with the field measurements yields the deformation loss of the tyre. The pulling force was measured with the pulled vehicle coupled behind the tractor (Fig. 1).

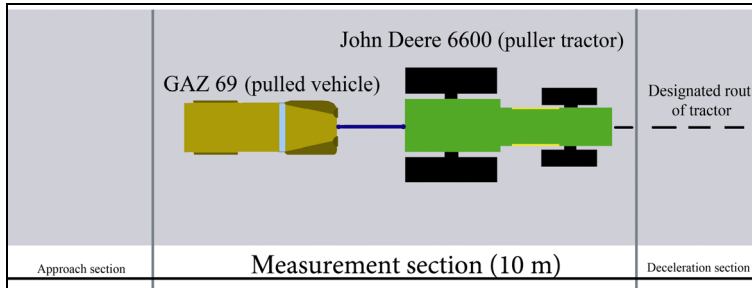


Figure 1. Pulling test on concrete.

2.3. Measurement on Arable Land

The measurements were performed on 60-m-long test courses (Fig. 2) in which the length of the designated measurement section was 10 m and that of both the approach and deceleration sections was 25 m. For each soil condition, the measurements were performed with four different tyre inflation pressures, so that there were four measuring sections marked out on stubble-covered, stubble-cultivated and cultivator-tilled land. To determine vertical soil deformation, every measurement was carried out on an undisturbed section so that the sinkage of the tyre into the soil could be measured. Another purpose of the arable land measurements, like that of the measurements on concrete, was to obtain basic data for calculating run-off speed. The measurements were designed to determine the rolling resistance factors on various soil conditions and at various tyre pressures.

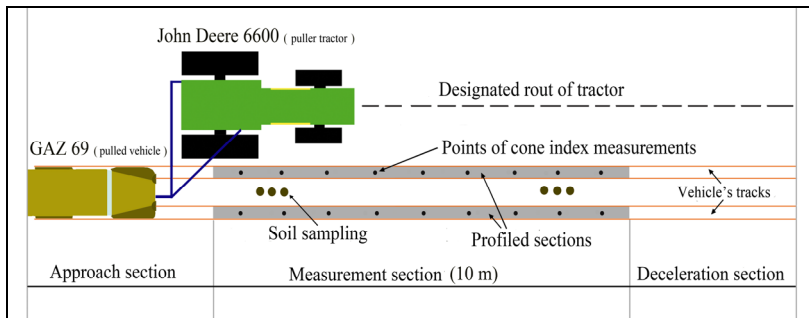


Figure 2. Pulling test on arable land.

2.4. Bulldozing Effect

Further field measurements investigated the phenomenon of bulldozing and determined the bulldozing resistance factor. The measurements were made on a towed vehicle. The tractor driver accelerated to three different speeds, and upon receiving a signal, applied the brakes so as to cause the wheel of the pulled vehicle to bulldoze. The measurements were made at speeds of 10, 15 and 20 km/h, always on undisturbed soil – on stubble-covered stubble-cultivated and cultivator-tilled land. After the wheel sank into the soil and caused bulldozing, the depression of the wheel and the height of the soil accumulating in front of it were measured. The pulling force was also measured.

2.5. Measurement of Soil Profile

Soil profile measurements determined the vertical depression caused in the pulling tests on various soil conditions. They were carried out on the undeformed measurement section and the rut left after pulling. The difference between the two gave the vertical deformation caused under the pulled vehicle.

2.6. Determination of Tyre Contact Surface

The tyre inflation pressure was a variable parameter in the tests. Since the tyre contact area changes with pressure, it was also measured for each pressure value and on every soil condition and on concrete. The method used on concrete was to measure the impression the tyre left on carbon paper. On terrain, marking powder was sprayed around the tyre. In both cases, the impression was assumed to be elliptical and its area was calculated by measuring the principal diameters.

3. Results

The measurements were carried out in accordance with the objectives stated in the introduction. This section gives the measured and calculated results and the new scientific results.

3.1. Determination of Coefficient of Rolling Resistance

The coefficient of rolling resistance factor was determined from the field tests on every soil type and at every tyre pressure. Table 1 summarizes the calculated travelling resistance, the measured pulling force, the set tyre pressures and the slope of the ground, which was calculated from the slope of the measured profile curve.

The rolling resistance factor (f_{rr}) may be written as follows (Eq. 1):

$$f_{rr} = \frac{F_t \mp m \cdot g \cdot \sin \alpha - F_{air}}{m \cdot g \cdot \cos \alpha} \quad [-] \quad (1)$$

In this form, the rolling resistance factor can only be determined if the pulling force is known. This was measured using a load cell. The vehicle weight was

measured by wheel load weighers and the data to calculate air resistance was available. Since the measurements were made at a constant speed of 10 km/h, the air resistance was taken as the constant value of $F_{air} = 6.3$ N. It is not given in Table 1, but was incorporated into the calculations.

Table 1. Summary of measured pulling force, calculated resistances and coefficients of rolling resistance.

	TIP [bar]	Ft [N]	A [°]	Frr [N]	Fs [N]	Frr [-]
Concrete	1.5	604.7	-1	596.4	-273.9	0.038
	1.8	527.1	-1	518.0	-273.9	0.033
	2.1	481.2	-1	470.9	-273.9	0.030
	2.4	434.9	-1	423.8	-273.9	0.027
Stubble	1.5	1237.5	0.92	941.6	252.0	0.060
	1.8	1607.3	1.10	1255.4	301.3	0.080
	2.1	1860.3	1.17	1490.8	320.5	0.095
	2.4	1944.6	0.90	1647.9	246.5	0.105
Stubble-cultivated	1.5	1435.3	1.13	1098.5	309.5	0.070
	1.8	1629.8	0.91	1334.0	249.3	0.085
	2.1	2105.2	1.22	1726.2	334.2	0.110
	2.4	2308.5	1.07	1961.7	293.1	0.125
Cultivator-tilled	1.5	2120.6	1.21	1647.7	331.4	0.105
	1.8	2459.2	1.29	1961.5	353.4	0.125
	2.1	2665.4	1.22	2196.9	334.2	0.140
	2.4	2879.2	1.11	2432.4	304.1	0.155

Knowledge of the rolling resistance factor is essential for determining the run-off speed of a vehicle entering terrain. It may be described by simply-defined parameters. The rolling resistance factor was determined in terms of terrain and vehicle characteristics using formulae given by Laib (2002). These give the rolling resistance for a single wheel (Eq. 2) and the rolling resistance factor (Eq. 3):

$$F'_{rr} = \frac{B \cdot p_{ground} \cdot z}{n + 1} \text{ [N]} \quad (2)$$

$$f'_{rr} = \frac{F'_{rr}}{Q} = \frac{B \cdot p_{ground} \cdot z}{(n + 1) \cdot Q} = \frac{B \cdot z}{(n + 1) \cdot A_{tire}} \text{ [-]} \quad (3)$$

where:

- f'_{rr} coefficient of rolling resistance in case of one wheel [-]
- F'_{rr} rolling resistance in case of one wheel [N]
- Q wheel load [N]
- z soil deformation (wheel sinkage) [m]

- B tyre width [m]
- p_{ground} ground pressure [Pa]
- A_{tire} tyre contact surface [m²]
- n factor of load bearing capacity of soil [-]

$$n = \frac{\frac{CI_{z_0=L} - 1}{CI_{z_0=0}} - 1}{2} \quad [-] \quad (4)$$

In Eq. 4, n is the exponent of the load curve, L is the length of the penetrometer head and z_0 is the distance between the penetrometer head and the soil surface, as indicated on Fig. 3.

The penetrometer used had a length $L = 3$ cm. In the notation of Fig. 3, the depth of penetration is 3 cm when $z_0=0$, and thus 6 cm when $z_0=L$, so that $CI_{z_0=0} = CI_3$ (cone index at 3 cm) and $CI_{z_0=L} = CI_6$ (cone index at 6 cm).

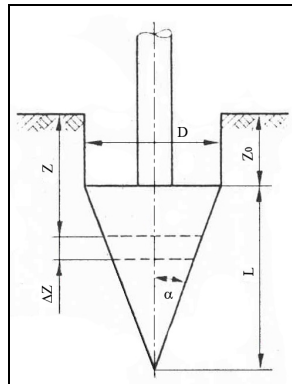


Figure 3. Geometry of cone penetrometer (Sitkei 1986).

Table 2. Determination of exponent n .

	TIP [bar]	Z [cm]	CI3 [MPa]	CI6 [MPa]	CI6/CI3 [-]	N [-]
Stubble	1.5	1.30				
	1.8	1.80	0.216	0.513	2.30	0.7
	2.1	2.05				
	2.4	2.15				
1.5	3.30					
Stubble-cultivated	1.8	3.43	0.245	0.974	3.98	1.5
	2.1	4.55				
	2.4	4.70				
	1.5	6.40				
Cultivator-tilled	1.8	6.80	0.03	0.139	4.93	1.8
	2.1	7.10				
	2.4	7.30				

Table 2, for each measurement area, summarizes the values of sinkage, CI_3 and CI_6 , their ratio in the sense of Eq. 4, and the derived exponent n .

The contact areas of the diagonal and radial tyres were determined from measurements. The contact area of a diagonal tyre is given by the formula:

$$A_{\text{tire(D)}} = \frac{Q}{10 \cdot \text{TIP} \cdot \left[1.2 - 1.2 \cdot \left(\frac{z}{D} \right)^{0.44} \right]} \text{ [cm}^2\text{]} \quad (5)$$

For a radial tyre, the applicable formula is:

$$A_{\text{tire(R)}} = \frac{Q}{10 \cdot \text{TIP} \cdot \left[0.75 - 0.75 \cdot \left(\frac{z}{D} \right)^{0.44} \right]} \text{ [cm}^2\text{]} \quad (6)$$

where Q is the load on one wheel [N], TIP is the tyre inflation pressure [bar] and z/D the relative wheel sinkage [-].

Equations 5 and 6 were used to produce the nomograms of Figs. 4 and 5. These are intended to give forensic investigators a simple and quick way of determining the contact area of a tyre knowing the relative sinkage, the inflation pressure and the wheel load. The contact area is an important input parameter for determining run-off speed.

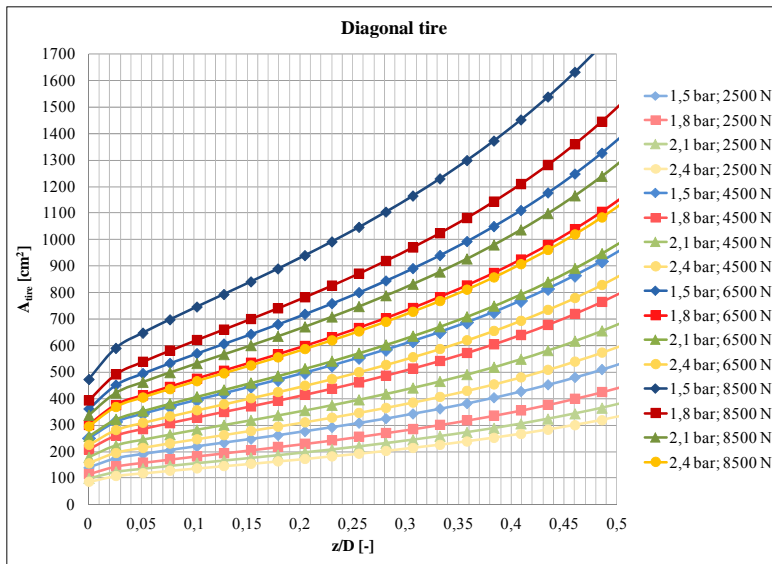


Figure 4. Contact area of diagonal tyre as a function of relative wheel sinkage.

On Figs. 4 and 5, curves for the same tyre pressure have the same colour but differing saturation according to the wheel loads, so as to clearly display the effect of the latter. The nomograms were produced for four tyre inflation pressures (1.5-1.8-2.1-2.4 bar) and four wheel loads: $Q_1 = 2500$ N, $Q_2 = 4500$ N, $Q_3 = 6500$ N, $Q_4 = 8500$ N.

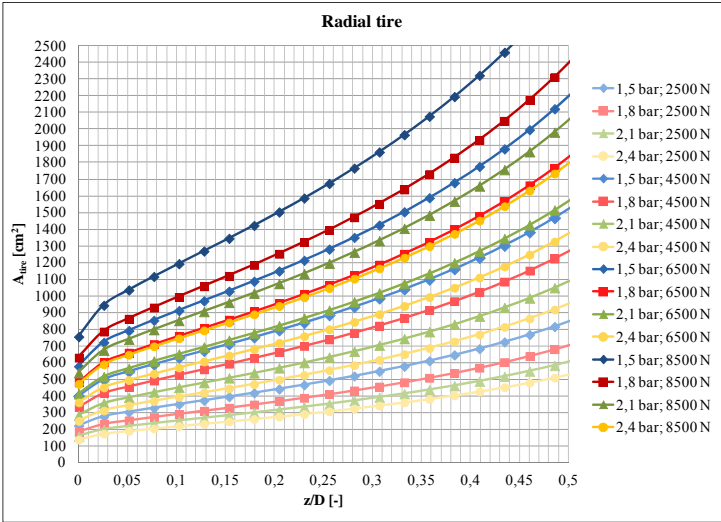


Figure 5. Contact area of radial tyre as a function of relative wheel sinkage.

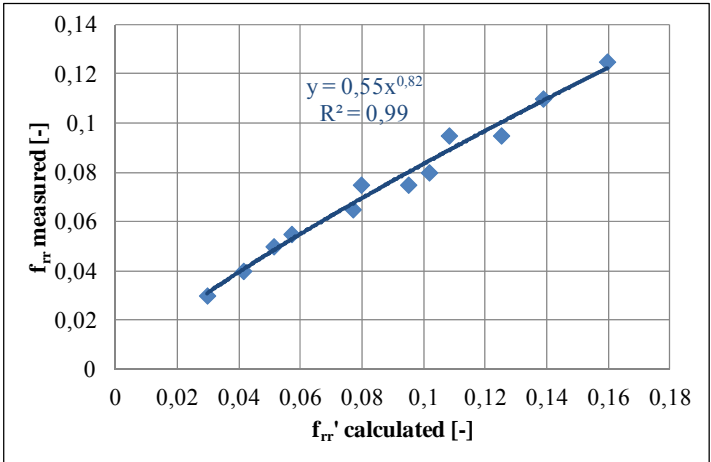


Figure 6. The rolling resistance coefficients determined by the field measurement data, as a function of calculated rolling resistance coefficient, valid for one wheel, without tyre deformation.

Since Eq. 3 applies to one wheel, there is a need to determine the functional relationship of the rolling resistance coefficients measured as the vehicle traverses the track, i.e. where the multipass effect is involved, with the rolling resistance for

a single wheel. This involves using Eq. 3 to calculate the f_{rr}' values for each measurement series.

To determine the resistance caused by the terrain, the resistance caused by tyre deformation – found from the measurement on concrete – was subtracted from both rolling resistance coefficients. This value ($f_{rr(def)}=0.03$) can later be added to the function describing the relationship, because it is a constant.

Figure 6 shows the functional relationship between the rolling resistance coefficient for all four wheels and that calculated for a single wheel. It is clear from the graph that the power function fits the points with the correlation value $R^2=0.99$.

The power function derived from the curve may be used to write a formula for the rolling resistance coefficient for the multipass case of four wheels traversing the track (Eq. 7):

$$f_{rr} = 0.03 + 0.55 \cdot \left(\frac{B \cdot z}{(n + 1) \cdot A_{\text{tire}}} \right)^{0.8} \quad [-] \quad (7)$$

3.2. Examination of Bulldozing Effect

Bulldozing is a special type of rolling resistance, and the bulldozing resistance coefficient (f_{bull}) is derived from the rolling resistance coefficient (f_{rr}).

The equation of motion of the vehicle in case of bulldozing has the general form:

$$F_t = F_{bull} + F_s \quad [N] \quad (8)$$

where:

- F_t tractive force [N]
- F_{bull} bulldozing resistance [N]
- F_s slope resistance [N]

The tractive force may be written as:

$$F_t = f_{bull} \cdot m \cdot g \cdot \cos\alpha \pm m \cdot g \cdot \sin\alpha \quad [N] \quad (9)$$

If the tractive force is known, the rolling resistance coefficient may be expressed as:

$$f_{bull} = \frac{F_t \mp m \cdot g \cdot \sin\alpha}{m \cdot g \cdot \cos\alpha} \quad [-] \quad (10)$$

The bulldozing resistance coefficient is required to determine the run-off speed of a vehicle which experiences bulldozing after it runs on to terrain. It must be described by parameters which forensic investigators can determine easily.

Equation 7, involving the terrain and vehicle characteristics, was used to determine the bulldozing resistance coefficient with the inclusion of the height of the displaced soil.

Table 3 shows the characteristics set and measured in the bulldozing test and those calculated from the results. The tyre inflation pressure (TIP=2.1 bar) and the tyre width (B=16.5 cm) were constant parameters and are not included in the table. The other set and measured characteristics are: n= index of load capacity curve; A_{abr}=tyre contact area; v=speed; F_{vmax}=maximum drawbar force; z=wheel sinkage; h=height of soil displaced by bulldozing; H= sum of z and h.

The measurement results were used to calculate the bulldozing resistance coefficient (f_{bull}) using Eq. 10, and the rolling resistance coefficients (f_{rr}) using Eq. 11.

$$f_{rr} = 0.03 + 0.55 \cdot \left(\frac{B \cdot H}{(n + 1) \cdot A_{tire}} \right)^{0.8} \quad [-] \quad (11)$$

The basis for calculating the rolling resistance coefficient was Eq. 7, with the sinkage z replaced by H. Where there is no bulldozing, and thus no displaced soil, H is equivalent to z. The vehicle brakes may be applied intermittently, and thus ride over the displaced soil. In this case, the sinkage and the height of soil displaced beside the rut are known. By taking these into account, the bulldozing resistance coefficient may be calculated to a good approximation.

Table 3. Measured coefficients of bulldozing resistance.

	N [-]	A _{tire} [cm ²]	V [km/h]	F _{tmax} [kN]	Z [cm]	H [cm]	H [cm]	f _{bull measured} [-]	f _{rr calculated} [-]
Stubble	0.7	186	10	12.78	9	11	20	0.798	0.599
			15	14.21	10	12	22	0.887	0.644
			20	11.17	7	10	17	0.694	0.530
Stubble-cultivated	1.5	228	10	16.31	13	30	43	1.012	0.685
			15	16.76	14	32	46	1.050	0.722
			20	19.28	16	34	50	1.211	0.769
Cultivator-tilled	1.8	248	10	20.73	20	45	65	1.303	0.809
			15	17.61	19	41	60	1.092	0.760
			20	18.54	22	40	62	1.164	0.780

The bulldozing resistance coefficients given in Table 3 are plotted against the rolling resistance coefficient in Fig. 7.

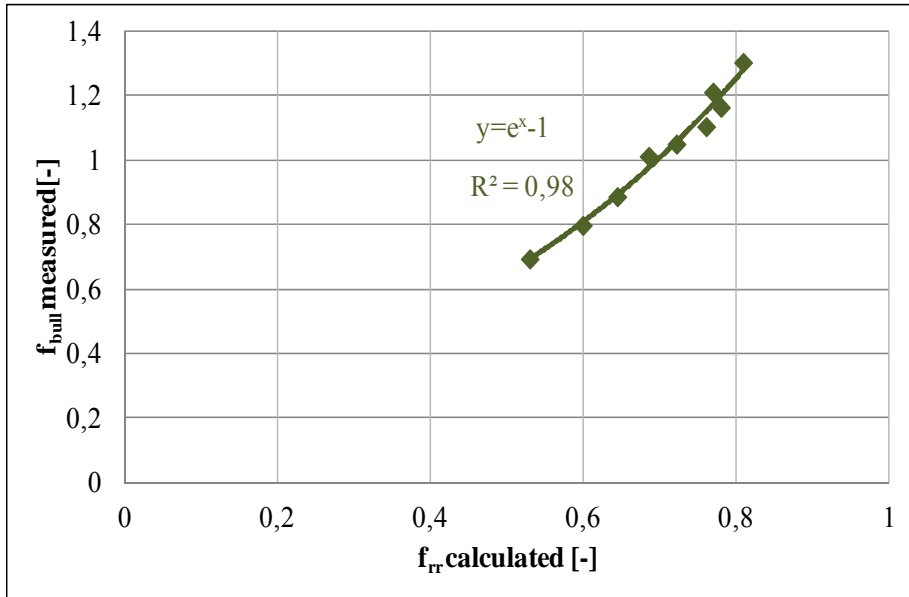


Figure 7. The coefficients of bulldozing resistance determined by field measurement data, as a function of calculated rolling resistance coefficients.

The curve fitted to the points on the graph is described by an exponential function with a correlation of $R^2=0.98$, which is very close. The equation of the curve was refined to describe the bulldozing resistance coefficient (f_{bull}) using the rolling resistance coefficient of Eq. 11:

$$f_{bull} = \exp(f_{tr}) - 1 = \exp \left[0.03 + 0.55 \cdot \left(\frac{B \cdot H}{(n + 1) \cdot A_{tire}} \right)^{0.8} \right] - 1 \quad (12)$$

4. Discussion

A vehicle entering terrain gradually loses the kinetic energy it possesses when it runs off the road and comes to a halt on the terrain. The kinetic energy is absorbed by motion resistances known from travel on terrain. These quantities are important for accident analysis. An accident investigator has no time for laboratory tests and must record the both the soil and vehicle characteristics on site.

The terrain data required to determine the run-off speed are the rolling resistance coefficient for the soil and, in case of bulldozing, the bulldozing resistance coefficient. At an accident, only the ruts are known; the cone index and rut depth may be measured and the soil type identified. The data for the vehicle may be obtained from catalogues and databases, and so may be regarded as known output parameters.

The outcome of this research is a means of determining the rolling resistance coefficient and the bulldozing resistance coefficient using rut data recorded on the terrain.

References

- [1] Ayun, S. (1983): Machinery mobility problem in mechanized rice production in Malaysia. Malaysian Agricultural Research and Development Institute Report No. 83.
- [2] Bekker, M. G. (1960): Track and Wheel Evaluation. *Journal of Machine Design*, 32 (1), pp. 50-95.
- [3] Bukhari, S. et al. (1988): Performance of selected tillage implements. *Agricultural Mechanization in Asia, Africa and Latin America*, 19 (4), pp. 9-14.
- [4] Crolla, D. A., Schwanghart, H. (1992): Vehicle Dynamics. *Journal of Terramechanics*, 29 (1), pp. 7-17.
- [5] Cronjé, P. H., Els, P. S. (2010): Improving off-road vehicle handling using an active anti-roll bar. *Journal of Terramechanics*. 47 (3), pp. 179-189.
- [6] Fan, H., Liu, F., Long, H. (2011): Locomotion of vehicles on hinged road mats. *Journal of Terramechanics*. 48 (1), pp. 47-55.
- [7] Hugemann, W. (2007): Unfallrekonstruktion (Accident reconstruction), Band 1: Grundlagen, Münster: Schönbach-Druck GmbH, pp. 222-226.
- [8] Laib, L. (2002): Terepen mozgó járművek. (Off-Road Vehicles). Szaktudás Kiadó Ház, Budapest
- [9] Liu, C. and Subramania, R. (2009): Factors Related to Fatal Single-Vehicle Run-Off-Road Crashes. NHTSA Technical Report. DOT HS 811 232. DC: National Highway Traffic Safety Administration, Washington, pp. 1-23.
- [10] Liu, J., Kushwaha, R. L. (2012): Effect of travel speed and vertical load on the subsoil force and displacement under a smooth steel roller. *Journal of Terramechanics*. 49 (5), pp. 263-270.
- [11] Mohsenimanesh, A., Ward, S. M. (2010): Estimation of a three-dimensional tyre footprint using dynamic soil–tyre contact pressures. *Journal of Terramechanics*. 47 (6), pp. 415-421.
- [12] Nguyen, V. N., Inaba, S. (2011): Effects of tyre inflation pressure and tractor velocity on dynamic wheel load and rear axle vibrations. *Journal of Terramechanics*. 48 (1), pp. 3-16.
- [13] Plackett, C. W. (1985): A review of force prediction model of an off-road wheel. *Journal of Agricultural Engineering Research*, 31 (1), pp. 1-29.
- [14] Rahman, A. et al. (2004): Mechanical properties in relation to vehicle mobility of Sepang peat terrain in Malaysia. *Journal of Terramechanics*, 41 (2), pp. 25-40.
- [15] Ridella, S. A., Rupp, J. D., Poland, K. (2012): Age-related differences in AIS 3+ crash injury risk, types, causation and mechanisms. Proceedings of the 2012 International IRCOBI Conference on the Biomechanics of Injury. September 12-14, Dublin, Ireland, pp. 43-60.

- [16] Ringdahl, O. et. al. (2012): Estimating wheel slip for a forest machine using RTK-DGPS. *Journal of Terramechanics*. 49 (5), pp. 271-279.
- [17] Sánchez-Girón, V., Andreu, E., Hernanz, J. L. (1998): Response of five types of soil to simulated compaction in the form of confined uniaxial compression tests. *Soil Tillage Research*, 48 (2), pp. 37-50.
- [18] Shoop, S. A. (2001): Finite Element Modeling of Tyre–Terrain Interaction. CRREL Report, US Army Corp of Engineers, Cold Regions Research & Engineering Laboratory, November, p. 69.
- [19] Sitkei, GY. (1986): *Mezőgazdasági és erdészeti járművek modellezése. (Modelling of Agricultural and Forestry Vehicles)*. Akadémiai Kiadó, Budapest
- [20] Tsuji, T. et. al. (2012): 3-D DEM simulation of cohesive soil-pushing behavior by bulldozer blade. *Journal of Terramechanics*. 49 (1), pp. 37-47.
- [21] Wesson, K. D. et. al. (2007): Instrumenting an all-terrain vehicle for off-road mobility analysis. CRREL Report, US Army Corp of Engineers, Cold Regions Research & Engineering Laboratory, January, p. 57.

Institute for Engineering Management



Associate Professor Dr. Miklós DARÓCZI
Director of the Institute

Dear Reader,

Our Institute consists of three professional areas called departments:

- Department of Applied Management,
- Department of Engineering Economics,
- Department of Material Handling and Logistics.

The activities and the research fields of our Institute can be separated by these departments, and had the following main research activities during 2016:

Department of Applied Management

- The main aspects and activities of the development of quality management systems in particular the new standards;
- According to the technical development of agriculture we examine some important elements of precision farming and strip-till;
- Concerning production management we study the application of lean management techniques to improve technical processes.

Department of Engineering Economics

- The importance of education and training in the mirror of human resource factor in agricultural machinery.
- Technical, economic and management analyses of the farm machinery of arable farming.

Department of Material Handling and Logistics

- Developing logistical processes by mathematical modeling and simulation.
- Research of material handling machines with special respect to conveyors.

The educational activity is very important in our Institute. We have reviewed the curriculum of our Engineering Management Programmes. We renewed some e-learning materials and several subjects like Quality Management, Strategic Management and Engineering Economics.

More details about our Institute are available at: <http://mumi.gek.szie.hu/>

Partial examination of the influencing factors in the use of IT applications in agricultural mechanization

Imre KOVÁCS¹, Viktor MEDINA², István HUSTI¹

¹Department of Applied Management, Institute of Engineering Management

²Institute of Engineering Management

Abstract

The agricultural machinery designers and manufacturers meet the information needs of users more and higher level through various innovative IT solutions. As a result of the developments, the determination of machine position in the field and thereby the facilitation of the operator's work is now an available daily practice. Not only the technical solutions and the hardware is important, but the selection of the right software, because it is the soul of the IT applications. It is not easy to find the optimal choice from the wide range of the possible modular software packages.

In the present paper we search answer based on the measurement of a company to the question, why the available IT applications are used or why not. To answer the question we made a "working-day shoot" and evaluated the obtained results.

Keywords

agricultural mechanization, time management of machines, precision farming, positioning, AutoTrack, ITecPro.

1. Introduction

Based on our country's ecological conditions the agriculture and its development has always been concerned by the theoretical and practical professionals. In recent years, IT solutions extend more and more dynamically to help carry out agricultural work more precise. [3] Such innovative new solutions become available which can place on new basis the traditional farm operations, particularly in arable crop production. Nowadays we can find so wide range of software and hardware like never before. [6] This abundance brought new challenges for the entrepreneurs. It is very difficult to find and select the optimal solution. During the election should be considered not only the technical services but the potential economic benefits and the real supply and usage costs. [2] In this situation always a big question: Is it worth for me?

The answer is not only a technical and economical approach. We would like to reveal with our measures and study that the rationalization of working time can answer the question. The use of information technology is also influenced by

many other factors (income conditions, user education, commitment to new solutions, age etc.). [1] In the present paper these factors won't be examined.

2. The available software packages

The striking appearance of IT achievements in the crop production is the exact positioning in the field. Without being exhaustive, the John Deere offers the following software solutions for the Hungarian farmers: [11]

- AutoTrac, automatic steering, trail tracking,
- iTecPro, automatic turning,
- Spray Star, automatic dosage control,
- Section Control, automatic section control,
- AutoTrac RowSense, automatic row sense,
- iSteer, active steering control,
- MachineSync, automatic machine synchronization,

The above mentioned software solutions are also offered by other manufacturers. Their common feature is they need different accuracy range for the positioning in the field. The price of the satellite based solutions increases with the accuracy which increases also the production costs. [10] We can see in the figure 1 the list prices based on signal accuracy provided by Claas in 2015.

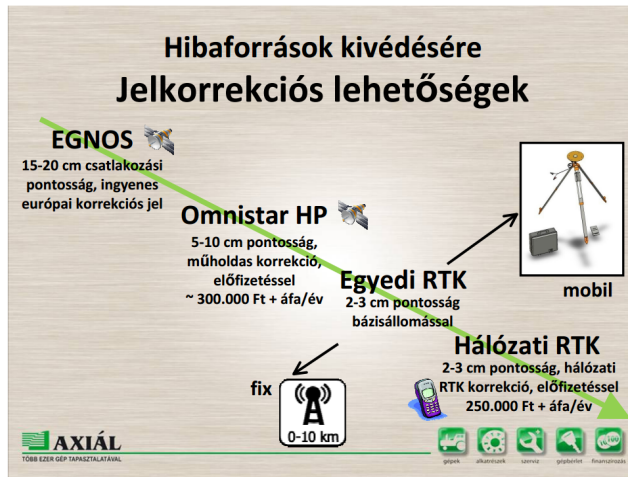


Figure 1. Signal accuracy and annual subscription fees
(Source: [12])

We examined two software based on the question: Is it worth for me? For the illustration we tested two applications in the maize seeding. The applied IT solution is the AutoTrack automatic steering solution developed by the John Deere. The seeding was made on a straight track trail. The iTecPro hasn't been

used to help at the headland turns. The main reason for not using iTecPro was that all turnings could do in less time in that parcel than it was needed for the preparation, programming and operation of the software.

3. Preparation of the examination

The farm test was carried out in the parcel D-52 of the “Galgamenti Mezőgazdasági Termelő és Szolgáltató Ltd.” The corn sowing was made by a John Deere 6150R universal tractor, and a John Deere 1760 Conservation Type 12 line seeding machine suitable for precision farming (Figure 2).

Our examination was focused on the time management of seeding. We tried to answer the question, how a working day can be divided into time consuming components. [4] The tested parcel D-52 has the following characteristics:

- Territory: 12.10 ha
- Length: 572 m
- Width: 211 m
- Shape: Rectangle



*Figure 2. The examined tractor with the seeding machine
(Source: [9])*

The GreenStar package consists of three components:

- StarFire 3000 receiver,
- GreenStar 2630 on board unit,
- AutoTrac automatic steering system.

The AutoTrac system helps the operator to follow the previously travelled route. During its use there is no need to use mechanical tracers. The AutoTrac

system uses the StarFire1’s differential correction signals. As the maize seeding need more precision, it is needed continuously take the correction signal of Real Time Kinematic (RTK). The use of RTK can reduce the overlapping of arable land, precision connection lines can be available, which are very important in the care of the crop. The higher level cultivation of linespacing can increase the yields. [7,8] An additional benefit is the increase of operator comfort, because less attention is required from the machine operator.

The total accuracy of AutoTrac system depends on several variables:

- signal accuracy;
- positioning of power machine;
- setting up the machine and
- field/soil physical condition.

The use of iTecPro makes the seeding more convenient, because it assists not only the headland turns. It operates fully all the features of tractor and seeding, so supplements the AutoTrac system. This includes the changing gear under load, turning on and off the PTO, and the front and rear three-point suspension structure accurately and timely lifting and lowering. However if the operator is sufficiently experienced in the implementation of the headland turns and the seeding machine has no session control, then the use of iTecPro is not always appropriate.

4. Results of measurements

During the measurement we followed a “working-day shoot” methodology mentioned in professional literature. Based on this method we measured on a traditional way the time elements of power machine and interface relationship during the seeding, then we systematized the results. [5] The table 1 shows the required time of the different activities.

Table 1. Summary of time elements of seeding

Code	Type	Activity	Time (min)	%
Total:			1h 50m 55s	100 %
T1	Basis time	Seeding	65:14:00	59
T21	Extension time 1	Turning	8:18:00	7
T22	Extension time 2	March	10:59:00	10
T23	Extension time 3	Loading the seeding machine	12:08:00	11
T24	Extension time 4	Empty round	0:44:00	1
T31	Technical service	Control of seeding machine	5:16:00	5
T5	External time	Orientation	8:16:00	7

(Source: [9])

The Figure 3 shows the distribution of the operational times.

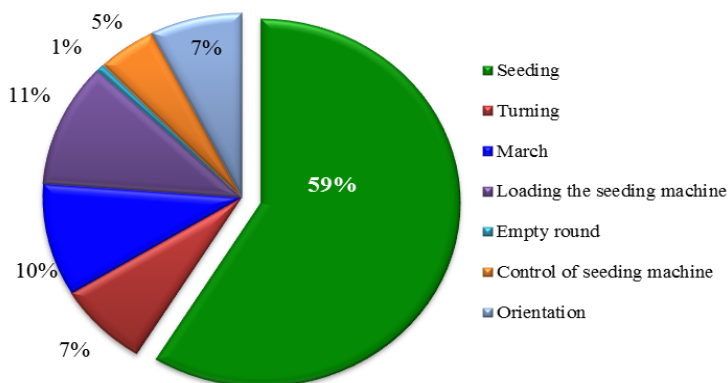


Figure 3. Percentage of the time requirements of the operations (Source: [9])

The results clearly show that due to the disciplined and well-organized work the machine group spent 80% of its working time with seeding. The overall quantity of the turnings was 8 minutes 18 seconds at the D-52 parcel, which is 7% of the working period. Meanwhile the machine group turned 50 times in the 24 tracks. The duration of a turn fell by 7 and 11 seconds.



Figure 4. The regular turning rays of the seed machine's lifting wheels (Source: [9])

This rate can be further reduced in the case of a longer parcel where the rate of the seeding and turning continues to improve. For the introduction of the iTecPro application it is required to input the borders of the parcel, then determine the point A and B, thereafter it is needed to record further data of the machines for

drawing the turning radius. But the required preparation time of the software (45 minutes based on our estimation) exceeds the total required time to the manually turns. The determination of the parcel borders takes the most time of the preparation. The admittance of the 1566 m long parcel takes 18 minutes.

Two additional factors helped to the manual turning. On the one hand the AutoTrac system assists returning to the original track after determining the tracks. As the taking of the limits didn't happen, the track showed over the parcel borders. At the end of the track the tractor turned in the smallest possible radius, as the arc between the longitudinal axis of the tractor and track became smaller than 110 degree. The another factor that contributed to the rapid turning was the low turning radius due to the width of the seeding machine (Figure 4)

A few more derived results of the maize seeding:

- Average speed: 11,8 km/h
- Area capacity: 11,5 ha/h
- Specific fuel consumption I.: 2,7 l/ha
- Specific fuel consumption II.: 18,7 l/h
- Total fuel consumption: 27 l
- Travelled distance 15.610 m.

Conclusions

Manufacturers, distributors and various professional publications recommend the application of IT software's for the agricultural enterprises. But it is not easy to select from the wide and diverse range of solutions to find the most adequate one. The choice of software associated with the purchased device system needs particular attention. It must take into account the real needs and opportunities, as well as the relationship of the offered software with them. Once the software usage is usually planned for a long time, so it is needed to calculate not only with technical specification, but the economical and management aspects as well.

Eternal dilemma also in this case is: "what we gain from one side, we lose it on the other side". Although our research based on time measurement was made once, it shows clearly, that the management apply software solutions only when it gives them really advantages (eg, time-saving). They won't spend money for such kind of developments or investments because of uncritical acceptance of "technology push". Finally we can declare that our examinations must be repeated various times in the future to control our recent results.

References

- [1] Bak Á. – Szira Z. (2016): Kihívások és tapasztalatok a hazai kkv-k innovációs teljesítményének mérésében és értékelésében. Multidiszciplináris kihívások, sokszínű válaszok. BGE KVIK Közgazdasági Intézet, Budapest. ISBN 978-615-5607-15-8

- [2] Fekete A. (2000): A precíziós termesztés alapjai. Gyakorlati Agroforum. 11. évf. 14. sz.
- [3] Herdon M. - Rózsa T. (2011): Információs rendszerek az agrárgazdaságban. Szaktudás Kiadó Ház, Budapest
- [4] Husti I. (2011): A mezőgazdasági műszaki fejlesztés gazdasági vonásai. Szaktudás Kiadó Ház, Budapest
- [5] Husti I. (2016): Időgazdálkodás (általában és a mezőgazdaságban). Agroinform Kiadó, Budapest, ISBN 978-615-5666-01-8-0
- [6] Kalmár S. (2010): A precíziós növénytermelés üzemgazdasági összefüggései. Doktori értekezés, Nyugat-Magyarországi Egyetem, Mosonmagyaróvár
- [7] Magó L. (2008): A gépkihhasználás fokozásával megvalósítható alacsony költségű gépesítési megoldások különböző üzemi méretű növénytermelő gazdaságokban. Szent István Egyetemi Kiadó, Gödöllő. (OTKA-K 63231 kutatási téma)
- [8] Magó L.: (2002) „Economically Reasonable Using of Different Power Machines According to the Farm Sizes”, Hungarian Agricultural Engineering, Periodical of the Committee of Agricultural Engineering of the Hungarian Academy of Sciences, Vol. 15/2002. ISSN 0864-7410
- [9] Mészáros F. (2016): A mezőgazdasági informatikai fejlesztések időkihasználásra gyakorolt hatása. Szakdolgozat. Konzulens: Kovács I., SZIE GÉK, Gödöllő.
- [10] Németh T. - Neményi M. - Harnos Zs. (2007): A precíziós mezőgazdaság módszertana. Agrokémia és Talajtan, MTA Talajtani és Agrokémiai Kutatóintézet, Budapest
- [11] KITE Zrt.: KITE precíziós gazdálkodás – prospektus. Elérhetőség: http://www.kite.hu/termek/precizios_gazdalkodas
- [12] www.axial.hu/fomi-halozati-rtk-korrekcios-jelek

Institute for Mechanics and Machinery



Professor Dr. István SZABÓ,
Director of the Institute

Dear Reader,

The Institute of Mechanics and Machinery (IMM) is one of the key units of the Faculty of Mechanical engineering in Szent István University. Its focus area represents a wide range of scientific interests from fundamental engineering disciplines to the more practical applications in machinery design and technology development. As of today the Institute consists of 3 departments:

- Department of Mechanics
- Department of Machine construction
- Department of Agricultural and food Industrial Machines

Services provided by IMM is supported by two further so called “external departments”: Department of Biotechnics hosted by Oncotherm Ltd. and Department of Farm Machinery set up by Hungarian National Institute of Agricultural Engineering. The Institute is also housing the Computer Aided Engineering Center, a research and training unit dedicated to IT applications used in engineering procedures. This orientation gives emphases to the use of IT technologies in all areas of engineering activities, but lately it is extremely visible in the filed of agriculture and its related fields.

Selected papaers published in the following chapter of this journal may give the cross section of the work done by our staff during 2016. In case you may have questions regarding our work please feel free to visit our website at www.gepeszmernok.hu.

Dr.Istvan Szabó
Director

Calibration of discrete element models

István KEPPLER¹, István OLDAL¹, Ferenc SAFRANYIK¹,
Adrienn BABLENA²

¹Department of Mechanics and Technical Drawing, Institute for Mechanics and Machinery

²NARIC Institute of Agricultural Engineering, Hungary

Abstract

A Lagrangian description based model of granular assemblies is the so called discrete element modelling technique. In this model we describe the granular assembly as the collection of large number of small rigid bodies, and the modelling process of the assemblies' behaviour is based on solving the equations of motion of this large number of particles directly. The question that arises from the practical use is how we can determine the parameters which affect the interaction between the particles: the coefficient of static- and rolling friction, coefficient of restitution, Young modulus and Poisson's ratio of a given (in some cases very small) particle. The direct measurement of these quantities is of course impossible for really small particles. We demonstrate here, that the classical shear test and the penetration test are adequate methods for calibration. It is also demonstrated, that calibration time reduction is also achievable by carefully modifying the particle size in the discrete element model.

Keywords

mechanics of granular materials, discrete element method, calibration

1. Introduction

From the mechanical point of view, two different type of material model can be established: the so called discrete element model, where the physical parameters of the interaction between the distinct grain particles (the so called micromechanical parameters) are modelled, and the continuum model, where the whole granular assembly is modelled as a continuum. The difficulty of the mechanical modelling arises from the problem that the continuum model's (here called as macromechanical) parameters can be determined by measurements developed long ago, but the determination of the micromechanical parameters is difficult and sometimes impossible. Since the elaboration of discrete element method (Cundall and Strack 1979), the calibration of micromechanical parameters remained the most sensitive issue of the modeling process. In case of continuum models, the material parameters can be determined by using measurements, but in case of discrete element modeling, the relations between micromechanical parameters must be determined by simulating the macromechanical behaviour of the particle

system. However, multiple number of micromechanical parameters governing the model behavior must be considered which makes the adequate determination of the actual parameter values challenging. Direct measurement of the parameters would be the best solution, but in most of the cases it is impossible. It can also happen that even the measured parameters would not be suitable for modeling purposes, as the applied constitutive equations in the numerical calculations are only approximations. Due to this problem, in most of the cases the proper measured values of these parameters are not needed, but a combination of parameters ensuring the modeled macro behavior to be the same as the measured one. It is also possible, that there are multiple combinations of parameters resulting the same macro behavior of the granular assembly, and because of this phenomenon the calibration procedure must be very rigorous to get the proper discrete element model.

Large number of different methods are used for calibration. So called slump tests are used for calibration procedures by Grima (Grima 2011). Several other effective and simple calibration techniques were examined by (Grima 2011). Analysis of silo outflow process (González-Montellano, 2011) can also be used for calibration of DEM parameters. Coetzee and Nel (Coetzee and Nel 2015) calibrated the micromechanical properties of packed rock beds by doing angle of repose, confined compression, sliding friction test, and the calibrated micromechanical parameters were validated by measuring and simulating the particle discharge process from a hopper. Derakhshani et al. (Derakhshani 2015) made angle of repose-, conical pile-, and sandglass tests to determine the micromechanical properties of quartz sand, and they succeeded to get good correlation between the measured and DEM simulated behavior of the particle assembly. Tanaka et. al (Tanaka et. al 2000) modeled bar penetration tests using discrete element method. They evaluated the effect of the coefficient of friction between the element and wall. Their calibration was based on the same penetration method, which they modeled. For soil-tool interaction modelling purposes (Mak et al., 2012) used a method for calibration based on the modeling of soil-tool interaction and using the universal earthmoving equation. Simons et. al (Simons et. al 2015) used ring shear tester for calibration purposes. Their results showed dependence on the Young's modulus, the static and the rolling friction coefficients, and showed no significant influences of the Poisson's ratio, the coefficient of restitution and the particle-wall friction coefficients. Grima and Wypych (Grima and Wypych 2011) calibrated discrete element model parameters for particle-structure interactions under impact conditions. They found, that marginally scaling up the particle size of the spherical particles and the solid density in the DEM simulations to reduce the computation time proved to still provide accurate and reliable results compared to smaller non-spherical particles.

2. The discrete element method

The Discrete Element Method (DEM) is a fairly new proceeding to model the mechanical properties of bulk materials. By the use of DEM, the model problem

is solved by applying and solving the equation of motion on each singular particle of the bulk material assembly (Cundall and Strack, 1979). The discrete element based approach can be very useful because its results can be extended for more complex tool geometries than the results of the analytic approach.

For modelling the mechanical behaviour of the granular material, we used EDEM discrete element software with “Hertz Mindlin with bonding” contact model. In this model, the particles are glued with a finite sized bond. This model is based on the assumption that the capillary and dynamic viscous forces are causing the parallel bonding forces between the soil particles in case of cohesive soil.

In the discrete element model from the beginning of the simulation until “turning on the bonded contacts” (from $t_0 = 0$ until t_{bond}) the simulation evaluates the contact forces according to the “Hertz-Mindlin no slip” contact model: the material and interaction parameters have their effect on the normal- and tangential forces. This forces and moments acting between the interacting soil particles in the form of the following equations.

The normal force is

$$F_n = \frac{4}{3} E_0 \delta^{\frac{3}{2}} \sqrt{R_0} - 2 \sqrt{\frac{5}{6}} \frac{\ln C_r}{\sqrt{\ln^2 C_r + \pi^2}} \sqrt{2 E_0^{\frac{4}{3}} R_0 \delta} \sqrt{m_0 v_{\text{rel}}}, \quad (2)$$

where $\frac{1}{E_0} = \frac{1-\nu_1^2}{E_1} + \frac{1-\nu_2^2}{E_2}$ is the equivalent Young modulus of the two interacting soil particles, δ is the overlap between these two soil particles. This normal overlap represents the normal deformation of a particle. The normal overlap δ between two particles i and j at positions x_i and x_j (where x is the distance measured on the line connecting the centers of the two overlapping particles) with radii R_i and R_j is defined as: $\delta = R_i + R_j - (x_j - x_i)$.

$R_0 = \frac{R_1 R_2}{R_1 + R_2}$ is the equivalent radius, $m_0 = \frac{m_1 m_2}{m_1 + m_2}$ is the equivalent mass and v_{rel} is the normal component of the relative velocity of the soil particles.

The tangential force is

$$F_t = -8 G_0 \sqrt{R_0 \delta} \delta_t - 2 \sqrt{\frac{5}{6}} \frac{\ln C_r}{\sqrt{\ln^2 C_r + \pi^2}} \sqrt{2 G_0^{\frac{4}{3}} R_0 \delta} \sqrt{m_0 v_{\text{rel}}}, \quad (3)$$

where $\frac{1}{G_0} = \frac{2-\nu_1}{G_1} + \frac{2-\nu_2}{G_2}$ is the equivalent shear modulus of the two interacting soil particles, δ_t is the tangential overlap between the two particles and v_{rel} is the tangential component of the relative velocity of the soil particles. The tangential overlap is the tangential displacement of the contact point up to the point at which the contact ends or the particle begins to roll or slip. The

tangential overlap represents the tangential deformation of a particle. The tangential force is limited by Coulomb friction $\mu_s F_n$, where μ_s is the coefficient of static friction.

The moment from rolling friction is $M_r = -\mu_r F_n R_i \omega_i$, where R_i is the distance of the contact point from the centre of the i -th soil particles and ω_i is the unit angular velocity vector, which is a dimensionless quantity representing only the direction of rotation of the i -th soil particle. μ_r is the coefficient of rolling friction. The tangential force also has moment on the particle: $M_t = F_t R_i$.

From $t > t_{\text{bond}}$ (from the time, when bonding is “turned on”) at contact points and at points which are closer to each other than a pre-defined distance (called bonded disk radius) particles are glued to each other by bonding bridges (fig 1.). Bonds of finite stiffness can exist at contacts, and these bonds carry load and can break. An applied macroscopic load is carried by the grain and “glue” skeleton in the form of force chains that propagate from one grain to the next across grain contacts, some of which may be filled with “glue”. The forces arising in these bonding bridges can be calculated by taking into account their deformation and their material properties.

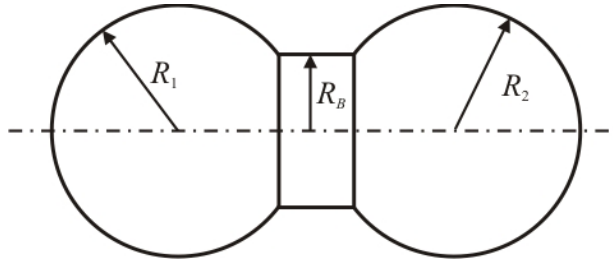


Figure 1. Bonded particle model

The bonding forces/moments acting on the particles are set to initial value zero, and are adjusted incrementally every time step:

$$\delta F_n = -v_n S_n A \delta t, \quad (4)$$

$$\delta F_t = -v_t S_t A \delta t, \quad (5)$$

$$\delta M_n = -\omega_n S_n J \delta t, \quad (6)$$

$$\delta M_t = -\omega_t S_n \frac{J}{2} \delta t, \quad (7)$$

where $A = R_b^2 \pi$, $J = \frac{1}{2} R_b^4 \pi$. R_b is the radius of the glue, $S_{n,t}$ are the normal and shear stiffness per unit area, δt is the timestep, $v_{n,t}$ are the normal and tangential

velocities of the particles and $\omega_{n,t}$ are the normal and tangential components of the angular velocity vector.

The bond is broken when the normal or tangential stress exceeds some predefined value (the strength of the bonding bridges):

$$\sigma_{\max} < -\frac{F_n}{A} + \frac{2M_t}{J} R_B, \quad (8)$$

$$\tau_{\max} < -\frac{F_t}{A} + \frac{M_t}{J} R_B. \quad (9)$$

These bonding forces/torques are in addition to the standard Hertz-Mindlin forces.

During the simulations, the linear- and angular momentum theorem is used to write the equation of motion for all the individual particles resulting multiple number of differential equations to be solved in a sufficiently large number of time steps. The used time step has a great impact on the stability of the numerical model. We selected for the simulation 25% of the Rayleigh-type time step:

$$\delta t = 0,25T_R = 0,25 \cdot (0,1631\nu + 0,8766)^{-1} \pi R \left(\frac{\rho_p}{G_p} \right)^{\frac{1}{2}}. \quad (10)$$

It is important to take into account, that the quality of the obtainable solution could sensitively depend on the value of this time step used during the simulations. The same time step must be used during the calibration process of the discrete element model and during the simulations.

3. The standard shear test

The standard shear testing technique for particulate solids is based on the so called Jenike shear cell (Jenike 1964). The Jenike Shear Cell (fig. 2.) consists [3] of a base (1) shear ring (2) and shear lid (3), the latter having a bracket (4) and pin (5). Before shear the ring is placed in an offset position and a vertical force F_v is applied to the lid and hence to the particulate solid within the cell by means of a weight hanger (6) and weights (7).

A horizontal force is applied to the bracket by a mechanically driven measuring stem (8) which is driven forwards at a steady rate of 1-3 mm/min. This stem is attached to the drive system through a force transducer which measures the shear force F_s . During the shear operation the shear ring moves from the original offset position to the opposite. During shear a shear zone develops inside the sample, and in this way the shear force vs. time plot can be transformed to a shear force – shear strain plot. Using Jenike shear cell, the friction between the granular material and the container wall (the so called wall friction) also can be determined [3].

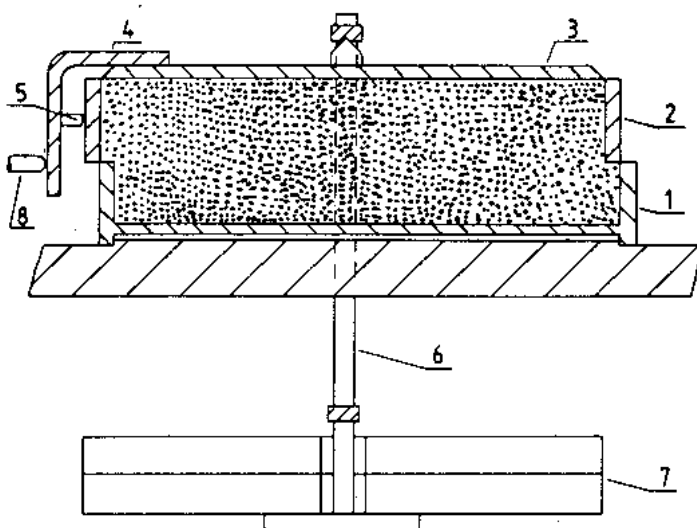


Figure 2. Jenike shear cell

Based on the description found in the literature we developed an automatic shear device making the same shear process described above.

By using this automatic shear testing device, we determined the yield loci (the envelope of the Mohr circles corresponding the failure at given normal load) of cement powder for demonstrating the usability of our calibration method. First we made critically consolidated samples of the cement powder, critically consolidated means that the shear force – shearing distance diagram has no local maximum point, but saturates within the shearing distance of the cell. A particulate solid is critically consolidated with respect to the state of stress applied, when it yields without change in bulk density at a constant state of stress.

By pre-shearing the material sample using the compressive force corresponding to critically consolidated sample of cement, then lowering the compressive force successively to smaller normal forces, we made the points of the yield loci for cement powder. Using linear approximation, we determined the yield line of the given powder by fitting a line to points determined by measurements.

4. DEM model of the standard shear test

By using commercial DEM software, we created a simple shear cell model. The model consisted of two cylinders (having the same size as the standard Jenike cell), an upper plate and a plane dividing these two. We filled the cylinders with spherical particles having radius randomly distributed radiuses varying around m $r=0,003m$ with a variance $\pm 0,0005m$ (in DEM models, the particle sizes must not

be inevitably the same as the sizes of the real particles). The first phase of modelling was the filling of the cylinders with granular materials, then a pre-compression phase followed the filling. The pre-compression was made by the upper plate, as it was forced to move downwards until pressure on it resulted the vertical force needed to reach critically consolidated sample in the virtual tester.

After reaching critically consolidated state of the sample, the upper cylinder has started to move in the horizontal direction, modelling the shear process. From the pressure arising from the particles in the cylinder, the vertical force acting on the cylinder wall was determined.

By successive modelling of the shear process with DEM using different micromechanical parameters we managed to get yield loci from the “virtual” shear test being in a good match with the line determined by measurements (fig. 3.).

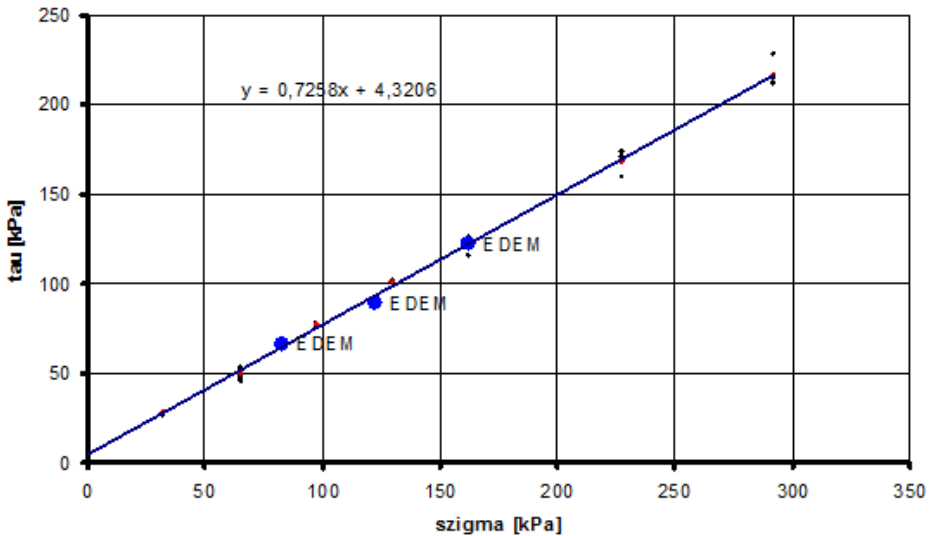


Figure 3. Yield loci in linear case from measurements, and yield points from DEM model

On fig. 3 small black dots are the measured yield points of cement powder, red dots denote the average values and blue dots correspond to the yield loci from the virtual DEM model of the given powder.

5. Penetrometer tests

For calibration of our soil-wheel interaction model penetration test can be chosen and discrete element model of penetration measurement on tilled soil was made. From penetration test the cone index (CI) of soil can be determined. CI describes the vertical load carrying capacity of soil and it is used for calculating of soil deformation work.

For penetration test cone penetrometer has been used. This penetrometer has a cone in its measure bar and it must be pressed in the soil in defined depth. By using penetrometer we are able to measure the soil resistance and save measured data (fig. 4). On the diagram can be seen that the deviation of measured data is considerable therefore huge amount of measurements must be accomplished to get proper CI data.

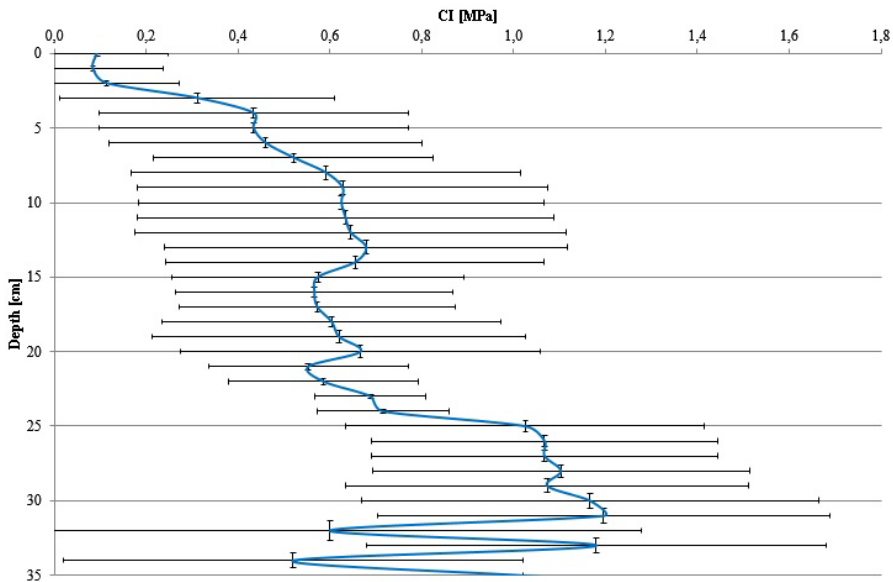


Figure 4. Average penetration diagram of 8 measurements

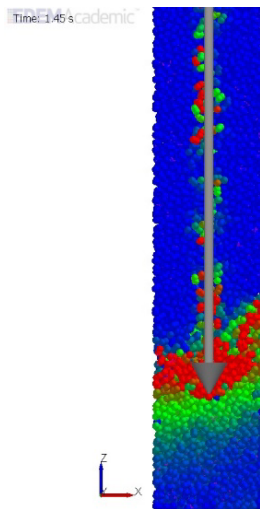


Figure 5. Simulation of penetration test

Cone index is related to given depth, generally CI on 15 cm depth is used. It is marked as an index so CI on 15 cm depth is marked as CI0-15. This means that measured data per centimeter are read from the diagram and average value of data are calculated. This method accomplishes on each diagram then average value of average values becomes cone index.

In this case soil particles were assembled from two balls (Keppler et al. 2012). Particles are generated in a cylinder. Model of the penetrometer is a cone and a bar, this model penetrometer was pressed into the granular assembly with given velocity (fig. 5.).

Two types of soil model has been used in penetration test simulations, a cohesionless and a cohesive sand model. Penetration test models were repeated three times.

By knowing Z components of forces cone index were determined and illustrated in a diagram as a function of depth. On fig. 6, diagrams from measured and simulated data can be seen.

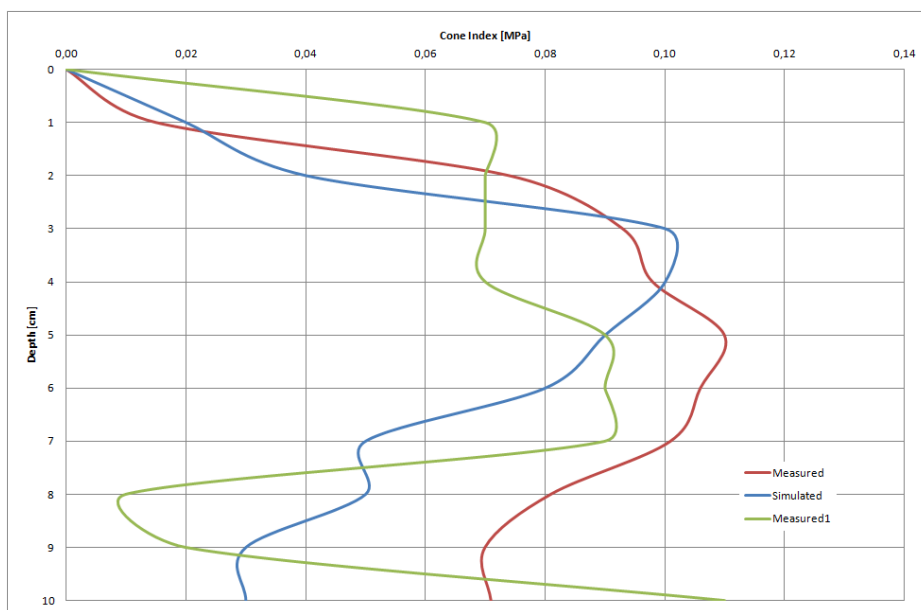


Figure 6. Measured and simulated cone indexes

6. On the reduction of the computational time

Reducing of computational time is capable solution for reduction calibration procedure. The most effective solution is enlarging of particle radius. The relationship between computational time and particle radius was examined in (Oldal et al. 2017). The simulation time decreased with enlargement of particle radius according to hyperbolic function (fig 7), because of this doubling of

particle radius results very serious computational time reduction with 94.9% in case of cohesionless assemblies.

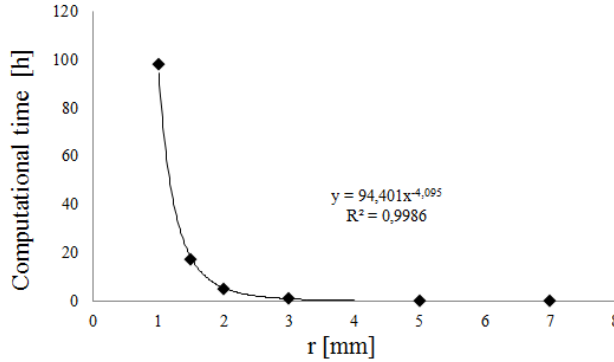


Figure 7. Computational time in function of particle radius (Oldal et al. 2017)

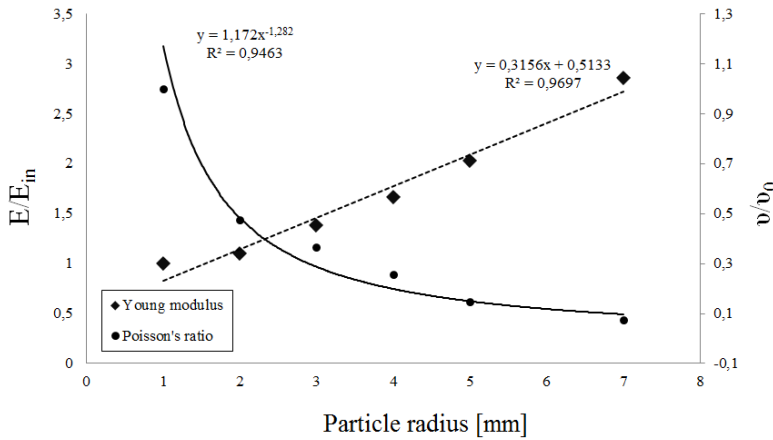


Figure 8. Young modulus and Poisson's ratio change in function of particle radius (Oldal et al. 2017)

In next step based on above parameter sensitivity test (Keppler et al. 2016) and effect of particle scaling up we had to select which micromechanical parameter need to change to get reference macro behavior of the granular assembly. According to phenomenon of particle clustering the deformation of whole assembly proceeds with displacement of particle groups, and these clusters are less rigid than individual particles, because the particles can move internally the cluster. Consequently the elastic properties of clusters are different than the behavior of single particles, hence Young modulus and Poisson's ratio were changed for scaled up particles. To get reference macro behaviors with scaled up

particles the Poisson's ratio need to change with a hyperbolic function referring to particle radius Young modulus need to change with a linear function referring to particle radius (Fig. 8). (Oldal et al. 2017)

Consequently in this work introduced DEM simulation time reducing technique can be generally used in case of different initial set of micromechanical parameters, however the Young modulus and Poisson's ratio need to determine in every cases.

Conclusions

The direct measurement of micromechanical parameters for discrete element modeling of granular assemblies is not possible. So called calibration procedure is needed for finding the adequate values of these mechanical quantities. Shear test and penetration test are good choices for discrete element calibration procedures. Both of these methods do compare the measured and simulated behaviour of the granular assembly, and by systematically changing the micromechanical parameters used in the discrete element model, try to achieve statistically acceptable correspondence between the two dataset. The procedure is so time consuming, that in most of the cases the calibration procedure takes significantly more time, than the modeling of the real process inspected. Because of this, the reduction of the time needed for the whole modeling procedure is important from practical point of view. In this article, we demonstrated that such time reduction is possible.

References

- [1] P.A. Cundall, O.D.L. Strack: A discrete numerical model for granular assemblies, *Geotechnique*, 29 (1). pp. 47–65. 1979.
- [2] A. P. Grima, P. W. Wypych: Development and validation of calibration methods for discrete element modelling. *Granular Matter*, 13 (2). pp. 127-132. 2011.
- [3] A. P. Grima, P. W. Wypych: Discrete element simulations of granular pile formation: Method for calibrating discrete element models, *Engineering Computations*, 28(3). pp. 314-339. 2011.
- [4] C. González-Montellano, Á. Ramírez, E. Gallego, F. Ayuga: Validation and experimental calibration of 3D discrete element models for the simulation of the discharge flow in silos, *Chemical Engineering Science* 66 (21). pp. 5116–5126. 2011.
- [5] Sayed M. Derakhshani, Dingena L. Schott, Gabriel Lodewijks: Micro–macro properties of quartz sand: Experimental investigation and DEM simulation, *Powder Technology* 269. pp. 127–138. 2015.
- [6] Tom A. H. Simons, Rouven Weiler, Stefan Strege, Sven Bensmann, Martin Schilling, Arno Kwade: A ring shear tester as calibration experiment for DEM simulations in agitated mixers - a sensitivity study, *Procedia Engineering* 102. pp. 741–748. 2015.

- [7] A.P. Grima, P.W. Wypych: Investigation into calibration of discrete element model parameters for scale-up and validation of particle–structure interactions under impact conditions, *Powder Technology* 212. pp. 198–209. 2011.
- [8] Hiroaki Tanaka, Masatoshi Momozu, Akira Oida, Minoru Yamazaki: Simulation of soil deformation and resistance at bar penetration by the Distinct Element Method, *Journal of Terramechanics* 37. pp. 41-56. 2000.
- [9] Mak, J., Chen, Y. and Sadek, M.A. (2012): Determining parameters of a discrete element model for soil – tool interaction, *Soil & Tillage Research*, 118(1), pp. 117-122.
- [10] Jenike, A. W.: Storage and Flow of solids, Bulletin No. 123, Utah Engineering Experiment Station, University of Utah, Salt Lake City, 1964.
- [11] The Institution of Chemical Engineers: Standard shear testing technique. Published by the institution of chemical engineers, England, 1989. ISBN 0 85295 232 5.
- [12] C.J. Coetzee, R.G.Nel: Calibration of discrete element properties and the modeling of packed rock beds, *Powder Technology* 264. pp. 332-342. 2014.
- [13] I. Oldal, F. Safranyik, I. Keppler: Reducing computational time of cohesionless discrete simulations based on particle clusters, *Engineering Computations*, Accepted manuscript. 2017
- [14] Keppler I., Safranyik F., Oldal I.: Shear test as calibration experiment for DEM simulations: a sensitivity study, *Engineering Computations*, Volume 33, Issue 3, pp. 742 – 758. 2016.

Terrain classification with IMU

Zoltán BLAHUNKA, Zoltán BÁRTFAI, Dezső FAUST

Department of Agricultural and Food-industrial Machines,
Institute for Mechanics and Machinery

Abstract

Stochastic processes are always changing. Measuring the process parameters never gives us a stable end value. In our institute we develop a statistical surface metrology method. To calculate the optimal length of measurement we use information entropy. The entropy is a saturating function. By exponential regression we are able to forecast the optimal length of measurement. Using the optimal measuring we are able to classify the terrain.

Keywords

soil surface, terrain classification, IMU, roughness, entropy, optimization, mobile robot

1. Introduction

In our institute we developed a new method for soil surface monitoring (Blahunka, Faust, Bártfai, & Lefénti, 2011) (Blahunka, Bártfai, & Lefánti, 2012). A mobile robot is moving over the field. The mobile robot has and 6 DOF IMU device (Bose, 2009). The IMU measures the acceleration (all three dimensions, 3 DOF) and angle speed (all three dimensions, 3 DOF). At the beginning we used the vertical acceleration. There are many issues with this acceleration. The IMU measures the sum of gravity and kinetically acceleration. The vertical axle changes by the mobile robot body. Finally we are calculating the height different between the axles by the angel speed.



Figure 1. Pioneer P3-AT mobile robot on the field

The method give us a distribution which specific to the field. The classification based on agricultural needs, the site of the clots.

Like every stochastic process monitoring, we had a question: how long should it take? To answer this question we used information entropy.

2. Entropy

The entropy shows how much new information we get. Shannon defines it at 1949 (Shannon & Weaver, 1949).

$$H = -\sum p_i \log_2 p_i \tag{1}$$

Equation 1 shows the entropy for discrete events. p_i -s are the probabilities of events. Because of \log_2 the entropy is calculated by binary bits.

How can the entropy changing (increasing, decreasing). To calculate the entropy we need a distribution (probabilities for all events). The entropy depends on the number of the events, probabilities. With the same number of events the entropy is higher when the probabilities are the same. Let's see two examples: coin, dice.

3. Coin

The coin has two events. At first we use normal coin, both side has the same probably. Calculating the entropy for this case gives 1. Throwing a (normal) coin gives us 1 bit new information.

$$H = \left(\frac{1}{2} \log_2 \frac{1}{2} \right) + \left(\frac{1}{2} \log_2 \frac{1}{2} \right) = 2 \left(\frac{1}{2} \log_2 2 \right) = 2 \frac{1}{2} = 1$$

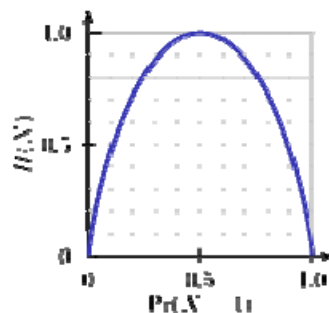


Figure 2. Entropy for two events (coin), source: (Wikipedia contributors, 2012)

However if we cheat, the probabilities are not the same. One side has a bigger probability. This way the entropy is smaller. Worst case the coin fallen always at one side. At this case the entropy is 0. We know the result, there is no new information by the measurement.

4. DICE

The dice has 6 sides. All sides have the same probability. This way the entropy is equal $\log_2 6$.

Big question of dice? How many times should we throw to get the 1/6 probabilities. For example 1000. 1000 is not divisible by 6, it means not all events will be 1/6. Every throwing makes a new distribution and new entropy. The entropy has a limit, the theoretical value $\log_2 6$. We can get this value when all events have the same probability. If we are lucky it can be after 6 throwing. But for 7th throwing the entropy will decreasing.

$$H = n \left(\frac{1}{n} \log_2 \frac{1}{\cancel{1/n}} \right) = n \frac{1}{n} \log_2 n = \log_2 n = \log_2 6 = 2,5850$$

We use this experience to define the optimal length of (stochastic) measurement.

Based on dice we introduce three type of relative entropy. As we throwing the dice, we know the final entropy. Calculating the rate of current entropy and the final (H_∞) is a relative entropy based on H_∞ .

$$h_\infty = \frac{H}{H_\infty} \quad (2)$$

h_∞ shows us how many information we get. The theoretical maximum is 100%. If we plan a measure error level, we can check if the relative entropy reached this level.

Another opportunity to calculate relative entropy is based on theoretical maximum entropy. In this case (all events have the same probability) the H_{\max} and H_∞ is equal.

$$h_{\max} = \frac{H}{H_{\max}} \quad (3)$$

Based on theoretical maximum entropy (it is depend on the number of events) we can check how many information we get based on the maximum. In general

(events have different probabilities) it cannot reach 100%. Also the smaller value can describe a good measurement.

Finally we calculate the rate of h_{\max} and h_{∞} . It shows the difference between all events are the same probability and the current process distribution.

$$h_{rel} = \frac{h_{\infty}}{h_{\max}} \quad (4)$$

We throw 500 times a dice. The last result are in the next table.

Table 1. Entropy after 500 times throwing a dice

Number	Dice	Number of value						2,5850	Entropy	Relative
		1	2	3	4	5	6			
495	2	78	85	86	75	84	87	2,5829	99,9186%	
496	2	78	86	86	75	84	87	2,5828	99,9149%	
497	2	78	87	86	75	84	87	2,5826	99,9101%	
498	4	78	87	86	76	84	87	2,5829	99,9208%	
499	6	78	87	86	76	84	88	2,5828	99,9151%	
500	6	78	87	86	76	84	89	2,5826	99,9085%	

The first column shows the number of throwing. A second yellow column shows the current value of the dice. For example the last throwing was 6. The next 6 columns show the number of value throwing. Theoretical it should be $500/6=83.333$. It is very interesting that some values have big different from it ± 5 , but the entropy is 99,9% of the maximum value.

Method

Our measurement result is a histogram. The soil surface is classified by clot size and a distance between clots. This histogram gives a distribution which is specific for the surface. We calculate the entropy after every clot.

The entropy shows a saturating function. Why should it be a saturating function?

At the beginning there are new columns in the histogram. More events make higher entropy. That's way at the beginning it raising fast.

When all events appear the value of entropy depend on the final distribution. As we measure more the final distribution stabilizing. Of course every clot makes a small change on the distribution but the main concept doesn't change. That's why the ending section approximate the theoretical limit of the entropy.

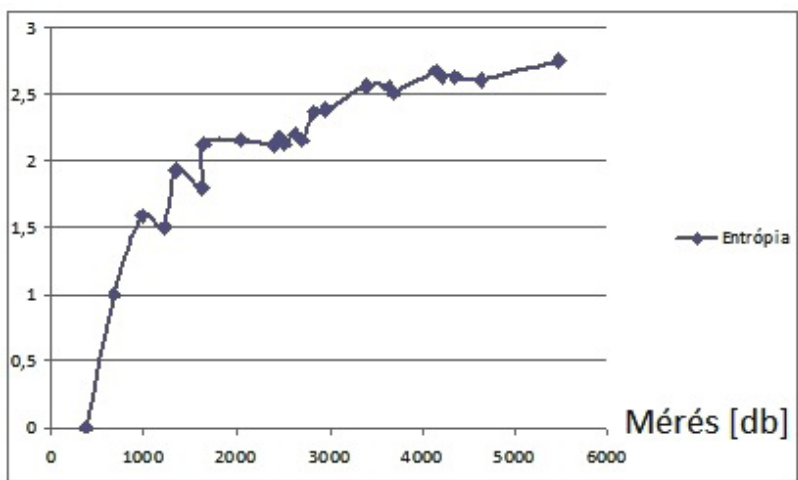


Figure 3. Entropy by distance

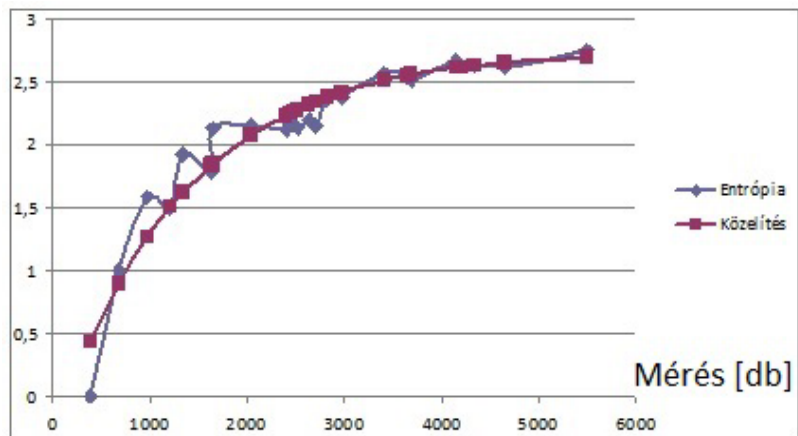


Figure 4. Exponential regression

Figure 3 shows the measured entropy and the result of the exponential regression (Seber & Wild, 2005). The regression find the parameters for the following equation:

$$H(t) = H_{\infty}(1 - e^{-(t/T)}) \tag{5}$$

Where, H_{∞} is the theoretical limit of entropy, t is the time of the measurement, T is the parameter of growing, saturating. Parameter T shows, how fast the saturation.

Results

In our method every clot changes the distribution. After histogram changing we calculate the entropy. Based on the entropy function we calculate the regression.

Our previous publication (Blahunka, Bártfai, & Faust, 2013) on this topic used different equation.

$$H = H_{\infty} - e^{-(ax+b)} \tag{6}$$

We found parameter b is zero. T is $1/a$.

Before the measurement we know the level of precision. Based on this level and equation number 5, the optimal time is:

$$T_{opt} = T \ln(\text{error}) \tag{7}$$

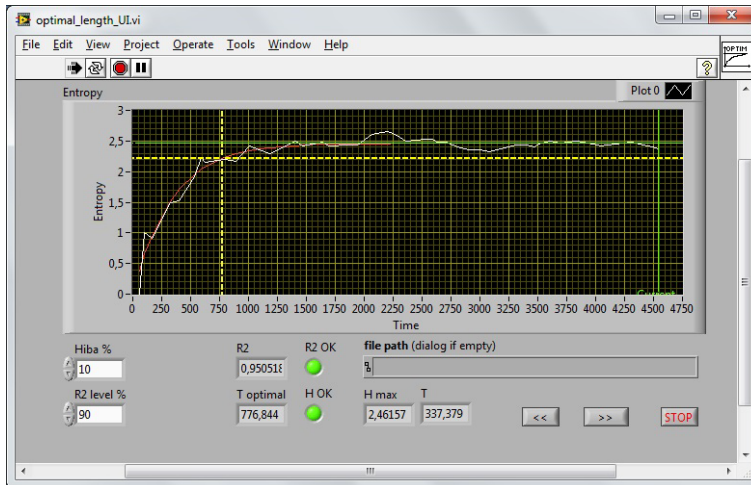


Figure 5. Exponential regression user interface

Finally we implement this algorithm at National Instruments LabVIEW environment. The software gets the entropy values and calculates the exponential regression. At figure 4 the white graph shows the measured and calculated entropy. The red exponential graph shows the calculated entropy based on the

regression. The green line is the maximum entropy level. It is interesting that in the measurement the entropy can be higher than the final. It is because the entropy shows how equals the events probability. If they getting equals the entropy increasing, if it is getting different the entropy value is decreasing.

Based on the green line and the given error level, the horizontal yellow line shows the level of entropy for a good measuring (entropy is bigger than the lowest limit). The vertical yellow line shows where crossing the horizontal level and the regression graph. The vertical yellow line shows the optimal length of the measurement.

We validate the calculation by R^2 . When R^2 is lower than 90% the calculation is not valid. This can be at the beginning of the measurement. There are just a few result and the R^2 is low. As figure 4 shows it is 95% so the entropy regression calculation is valid.

Conclusion

To know a stochastic process is an endless measurement. A process, surface is changing continuously. Also if we know that this is a homogeny surface, the statistical parameters became nearly constant. In other hand nowadays the precision agriculture technologies try to serve every clods like a unique item. It is good for general working (the tractors are working on the whole fields) but control measurements should be optimal length.

Our method big advantage is, that we are able to **forecast** the optimal length of a stochastically measurement. Using exponential regression we get the parameters of entropy function. With a given accuracy we are able to calculate the optimal length of measurement. After this point we will have more value about surface but our knowledge won't be more.

We planned and made a lot of measurement on different surfaces.

First validation measurements was taken inside the university building, using different size of obstacles. Based on these measurements we saw, this method is useful to get information about surface after implement worked on. We also planned measurements on field side. We measured surface prepared by different type of soils, implements.

Using this distribution is difficult the qualify the soil. The get easy, fast result we develop new categories for optimal soil surface for seeding.

We make 3 categories (mentioned by prof. Márta Birkás):

- steady,
- moderately bumpy,
- rugged.

The main target to make steady surface. It has a lot of advantages, based on water usage, seeding...

Moderately bumpy has some bigger rigs, which caused less efficient seed growing. In this case there should be more power/force the reach the steady level surface.

Rugged surface, contains more rigs than optimal size of rigs. This can be by special soil parameters, too much water when implement was working, etc.

Based on prof. István Jóri and prof. Márta Birkás quality requirements, we are able to define the level of steady rigs (3-4-5 cm, different by plants). Important to notice again, that we calculated of vertical level different, which is correlate to rig size.

Table 1. Rates of over size by categories

Category	Rate of over size
Steady	rate <10%
Moderately bumpy	10% < rate < 30%
Rugged	30% < rate

Nomenclature

DOF Degree-of-freedom
 IMU Inertial Measurement Unit

References

- [1] Blahunka, Z., Bártfai, Z., & Faust, D. (2013). Measurement optimization by information entropy. *Synergy 2013 - Book of Abstract: 3rd International Conference of CIGR Hungarian National Committee and Szent István University, Faculty of Mechanical Engineering & 36th R&D Conference of Hungarian Academy of Sciences, Committee of Agricultural and Biosystem Engineering, "Engineering, Agriculture, Waste Management and Green Industry Innovation".*, 23.
- [2] Blahunka, Z., Bártfai, Z., & Lefánti, R. (2012). Soil surface monitoring with gyroscope. *Mechanical Engineering Letters*, 8, 10–16.
- [3] Blahunka, Z., Faust, D., Bártfai, Z., & Lefánti, R. (2011). Mobile robot soil surface monitoring. In L. Magó, Z. Kurják, & I. Szabó (Eds.), (p. 104). Gödöllő: SZIE Gépészmérnöki Kar.
- [4] Bose. (2009). *Modern Inertial Sensors And Systems*. PHI Learning Pvt. Ltd.
- [5] Seber, G. A. F., & Wild, C. J. (2005). *Nonlinear Regression*. John Wiley & Sons.
- [6] Shannon, C. E., & Weaver, W. (1949). *The mathematical theory of communication*. University of Illinois Press.
- [7] Wikipedia contributors. (2012, August 15). Entropy (information theory). In *Wikipedia, the free encyclopedia*. Wikimedia Foundation, Inc. Retrieved from [http://en.wikipedia.org/w/index.php?title=Entropy_\(information_theory\)&oldid=507540588](http://en.wikipedia.org/w/index.php?title=Entropy_(information_theory)&oldid=507540588)

Experimental study: Operator's behavior measuring inside Off-road vehicle Cabin (Operator's focusing matrix and response time)

Mohammad HUSHKI, Laszlo KÁTAI, Istvan SZABÓ
Department of Machine Construction, Institute for Mechanics and Machinery

Abstract

Operator's workplace design takes a priority to be developed in order to reach the highest possible level of Quality, Safety and productivity. Continual improvement of the workplace is yield from studies carried out on different approaches, each approach shall keep into consideration many aspects, in this research; the results will be used for feeding the productivity and safety aspects with valuable and dependent input data using relatively simple engineering solutions. This research is made based on literature of the accumulated knowledge from diverse fields in which different studies and analysis are made to provide the necessary input for Human Centered Design process, adopting the-state-of-the-art technologies and methodologies used for data collection and analysis for Human behavior inside the dedicated workplace. Better understanding of the operator's behaviors and its change according to the mental and physical workloads inside the workplace will lead to optimal designs for higher productivity and safer operation.

1. Introduction

Human-centered-design approach is considered one of the most effective factors enhancing the productivity of vehicles used in the industrial and agricultural fields. The development of operator's workstation needs to be based on deterministic data which is validated, verified and dependable.

Due to the operational nature of multi-tasking off-road vehicles, operators need to spend long working hours; which increases the level of mental workload leading to human error. [1] Introduced similar conclusion of which the vehicle design should be human oriented in order to maximize comfort and ability to perform the driving task perfectly and safely by reducing the human error possibilities.

Generating dependable and deterministic data to represent Human behaviors inside the workplace using validated method will be beneficial for enhancing current cabin designs as well as the future cabin designs.

This research is focusing on studying operator's selected behaviors inside the tractor's cabin using simple engineering solutions to obtain useful results to be considered in the improvement of tractor's cabin design (i.e. upgrading notification system inside the tractor's cabin and allocating new equipment or

components inside the tractor's cabin) and the operation's work procedures design to increase the productivity of a specific agricultural operation (i.e. break time scheduling and feeding the risk analysis process with deterministic and/or probabilistic inputs).

No solid single definition for the mental workload has been reached by researchers, but it could be defined as the relation between demands resulted from various tasks to be performed on the operator and his ability to fulfill; with satisfactory; these demands. [2] Described those demands as multidimensional, as it involves tasks, operator and system demands together with other factors. [2] Studies showed that the need for well fitted architectural space to the operator's dimensions is considered crucial, additionally; the mental workload level is found to be increasing with the time passing.

For the purpose of this research, we focus on passive fatigue. This type of fatigue is characterized by being the indirect product of the human driver's exertion of a set of tasks whose demands are low, monotonous or repetitive [3]. This rules out any sort of physical fatigue or mental active fatigue.

A study conducted in 2015 by Joel Gonçalves and Klaus Bengler [4] claims that Highly Automated Driving (HAD) will be commercially available in a near future, yet human factors issues like the influence of driver state can have a critical impact in the success of this driving paradigm and also in road safety. It is very likely that Driver State Monitoring Systems (DSMS) will play a bigger role than they have played so far.

However with this new driving paradigm shift is important to select highlight what is transferable from the previous systems. Due to lack of driving task engagement, driving performance metrics are no longer viable, creating opportunities for other approaches like detecting non-driving task engagement or fatigue countering behaviors. Eye based metrics will remain important.

2. Methodology

The target behavior: Operator's focusing matrix is developed as accumulated scenes and focusing by operator on sites inside the workplace. The most sited locations are identified as targets inside the workplace, additionally, some of safety related or research interest locations will be considered as well.

Additionally; Operator's focusing matrix change along working hours are done by dedicating fixed numbers for the frequency of sited locations at the end of each working hour. Change of that value will be the change of Operator's focusing matrix along working hours.

Selection of Operators

5 operators are selected to conduct the same agricultural operation using the same tractor vehicle, operators are categorized according to their job experience into 3 categories as follows:

Category A: High Experienced operators (2 operators).

Category B: Low experienced operators (2 operators) with less than one year experience.

Category C: None experienced operator (1 operator).

Operators' details are registered in the Appendix A. showing the name, gender, age and years of experience in addition to the physical details like the tall and weight.

Selection of vehicle

CLAAS tractor (Model: XXXX) is selected to the purpose of accommodating the number of experimental trials. This model has a covered workplace for the operator, which is helpful to control some of experimental conditions (i.e. temperature and humidity) keeping on the consistency of those parameters and conditions.

Selection of experimental field and operation

Experimental trials are conducted in several work fields for the same agricultural operation for 3 times for each operator along 6 working hours. The details of experimental execution conditions and fields are registered in Appendix B.

Recording cameras

Number of used cameras are 2 cameras, one is inside vehicle (DVR) in addition to the camera fixed to the operator's Tobii Pro glasses. The recording system configuration is shown in Figure [1].



Figure 1. System Configuration Layout.

Tobii Glasses 2 equipment

Tobii Glasses 2 Figure 2 is used to the purpose of obtaining the operator's focusing matrix from his/her real-time gaze analysis to predefined areas of interest. Which is feeding the research results with the main source of data regarding the target behavior to be studied.

Building the mental-load topographical map on the areas of interest inside the workplace and accumulate it at the end of each working hour, will lead to measure the change of this topographical readings along working hours. Which is the second behavior to be studied “Operator’s focusing matrix change along working hours”.

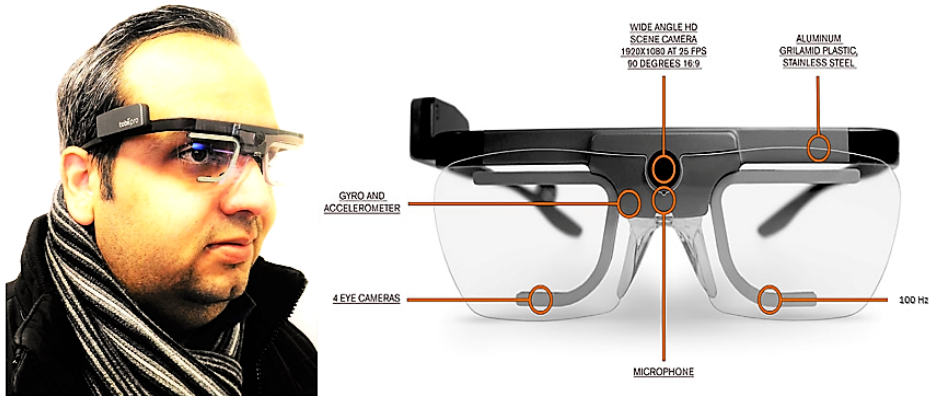


Figure 2. Tobii glasses 2

DVR for interior recording camera

A commercial DVR camera Figure 3 is used to monitor the tractors cabin interiors, the vision is showing the operator and his/her front and side areas which contain important controls selected as areas of interest. The main purpose of the DVR camera usage is to help researchers to make the decision of excluding any misleading records from the raw data.



Figure 3. DVR camera

Communication Module

The used vehicle is provided with a communication module to enable the operator to listen to directive orders from the monitoring laboratory, in order to

give certain directive orders as an inducer to measure; through the recorded videos; the response time of the operator to the induced order.

Processing of raw data

The main processing tool of the operators' gazes is the Tobii Pro Lab Figure 4 which has a powerful post-analysis and visualization tools provide a full spectrum of qualitative and quantitative gaze data analysis and visualizations. Tobii Pro Lab logs events, defines areas of interest, calculates statistics, creates heat maps, and exports data for further analysis in other software.

Researchers are tasked to go through all recorded videos of experiments resulted from the Tobii glasses 2 recordings and DVR recordings Figure 5 to make fair and evidences-based judgement regarding any misleading moments and exclude it from the raw data.

For linkage of the status of excluded periods, 2 screens are used to be compared to decide if the scene is a candidate to be excluded from analyzed data or just to be considered in the final result.



Figure 4. Tobii pro lab – analyzer software



Figure 5. DVR software for the exclusion procedure

Appendix C is used to keep the hard copy of excluded scenes. And other results are depending on the Tobii Pro Lab software package options for report generating.

Experimental procedure

The experiment is conducted on 3 phases:

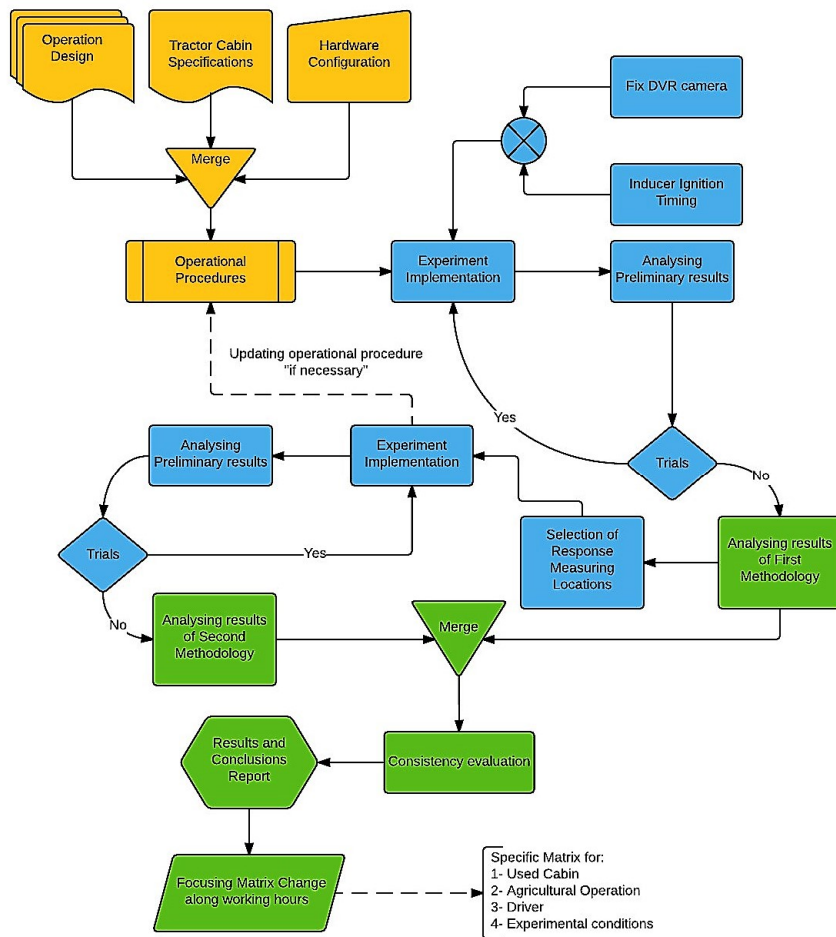


Figure 6. Experimental procedure flowchart

Phase 1: in which the consistency and similarity of the used work field and timing of operations will be ensured. Which applies as well for the experimental execution procedure. Operators are mandated to conduct the same operational procedures along trials. A calibration process for the Tobii glasses 2 is conducted via its dedicated software Tobii glasses controller software. Each operator is stored in the software, the software and the equipment have the capability to keep on each operator’s profile stored, and no recalibration is required to start the next experiment or to restart the recording during the same experiment in case of interruptions.

Phase 2: in which the execution of the experimental trials and data gathering are conducted. The operator is requested to wear special Eye-tracking Tobii glasses 2 providing the operators vision area and defining the point of focusing. Connected to the central station Cameras which are synchronically started at the beginning of each experimental trial, and synchronically stopped as well. The recording time is synchronized for all resulted video records.

According to the experiment execution procedure, several areas of interest is added to a representing matrix [M], each element in the matrix will store the accumulated time of operators glances (gaze) to that area of interest [AM].

Several inducers are ignited on previously defined times to request the operator checking a certain area of interest in the matrix. Upon the acknowledgement of operator, the response time is measured for each inducer providing the response time matrix for the areas of interest [RM].

Phase 3: in which data analysis and discussion are conducted. The recorded video films from all synchronized cameras are studied and analyzed by the research team to decide and document all none beneficial periods that includes abnormal behaviors or reactions to a random external inducer of the operators describing the reason of period exclusion.

Thereafter; the resulted data from the used eye-tracking glasses technology after exclusion procedure is represented in the matrix [AM].

Elements of [AM] are integrated at selected periods of working hours (i.e. at the end of each working hour or based on the nature of the operation) to produce the matrix [IM]_k. where k is the selected period number from 1 to K times.

Similarly; the response time matrix [RM] is separated along selected periods of igniting induces to produce the matrix [RM]_l. where l is the selected period number from 1 to L times as shown in Figure 7.

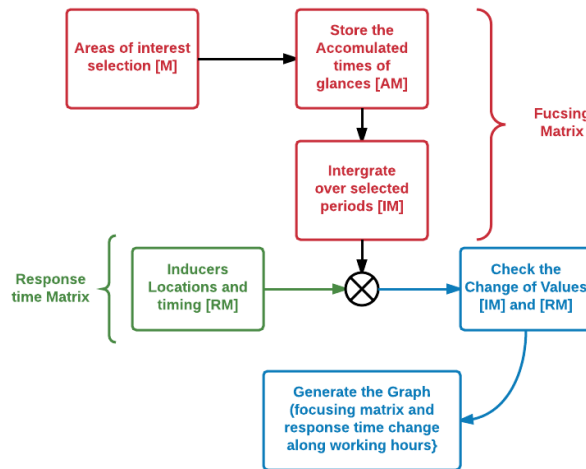


Figure 7. Generating the Change of Focusing Matrix [MI] and Change of Response Time Matrix [RM] along working hours.

Along working hours, the change of [IM] with increment of k and the change of [RM] with increment of l will be placed on a graph showing the change of the operator's focusing matrix and response time. Which are the target behaviors studied for each operator along several experimental trials.

Results

The final output of this research is to produce parallel methodologies to realize the change of operator's behaviors inside a specific tractor cabin used in specific agricultural operation and integrating those methodologies into one model with its operational procedure, research results are expected as follow:

a) Decreasing rate of operator's focus on several locations of components inside tractor cabin according to his/her head movement along working hours.

b) Decreasing rate of operator's response time to induced notifications in different locations inside tractor's cabin along working hours.

c) Correlating all mentioned measured rates with operator's tiredness and/or productivity formula of specific agricultural operation using specific tractor operated by specific operator.

d) Producing an engineering model with ability to provide valuable readings about operator's interaction with his/her workplace along working hours for different workplaces and/or agricultural operations "with mobility feature", the model will be useful as a tool for describing comparison's outcomes between different off-road vehicle cabins and/or agricultural operations in terms of Human Factor Engineering.

Highly Automated Driving (HAD) concept tries to automate as much as possible the driving task, this way freeing the driver to engage in other tasks. Yet, the human driver still retains the responsibility to resume the vehicle control in situation where the automation cannot handle. The Take Over Request (TOR) process contains many challenges that must be address in order to achieve the goal of allowing the driver to engage in other tasks and effectively support him to resume control in a safe manner.

One way to compromise the safety of a TOR process is to assume the driver is in a good status every time the TOR initiates. This process should not be set with fixed time buffers [5], but adjust the time buffer to the driver state. In practice, this is an application of the knowledge produced in the context of manual driver, for instance fatigued drivers have higher reaction times.

Analysis

CAT-A: experienced operators will be under focusing by the research, where they are looking and how they response to any inducer will be the question to be answered in the results. As well how it is changing along the time of working hours passing.

CAT-B: low experienced operators will show how it is different to be eager to an inducer by new or low experienced operator. The difference between CAT-A and CAT-B response change in time of working hours will be a useful result.

CAT-C: none experienced operators will be giving the shape of trend how change of experience is changing the response time and attention along working hours. As shown in Figure 8.

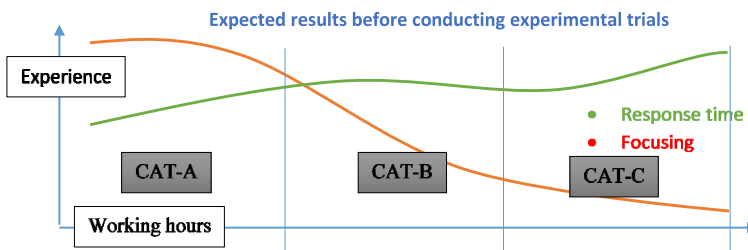


Figure 8. Expected results before conducting experimental trials.

Discussion

The confirming results of second target behavior “change of response time along working hours” of the expected results for the first target behavior “the change of operator’s focusing matrix along working hours” will be considered an indicator of the research methodology validity. However, many enhancement opportunities are proposed to the research methodology upon specifying more precise target behaviors of the operator in a certain production operation, workplace, field, timing, tool and/or vehicle ... etc.

Usability of research results

Increasing the efficiency and effectiveness of any agricultural or industrial operations that involves human operator – workplace interaction will be the main benefit of implementing this research methodology.

Current cabin designs are subjected to be enhanced with interactive guides and/or equipment for operators at the time in when and/or where it is expected to be needed because of the resulted numbers showing a decrement of focusing or response time.

Additionally, this research methodology is expected to be efficient comparison tool between prototypes of new cabin designs based on deterministic measures.

Future research usability

This research methodology is proposed to be developed for producing deterministic safety related measures to feed operator’s workplace and operation design with the necessary inputs. Which might be dependable to produce the safety or risk assessment reports for certain vehicle or operation design.

References

- [1] Li, G., and Haslegrave, C., M., (1999). Seated work postures for manual, visual and combined tasks. *Ergonomics*, 42(8). Taylor and Francis. pp. 1060-1086.
- [2] Sporrang, H., Palmerud, G., Kadefors, R., Herberts, P., (1998). The effect of light manual precision work on shoulder muscles-an EMG analysis. *Journal of Electromyography and Kinesiology*, 8. Pp. 177-184.
- [3] D. J. Saxby, G. Matthews, J. S. Warm, E. M. Hitchcock, and C. Neubauer, “Active and passive fatigue in simulated driving: discriminating styles of workload regulation and their safety impacts.,” *J. Exp. Psychol. Appl.*, vol. 19, no. 4, pp. 287–300, 2013.
- [4] J. Gonçalves and K. Bengler, “Driver State Monitoring Systems–Transferable knowledge manual driving to HAD”, *AHFE*, 2015.
- [5] C. Gold, D. Damböck, L. Lorenz, and K. Bengler, “‘Take over!’ How long does it take to get the driver back into the loop?,” in *Proceedings of the Human Factors and Ergonomics Society 57th Annual Meeting*, 2013, pp. 1938–1942.

Invited Papers

1. Zsolt HORVÁTH, András EDELMAYER:

LTI-modelling of the Air Path of Turbocharged Diesel Engine for Fault Detection and Isolation

The authors' team is research partner of the faculty in the field of energetic research and process modelling.

2. Jozef RÉDL, Juraj MAGA, Gábor KALÁCSKA:

Mathematical model of lateral stability of agricultural machine

The authors' team is research partner of the faculty in the field of energetic research and process modelling.

LTI-modelling of the air path of turbocharged diesel engine for fault detection and isolation

Zsolt HORVÁTH¹, András EDELMAYER^{2,3}

¹Postgraduate School of Multidisciplinary Engineering Sciences
Széchenyi István University, Győr, Hungary

²Department of Informatics, Faculty of Technical Sciences,
Széchenyi István University, Győr, Hungary

³Department of Applied Informatics (operated by MTA SZTAKI, Budapest), on behalf of the
Institute of Mathematics and Informatics, Szt. István University of Gödöllő, Hungary

Abstract

Combustion engines are complex, hybrid dynamical systems. They are characterized by the very fast dynamics in its mechanical and thermodynamic processes which are controlled by mechatronic components that can be commonly described by complex nonlinear representations. The application of nonlinear models of internal combustion engines in the solution of various control and fault detection problems, in real-time, constitutes a real engineering challenge. This paper discusses a model linearization approach for the modelling of the air path of diesel engines in an attempt to construct system representations for control and filtering applications. At first the issues of nonlinear modeling of the engine processes are reviewed, then the approach of linearization is discussed. The model verification, based on the comparison of the linear and nonlinear model performances through Matlab simulations is presented too. It is shown that, under specific conditions, the linearization, which is based on the Jacobian approach, provides suitable results to approximate the nonlinear model of the diesel engines air path. Our aim is to provide lower complexity LTI-models that can be used for the design of robust fault detection filters which can be implemented on the engine's microcontrollers.

Keywords

Mean-value engine model, model of the air path of diesel engines, Jacobian linearization, LTI-modelling, Fault detection and isolation

1. Introduction

In the past few decades steadily increased performance and environmental requirements for diesel engines are making it necessary to improve the modelling efforts for the purposes of robust control and fault diagnosis. Combustion engines can be typically represented by highly nonlinear processes that may have very fast dynamics. These properties pose additional requirements for the design, modelling and implementation of fault detection filters.

Complexity of modelling and simplicity of implementation are mutually two opposing design properties.

The creation of an accurate mathematical model of the system is not an easy engineering task. Combustion engines, for instance, are complex, nonlinear physical systems that are subject of noise and other disturbances coming from many sources. These physical processes can best be approximated by using nonlinear system models. By making reasonable simplifications and conditionally neglecting nonlinearities, the complexity of the models can be effectively reduced on the price that modelling will necessarily contain uncertainties.

Mean-Value Engine Models (MVEMs) are currently most commonly considered for model-based engine control and fault diagnosis purposes. There are many MVEM models available recently, see e.g., the studies (Jankovic and Kolmanovsky, 1998), (Jung, 2003) and (Herceg, 2006) which considered MVEMs for model-based control of the diesel engines air path. In the papers (Gertler et al., 1991) and (Krishnaswami et al., 1994) the application of MVEMs on the air intake system of SI-Engines for fault diagnosis purposes were proposed. The study (Buckland et al., 2009) presented an approach, which uses state observers for the estimation of unmeasured states in turbocharged gasoline engines. In (Chauvin et al., 2007) transient control of a diesel engine air path was presented. MVEMs have been also considered in numerous other studies and books, see e.g., the textbooks of (Guzella and Onder, 2010) and (Kiencke and Nielsen, 2004).

Because the complexity of the model impacts on the controller or fault detection filter design, in some cases a linearization approach of the nonlinear model is to be considered. The case-study (Guzella and Onder, 2010) uses a linearized model of the air path for air/fuel ratio control. (Kiencke and Nielsen, 2004) proposes the linearized model for engine idle-speed control implementation. An application of the Linear-Quadratic-Gaussian approach with Loop-Transfer-Recovery (LGQ/LTR) methodology in the design of the control system for a petrol engine using a linearized engine model was also considered in (Onder, 1993).

A detailed survey about the theory of the linearization approach for multivariable systems with some applications can also be found in the control literature e.g. in (Albertos and Sala, 2004) and (Gu, D., W., Petkov, P., H., and Konstantinov, 2013).

The robust model-based fault detection filter design methodology that we use in our study requires LTI models. From this reason this paper presents a linearization approach for the modelling of the air path processes of diesel engines. The model we are interested in is an LTI model suitable for the design of the fault detection filter. It is important to note that the above-mentioned methodologies can be applied by using a Linear Parameter Variable (LPV) modeling technique too. This modeling concept, however, is not the subject of this paper.

A simplified nonlinear model of the air path, that we used for linearization, was first suggested by (Jankovic and Kolmanovsky, 1998) for purposes of nonlinear control of diesel engines. The simplified third order nonlinear model that we used for linearization in a chosen operating point includes the gas dynamics in the intake and the exhaust manifolds. The nonlinear model of the plant should be approximated by the linearized model under the assumption of small deviations of the variables at the chosen operating point.

Obviously, for big deviations from the operating conditions where the linearization was done the approximation does not hold true and the detection performance of the fault detection filter may be badly compromised. To avoid this problem a set of local LTI models is created for different operating points and the corresponding filter gains are calculated to each of the LTI conditions. In our approach the Jacobian linearization method was implemented to obtain the local LTI models.

The detection method is based on the application of multiple LTI models, linearized around a representative set of operating conditions each, and switching between these LTI models by using scheduling variables. In this way, it is possible to set up a switchable set of filters whose dynamics adjust according to the variation of the nonlinear system (gain scheduling).

2. Model of the diesel engines air path

2.1 Model structure

The model of an examined system is always a partial representation of its behavior. From this comes, that the focus will be posed on behavior in which we are interested. The most complex part of the air path of the diesel engines is the turbocharger, which provides a substantial coupling between the engine exhaust and intake sides.

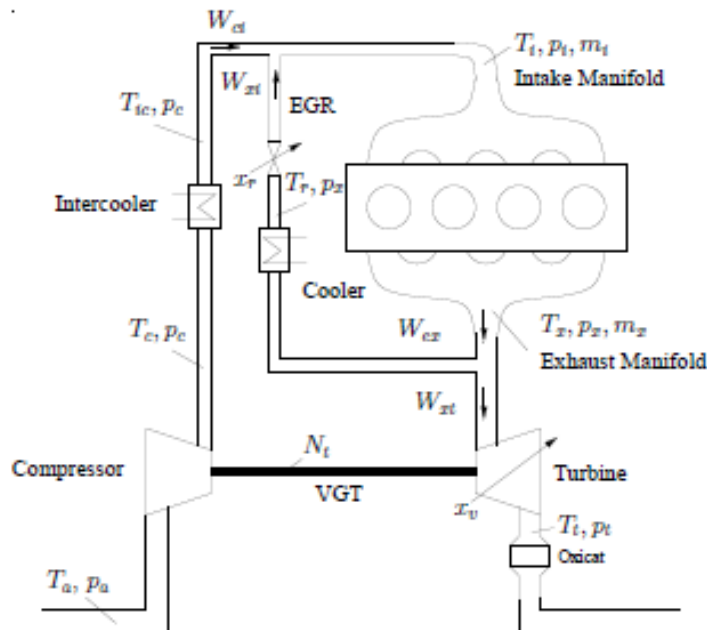


Figure 1. The scheme of the modelled turbocharged diesel engine (Jung, 2003)

The turbocharger dominates the air path; it consists of the turbine and compressor. The turbine is driven by the exhaust gas flow and it has a variable geometry turbocharger (VGT), whose position corresponds to closing or opening the guide vanes, that increases or decreases the turbine speed respectively. When the turbine speed is increased, the air in the inlet charge is more compressed, i.e., increased intake manifold pressure.

The second path from the exhaust gas to the intake manifold is the exhaust-gas recirculation, which is needed for NO_x reduction. The burned gas fraction is recirculated into the intake manifold and it displaces fresh air in it. This is lowering the flame temperature and hence decreasing of NO_x in the exhaust gas.

The basic structure of the system to be modelled is shown in Fig 1.

A detailed theoretical survey about the function of diesel engines can also be found in the literature see e.g., (Guzella and Onder, 2010), (Merker and Teichmann, 2014) and (Basshuysen, 2010).

2.2 Nonlinear modeling of the air path

A simplified third order nonlinear mean-value model of the air path is derived under various assumptions on the dynamics and the ideal gas law for intake and exhaust manifolds. This approach was first proposed by (Jankovic and Kolmanovsky, 1998).

The details of the applied modeling are determined by the ultimate goal of the actual engineering design; thus the modelling approach depends on the fault detection methodology as well. In this sense and also according to the concept of MVEMs the following modelling assumptions were taken:

- the potential energy is neglected
- the fluid can be modelled as an ideal gas
- constant intake, exhaust, manifold temperatures
- constant volumetric efficiency of the engine
- constant efficiency of turbine and compressor
- specific gas constant and adiabatic exponent are constant

The model (Jankovic and Kolmanovsky, 1998) is derived and parametrized for low and medium speed load points, which covers the New European Driving Cycle (NEDC) directive designed to assess the emission levels and fuel economy of car engines. NEDC was also taken into consideration by (Jung, 2003) which described the process by using the following set of equations:

The pressure of fluid flowing into the intake manifold can be formulated as

$$\dot{p}_i = \frac{RT_i}{V_i}(W_{ci} + W_{xi} - W_{ie}). \quad (1)$$

The pressure of fluid flowing into the exhaust manifold is

$$\dot{p}_x = \frac{RT_x}{V_x}(W_{ie} - W_{xi} - W_{xt} + W_f). \quad (2)$$

The compressor power of the turbo charger can be written in function of the turbine power with a time constant τ as

$$\dot{P}_c = \frac{1}{\tau}(-P_c + \eta_m P_t). \quad (3)$$

The compressor efficiency is treated as constant and the mass flow rate can be written as

$$W_{ci} = \frac{\eta_c}{c_p T_a} \frac{P_c}{\left(\frac{p_i}{p_a}\right)^\mu - 1}. \quad (4)$$

The mass flow through the EGR-valve assumed to be as subsonic is written as

$$W_{xi} = \frac{A_{egr} P_x}{\sqrt{RT_x}} \sqrt{\frac{2p_i}{p_x} \left(1 - \frac{p_i}{p_x}\right)}. \quad (5)$$

The mass flow from the intake manifold to the cylinder of the engine with the engine volumetric efficiency is

$$W_{ie} = \eta_v \frac{p_i N V_d}{120 T_i R}. \quad (6)$$

The turbine flow is given by

$$W_{xt} = (ax_{vgt} + b) \left(c \left(\frac{p_x}{p_a} - 1 \right) + d \right) \frac{p_x}{p_{ref}} \sqrt{\frac{T_{ref}}{T_x}} \sqrt{\frac{2p_a}{p_x} \left(1 - \frac{p_a}{p_x} \right)}. \quad (7)$$

The turbine power is written

$$P_t = W_{xt} c_p T_x \eta_t \left(1 - \left(\frac{p_a}{p_x} \right)^\mu \right). \quad (8)$$

All the model parameters proposed by (Jung, 2003) are summarised in the Table 1.

Table 1. Nonlinear model parameters

Parameter	Name	Value	Units
τ	turbocharger time constant	0,11	s
η_m	turbocharger mechanical efficiency	0,98	-
V_i	volume of the intake manifold	0,006	m ³
V_x	volume of the exhaust manifold	0,001	m ³
η_c	compressor efficiency	0,61	-
T_a	ambient temperature	298	K
c_p	specific heat at constant pressure	1014,4	J/kgK
c_v	specific heat at constant volume	727,4	J/kgK
$\mu = \frac{c_p - c_v}{c_p}$	specific heat ratio	0,286	-
P_a	ambient pressure	101325	Pa
T_x	exhaust gas temperature	509	K
R	gas constant	287	J/kgK
η_v	engine volumetric efficiency	0,87	-
T_i	gas temperature in the intake manifold	313	K
V_d	total engine displacement volume	0,002	m ³
P_{ref}	reference pressure	101325	Pa
T_{ref}	reference temperature	298	K
η_t	turbine efficiency	0,76	-
n	number of cylinders	4	-

Table 2. States and input/output variables of the linearized system

Variable	Notation	Function
EGR-Actuator effective area	A_{egr}	Input
VGT-Actuator position	x_{vgt}	Input
Engine speed	N	Disturbance
Fuelling	W_f	Disturbance
Intake manifold pressure (pi)	x_1	State variable 1.
	y_1	Output 1.
Exhaust manifold pressure (px)	x_2	State variable 2.
	y_2	Output 2.
Turbine power (Pc)	x_3	State variable 3.
Air mass	W_a	Output 3.
	y_3	

With substituting the above described constitutive equations into the differential conservation balances the model equations can be written as defined below

$$\dot{p}_i = \frac{RT_i}{V_i} \left(\frac{\eta_c}{c_p T_a} \frac{P_c}{\left(\frac{p_i}{p_a}\right)^\mu - 1} + \frac{A_{egr} P_x}{\sqrt{RT_x}} \sqrt{\frac{2p_i}{p_x} \left(1 - \frac{p_i}{p_x}\right)} - \eta_v \frac{p_i N V_d}{120 T_i R} \right),$$

$$\dot{p}_x = \frac{RT_x}{V_x} \left(\begin{array}{l} \eta_v \frac{p_i N V_d}{120 T_i R} - \frac{A_{egr} P_x}{\sqrt{RT_x}} \sqrt{\frac{2p_i}{p_x} \left(1 - \frac{p_i}{p_x}\right)} - \\ - (ax_{vgt} + b) \left(c \left(\frac{p_x}{p_a} - 1 \right) + d \right) \frac{p_x}{p_{ref}} \sqrt{\frac{T_{ref}}{T_x}} \sqrt{\frac{2p_a}{p_x} \left(1 - \frac{p_a}{p_x}\right)} + W_f \end{array} \right),$$

$$\dot{p}_c = \frac{1}{\tau} \left(-P_c + \eta_m (ax_{vgt} + b) \left(c \left(\frac{p_x}{p_a} - 1 \right) + d \right) \frac{p_x}{p_{ref}} \sqrt{\frac{T_{ref}}{T_x}} \sqrt{\frac{2p_a}{p_x} \left(1 - \frac{p_a}{p_x}\right)} c_p T_x \eta_t \left(1 - \left(\frac{p_a}{p_x} \right)^\mu \right) \right). \quad (9)$$

3. Linearized model of the diesel engines air path

3.1 Jacobian linearization of the nonlinear model

As it was previously mentioned, robust model-based fault detection filter design methodologies require a linear time-invariant model. According to this, it is

necessary to linearise the nonlinear engine model from Eq. (9). For this reason, we develop the Jacobian linearization of the nonlinear system about a specific operating point, called an equilibrium point. In order to introduce our concept for LTI modelling, we need to review the short theory of the Jacobian linearization.

The state space realization of a nonlinear system can be formulated with following description

$$\begin{aligned} \dot{x} &= f(x(t), u(t), t), \\ y &= g(x(t), u(t), t). \end{aligned} \tag{10}$$

where $x \in \mathbb{R}^n$ is the state vector, $y \in \mathbb{R}^p$ is the output vector, $u \in \mathbb{R}^m$ is the input vector, f is an n -dimensional vector of non-linear functions finally g is an p -dimensional vector of nonlinear functions.

A point $\bar{x} \in \mathbb{R}^n$ called equilibrium point is defined as state vector (set of variables) such as

$$0 = f(\bar{x}, \bar{u}), \quad \Rightarrow \quad \bar{y} = g(\bar{x}, \bar{u}). \tag{11}$$

For small and constant input amplitudes the deviation to measure the difference states and inputs respectively can be expressed by

$$\begin{aligned} \Delta x(t) &= x(t) - \bar{x}, \\ \Delta u(t) &= u(t) - \bar{u}. \end{aligned} \tag{12}$$

With substituting Eq. (12) in Eq. (10) we get

$$\Delta \dot{x}(t) = f(\bar{x} + \Delta x(t), \bar{u} + \Delta u(t)). \tag{13}$$

With performing a Taylor expansion of the right-hand side, and neglecting the term that higher than 1st are we obtain

$$\Delta \dot{x}(t) \approx f(\bar{x}, \bar{u}) + \left. \frac{\partial f}{\partial x} \right|_{x=\bar{x}, u=\bar{u}} \Delta x(t) + \left. \frac{\partial f}{\partial u} \right|_{x=\bar{x}, u=\bar{u}} \Delta u(t). \tag{14}$$

But

$$f(\bar{x}, \bar{u}) = 0, \tag{15}$$

leaving

$$\Delta \dot{x}(t) \approx \frac{\partial f}{\partial x} \Delta x(t) + \frac{\partial f}{\partial u} \Delta u(t). \tag{16}$$

In this sense the original nonlinear system Eq. (10) can be approximated by the linearized Eq. (16) as long as the deviation variables $\Delta x(t)$ and $\Delta u(t)$ remain small. The corresponding matrices

$$A_{i,j} = \left. \frac{\partial f_i(x_1, x_2, \dots, x_N, u)}{\partial x_j} \right|_{x=\bar{x}, u=\bar{u}},$$

$$b_i = \left. \frac{\partial f_i(x, u)}{\partial s} \right|_{\bar{x}, \bar{u}}, \quad c_j^T = \left. \frac{\partial g(x, u)}{\partial x_j} \right|_{\bar{x}, \bar{u}}, \quad D = \left. \frac{\partial g(x, u)}{\partial u} \right|_{\bar{x}, \bar{u}}. \quad (17)$$

are constant.

With the matrices A, B, C and D, called Jacobian components of the nonlinear functions, the obtained linear system

$$\begin{aligned} \dot{\tilde{x}} &= A\tilde{x} + b\tilde{u}, \\ \tilde{y} &= c^T \tilde{x} + D\tilde{u}. \end{aligned} \quad (18)$$

is called the Jacobian linearization of the nonlinear system Eq. (10), about the specified equilibrium point (\bar{x}, \bar{u}) . It is worth noting, that if the process evolves to another equilibrium point, the Jacobian components change.

3.2 Realisation of the linearized model of the diesel engines air path

In the following part the linearized model of the air path should be realized with the given parameters and operating condition. For this reason, at first the nonlinear model of the plant is formulated in state space form. With defining the following states as written below

$$\begin{aligned} x_1 &= p_i, \\ x_2 &= p_x, \\ x_3 &= p_c. \end{aligned} \quad (19)$$

The state space representation of the nonlinear model can be written

$$\begin{aligned} \dot{x}_1 &= \frac{RT_i}{V_i} \left(\frac{\eta_c}{c_p T_a} \frac{x_3}{\left(\frac{x_1}{p_a}\right)^\mu - 1} + \frac{A_{egr} x_2}{\sqrt{RT_x}} \sqrt{\frac{2x_1}{x_2} \left(1 - \frac{x_1}{x_2}\right)} - \eta_v \frac{x_1 NV_d}{120T_i R} \right), \\ \dot{x}_2 &= \frac{RT_x}{V_x} \left(\eta_v \frac{x_1 NV_d}{120T_i R} - \frac{A_{egr} x_2}{\sqrt{RT_x}} \sqrt{\frac{2x_1}{x_2} \left(1 - \frac{x_1}{x_2}\right)} - \left(ax_{vgr} + b \right) \left(c \left(\frac{x_1}{p_a} - 1 \right) + d \right) \frac{x_2}{p_{ref}} \sqrt{\frac{T_{ref}}{T_x}} \sqrt{\frac{2p_a}{x_2} \left(1 - \frac{p_a}{x_2}\right)} + W_f \right), \\ \dot{x}_3 &= \frac{1}{\tau} \left(-x_3 + \eta_m \left(ax_{vgr} + b \right) \left(c \left(\frac{x_2}{p_a} - 1 \right) + d \right) \frac{x_2}{p_{ref}} \sqrt{\frac{T_{ref}}{T_x}} \sqrt{\frac{2p_a}{x_2} \left(1 - \frac{p_a}{x_2}\right)} c_p T_x \eta_i \left(1 - \left(\frac{p_a}{x_2} \right)^\mu \right) \right). \end{aligned} \quad (20)$$

According to study in (Jung, 2003) the control inputs of the LTI-system are the position of the exhaust gas recirculation valve (EGR-Actuator) and variable geometry turbocharger (VGT-Actuator), the outputs are the sensor for air mass flow into the intake manifold (MAF), the sensor for exhaust gas pressure (EMAP) and the sensor for intake manifold pressure (MAP).

Noting that in the original model (Jung, 2003) two outputs, namely MAF and MAP were used, but for the reason of better observability of the system we extended this to one additional output namely EMAP, which may be realized nowadays in the real applications without any problem. Using three outputs means that the exhaust manifold pressure is additionally measured too. This could result a better performance of the fault detection filtering.

The engine speed (N) and fueling (W_f) are considered as disturbance from view of the air path for the sake of the simplification of the control (Jung, 2003) and (Herceg, 2006).

We linearise this model around the specified equilibrium point, which's setting values and model variables are summarized in the Table 3.

Table 3. States and Input/Output variables of the linearized system

Variable	Notation	Function	Value in the equilibrium point
EGR-Actuator effective area	ΔA_{egr}	Input	$4 \times 10^{-5} \text{ m}^2$
VGT-Actuator position	Δx_{vgt}	Input	70 %
Engine speed	ΔN	Disturbance	1900 1/min
Fueling	ΔW_f	Disturbance	0.032 kg/s
Intake manifold pressure (p_i)	Δx_1	State variable 1.	124200 Pa
	Δy_1	Output 1.	
Exhaust manifold pressure (p_x)	Δx_2	State variable 2.	131000 Pa
	Δy_2	Output 2.	
Turbine power (P_c)	Δx_3	State variable 3.	930 W
Air mass	ΔW_a	Output 3.	-
	Δy_3		

It is important to note, that choosing the right operating point for linearization is a critical part for obtaining an accurate linear model. The operating point has been chosen in the medium speed region at 1900 rpm according to the requirements of NEDC, this can be seen in the study (Herceg, 2006).

To accomplish the linearization procedure, we also need to determine the control inputs and disturbances of the plant, they are defined as

$$\begin{aligned} A_{egr} &= 4 \cdot 10^{-5} \left[m^2 \right], \\ X_{vgt} &= 70 \left[\% \right], \\ W_f &= 0.0322 \left[kg / s \right], \\ N &= 1900 \left[1 / \text{min} \right]. \end{aligned} \tag{21}$$

One can perform the linearization in Matlab in an easy way by using the command *linmod* on the corresponded SIMULINK block-diagram of the nonlinear system. We applied a more sophisticated analytical procedure which is presented in the following. All the Matlab commands in this paper refer to the textbook (Angermann et al., 2007). The finding of the equilibrium point is carried out by implementing Matlab function *fsolve*, which returns a state vector value of the nonlinear system in a steady state for the chosen inputs

$$\bar{x} = [124200, 131010, 930]^T. \tag{22}$$

In the next step of linearization the Jacobian matrices will be also analytically computed by Matlab function *jacobian*. With substituting the values of the equilibrium point in the Jacobian matrices we obtain the LTI system (Eq. (23)).

$$\begin{aligned} \begin{bmatrix} \Delta \dot{x}_1 \\ \Delta \dot{x}_2 \\ \Delta \dot{x}_3 \end{bmatrix} &= \begin{bmatrix} -5.2643 & 4.7316 & 28.5021 \\ 50.7697 & -156.9827 & 0 \\ 0 & 0.4287 & -9.0909 \end{bmatrix} \begin{bmatrix} \Delta x_1 \\ \Delta x_2 \\ \Delta x_3 \end{bmatrix} + \\ &+ \begin{bmatrix} 1.6111 \cdot 10^9 & 0 \\ -1.5720 \cdot 10^{10} & 8.3514 \cdot 10^4 \\ 0 & -141.6484 \end{bmatrix} \begin{bmatrix} \Delta A_{egr} \\ \Delta x_{vgt} \end{bmatrix} + \\ &+ \begin{bmatrix} -47.7946 & 0 \\ 466.3408 & 1.46083 \cdot 10^8 \\ 0 & 0 \end{bmatrix} \begin{bmatrix} \Delta N \\ \Delta W_f \end{bmatrix}, \\ \Delta y &= \begin{bmatrix} \Delta y_1 \\ \Delta y_2 \\ \Delta y_3 \end{bmatrix} = \begin{bmatrix} 1 & 0 & 0 \\ 0 & 1 & 0 \\ 0 & 0 & 3.924 \cdot 10^{-5} \end{bmatrix} \begin{bmatrix} \Delta x_1 \\ \Delta x_2 \\ \Delta x_3 \end{bmatrix}. \end{aligned} \tag{23}$$

with the individual matrices

$$\begin{aligned}
 A &= \begin{bmatrix} -5.2643 & 4.7316 & 28.5021 \\ 50.7697 & -156.9827 & 0 \\ 0 & 0.4287 & -9.0909 \end{bmatrix}, \\
 B &= \begin{bmatrix} 1.6111 \cdot 10^9 & 0 \\ -1.5720 \cdot 10^{10} & 8.3514 \cdot 10^4 \\ 0 & -141.6484 \end{bmatrix}, B_{\omega} = \begin{bmatrix} -47.7946 & 0 \\ 466.3408 & 1.46083 \cdot 10^8 \\ 0 & 0 \end{bmatrix}, \\
 C &= \begin{bmatrix} 1 & 0 & 0 \\ 0 & 1 & 0 \\ 0 & 0 & 3.924 \cdot 10^{-5} \end{bmatrix}.
 \end{aligned} \tag{24}$$

where A , B , C and B_{ω} are appropriate constant matrices, B_{ω} is the disturbance input acting on the system.

The initial responses of the obtained LTI model are shown in Fig. 2, from this it can be stated that the LTI system in the chosen operating point is stable. This can be proved also by checking the eigenvalues of the system matrix A laying in the left-half-plane.

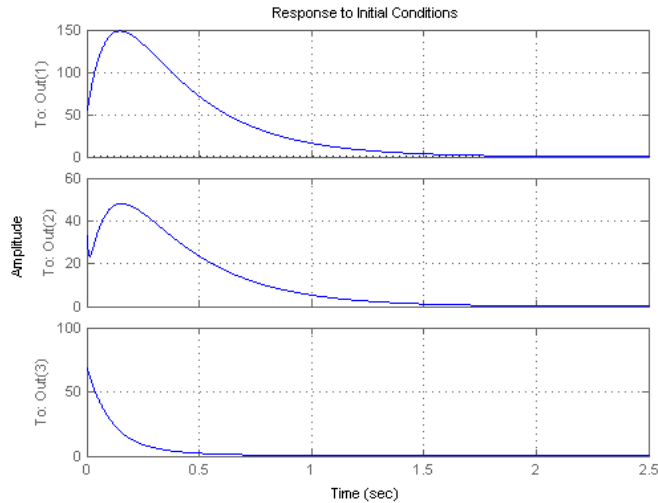


Figure 2. Initial responses of the obtained LTI model

It is worth noting if the process evolves to another equilibrium point, the Jacobian components change. In our paper for reason of simplifications, we referred only to the chosen equilibrium point. For further investigations in the sense of our application goal which is the robust fault detection filter design, more

equilibrium points could be considered, this would result more obtained LTI models.

3.3 Model simulations and results

In the following part the obtained LTI model will be simulated to get the MAF, EMAP and MAP responses. For this reason, four different input signals were created by the EGR - and VGT-Actuator. Both the linearization algorithm and simulation were computed in Matlab.

The initial conditions for the linearized system were

$$\begin{aligned} \Delta x_0(t) &= x_0(t) - \bar{x}_0, \\ \Delta x_0(t) &= [(124250 - 124200), (131050 - 131010), (1000 - 930)]^T. \end{aligned} \quad (25)$$

In order to examine the obtained LTI model, we applied slightly different inputs and disturbances and \bar{u}_ω respectively. We apply various input and disturbance signals. At first they are defined as

$$\begin{aligned} \Delta u(t) &= u(t) - \bar{u}, \\ \Delta A_{egr}(t) &= 0.2 \cdot 10^{-5} \cdot \sin(2 \cdot \pi \cdot 0.1(t)), \\ \Delta X_{vgt}(t) &= 4 \cdot \sin(2 \cdot \pi \cdot 0.1(t)), \\ \Delta W_f(t) &= 4 \cdot 10^{-4}(t), \\ \Delta N(t) &= 20(t). \end{aligned} \quad (26)$$

In the next step the input signal was also a sine wave but with a frequency of 0.5Hz excited by the EGR-Actuator and VGT-Actuator, the disturbance signals remain the same.

Finally, the input signals were replaced by a square signal with the same frequency as before. Thus, four simulations have been performed altogether.

In order to show the performance of the LTI model we compare the response of the nonlinear system to the response of the LTI model. To get a correct graph for LTI model response thus a comparison for the LTI model we plot $(t) = \Delta x(t) + \bar{x}$.

Figures 3-6 show the MAF, EMAP and MAP responses of the system respectively excited by different input signals. The graphs of the linearized model are plotted in blue color and the dashed red lines correspond to the plots of the original nonlinear model.

It can be seen, that the plots of the responses of the linearized model matches the nonlinear model at the chosen operating point. We can see that the response is slightly more different from the response of nonlinear system. It was excited with signal square wave of higher frequency that was 0.5Hz in our case. This can be explained by the effects of linearization, in our case the exhaust pressure does not change significantly around the chosen operation point.

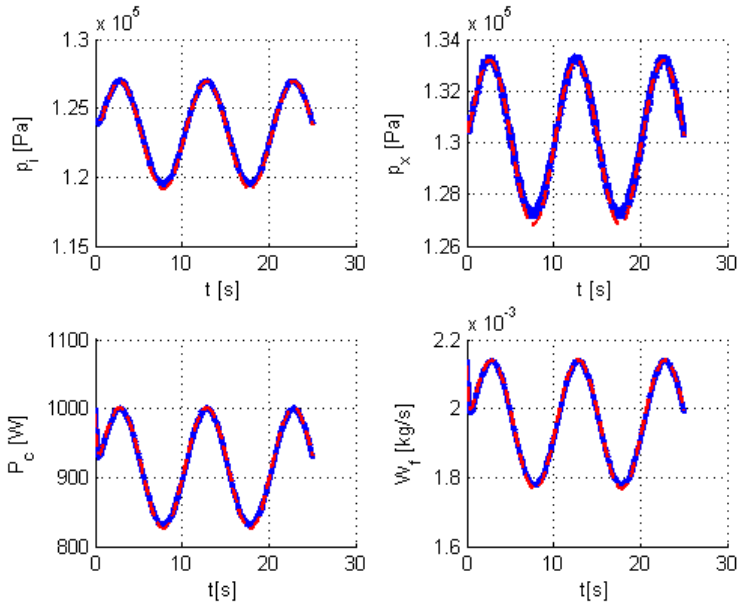


Figure 3. Comparison of the MAF, EMAP and MAP responses to sine inputs (0.1Hz) of an EGR- and VGT-Actuator blue line: nonlinear model, red dashed line: linearized model

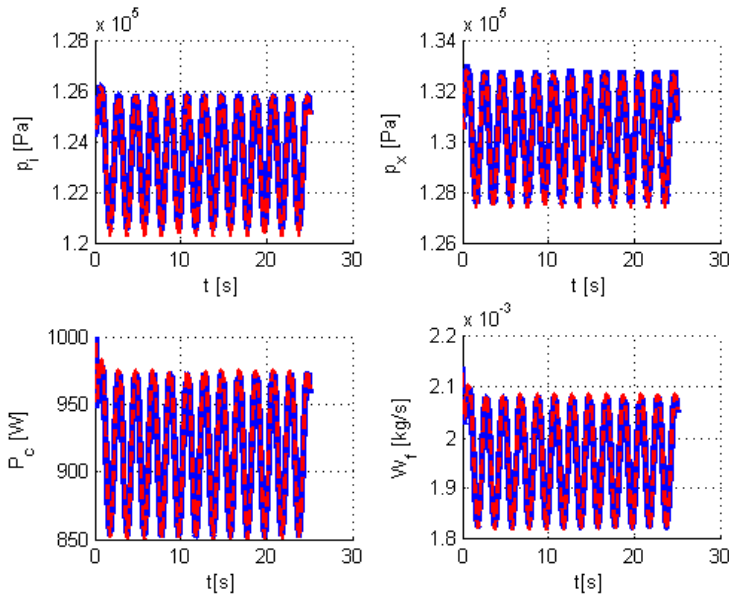


Figure 4. Comparison of the MAF, EMAP and MAP responses to sine inputs (0.5Hz) of an EGR- and VGT-Actuator blue line: nonlinear model, red dashed line: linearized model

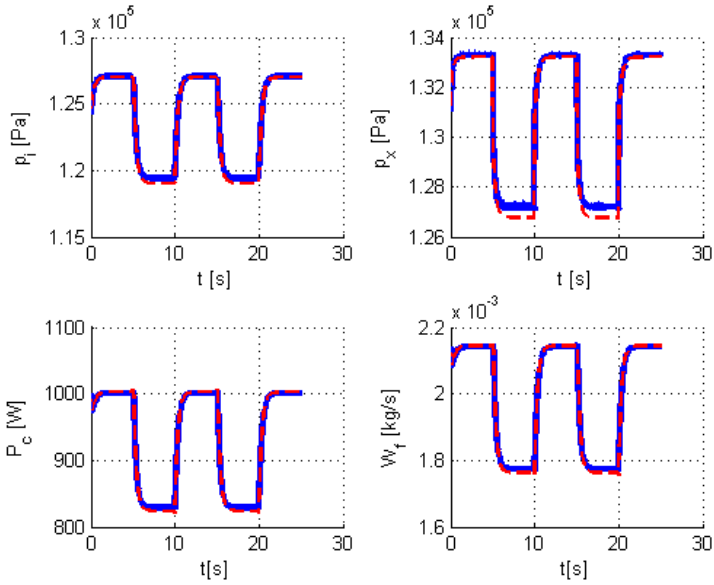


Figure 5. Comparison of the MAF, EMAP and MAP responses to square inputs (0.1Hz) of an EGR -and VGT-Actuator
blue line: nonlinear model, red dashed line: linearized model

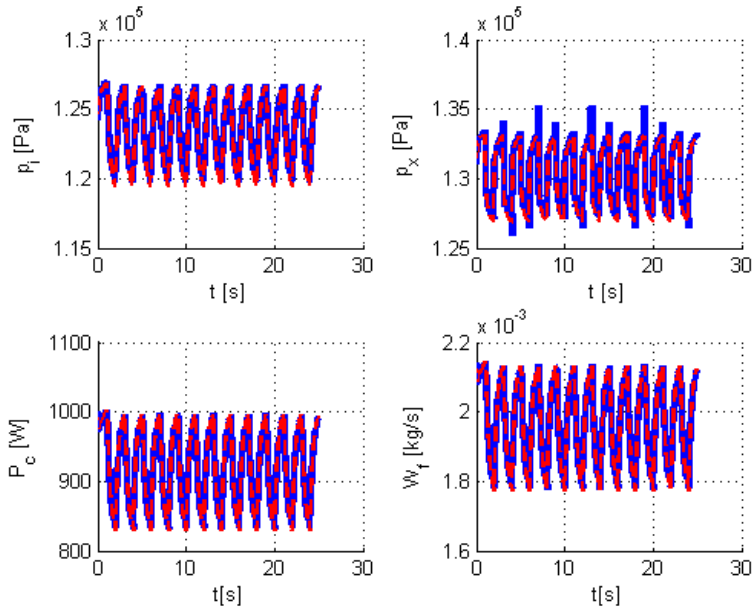


Figure 6. Comparison of the MAF, EMAP and MAP responses to square inputs (0.5Hz) of an EGR -and VGT-Actuator
blue line: nonlinear model, red dashed line: linearized model

Conclusion

In this paper the LTI-modelling problem of the air path of turbocharged diesel engines for fault detection and isolation purposes is discussed. Multiple LTI models, linearized in a set of distinguished operating conditions in the nonlinear process of the diesel engines air path with using the Jacobian linearization approach is used. The third order nonlinear mean-value engine model is parametrized for low and medium speed load points, which covers the New European Drive Cycle (NEDC), as proposed by (Jung, 2003) for robust control purposes.

The entire linearization procedure has been implemented in Matlab, namely finding the equilibrium point by the function *fsolve* and computing a Jacobian matrix by function *jacobian*. The procedure ended up in the modeling of the diesel engine air path by LTI approximation of the nonlinear state space.

In order to show the performance of the LTI modeling approach the results of four simulations have been performed, two with sine wave input signal and two with square wave, both with two different wave frequencies. The responses of the nonlinear plant and the approximate LTI model were compared to each other. It was shown, that the linearized model matches the nonlinear model at the chosen operating point quite well. Small acceptable differences could be observed when square wave input has been applied.

It can be seen that, in spite of the model complexity and strong nonlinearities under specific conditions, the Jacobian linearization is a suitable approximation for the nonlinear model of diesel engines air path. Our examination proved, that the proposed linearization approach can provide LTI models which can be used for a robust fault detection filter design.

References

- [1] Jankovic, M., Kolmanovsky, I.: Robust Nonlinear Controller for Turbocharged Diesel Engines, Proceedings of the American Control Conference, Philadelphia, PA (1998)
- [2] Jung, M.: Mean-value Modelling and Robust Control of the Airpath of a Turbocharged Diesel Engine, Ph.D Dissertation, University of Cambridge (2003)
- [3] Herceg, M.: Nonlinear Model Predictive Control of a Diesel Engine with Exhaust Gas Recirculation and Variable Geometry Turbocharger, Diploma Thesis, Slovak University of Technology in Bratislava, Bratislava (2006)
- [4] Guzzella, L., Onder, C., H.: Introduction to Modelling and Control of Internal Combustion Engine Systems, Springer, pp. 28-52 (2010)
- [5] Kiencke, U., Nielsen, L.: Automotive Control Systems for Engine, Driveline and Vehicle, Springer, pp. 167-171 (2004)
- [6] Gertler, J., Costin, M., Fang, X., Hira, R., Kowalczuk, Z, and Luo, Q.: Model-based On-Board Fault Detection and Diagnosis for Automotive Engine, IFAC Fault Detection, Supervision and Safety for Technical Processes, pp. 503-508, Baden-Baden, Germany (1991)

- [7] Krishnaswami, V., Chun-L, G., and Rizzoni, G.: Fault Detection in IC Engines using Nonlinear Parity Equations, Proceedings of the American Control Conference, pp. 2001-2005, Baltimore, Maryland (1994)
- [8] Buckland, J., H., Freudenberg, J., Grizzle, J., W., and Jankovic, M.: Practical Observers for Unmeasured States in Turbocharged Gasoline Engines, American Control Conference, St. Louis, MO, USA (2009)
- [9] Chauvin, J., Corde, G., and Nicolas, P.: Transient Control of a Diesel Engine Airpath, American Control Conference, New York, USA (2007)
- [10] Albertos, P., Sala, A.: Multivariable Control Systems, Springer, pp. 18-57 (2004)
- [11] Gu, D., W., Petkov, P., H., and Konstantinov, M., M.: Robust Control Design with Matlab[®], Springer, pp. 401-410 (2013)
- [12] Angermann, A., Beuschel, M., Rau, M., Wolfahrt, U.: Matlab[®]-Simulink[®]-Stateflow[®], Oldenburg Verlag, pp. 67-82, 236-241 (2007)
- [13] Merker, G., P., Teichmann, R.: Basics of the combustion engines, Springer Vieweg, pp. 176-266 (2014) (in German)
- [14] Basshuysen, R.: Combustion engine Handbook, Vieweg+Teubner, pp. 526-546 (2010) (in German)
- [15] Onder, H., C.: Model-based optimization of the control and regulation of an automobile engine, Ph.D. Dissertation, University of Zürich (1993) (in German)

Mathematical model of lateral stability of agricultural machine

Jozef RÉDL¹, Juraj MAGA², Gábor KALÁCSKA³

¹Department of Machine Design, Faculty of Engineering,
Slovak University of Agriculture in Nitra, Slovakia

²Department of Machines and Production Biosystems,
Faculty of Engineering,

Slovak University of Agriculture in Nitra, Slovakia

³Department of Maintenance of Machinery
Institute for Mechanical Engineering Technology

Abstract

In this contribution we deal with the mathematical model of lateral stability of agricultural off-road vehicle with respect to the elastic properties of the tires. The modeled machine was Reform Metrac H6X. The static properties of machine were obtained from manufacturer. Machine was modeled with 2D simple model with disposition on tilt table with initial tilt angle. To the mathematical model was included the deformation ratio of tires and its elastic properties. The tire properties were obtained from manufacturer. The simulation was realized for two options. Simulation for whole machine and for machine with front mounted tool. Created model also calculated the corrections of height of center of gravity and correction of tire section height. Results from simulation approved a serious influence of elastic properties of tire to machine static stability with and without mounted tool. The change of center of gravity due of mounted adapter has a serious influence to static stability of machine. Obtained results are useful in process of design and testing of prototypes.

Key words

Lateral stability, tire properties, mathematical modeling, tilt table

1. Introduction

Accidents of mountains machines and other agricultural machines operating on slopes are very often. The cases of these accidents we have select to two groups [11]. The first is the simple overturn, primarily is a lateral overturn. The second case occurs when the driver absolutely loss of steering of machine which is uncontrollable skidding. At the real conditions of this type uncontrollable moving we cannot predict the final position of machine. Off-road machine operating on slope have to respect this parameters:

- working characteristic which indicating loss of control,

- overturning stability,
- technical ability of vehicle eliminate the overturning process.

Ability of machine to moving on slopes safely is defined as sloping availability by [8]. Important work about vehicle rolls stability published by [13]. He applied the tire elastic properties to the lateral static stability of vehicle.

Very important predictable factor of side slope stability is determination of its static stability how are defined by [10]. Authors [10] refers about earth machine construction. Mostly of machines refers to construction for a low position of center of gravity and this improve the best stability on rough terrain. Researchers [12] present newly developed tire model for the *Overturning Moment (OTM)* characteristics and the analysis of the influence of OTM on vehicle rollover behavior. A new model for the tire overturning moment characteristics was developed based on the *Magic Formula* by adding a new term for the residual pneumatic scrub. The magic formula was published by [5]. The coupling interactions between vehicle anti-rollover and lateral stability, as well as the effect of road excitation, are taken into account on the vehicle rollover analysis. Authors [3] found that the some parameters influence the different vehicle stabilities diversely or even contradictorily and it has been found that there are contradictions between the vehicle rollover mitigation performance and the lateral stability. The direct cause for the contradiction is the lateral coupling between tires and road. Tires with high adhesion capacity imply that the vehicle possesses a high performance ability to keep driving direction, whereas the rollover risk of this vehicle increases due to the greater lateral force that tires can provide. Authors [2] declared that the static stability factor (SSF) may be a predictor of vehicle rollover propensity. Authors find the relation between the critical tilt angle and the static stability factor. They find the results were also involves the *tire/road* friction which is usually more dependent upon the *roadway/ weather* than the tires.

2. Material and methods

Systemic vehicle



Figure 1. Vehicle without tool



Figure 2. Vehicle with tool

The REFORM Metrac is a municipal services tool carrier designed for extreme slopes and difficult terrain. It is distinguished by cutting edge technology and highest efficiency. With its outstanding versatility, the Metrac is ready to roll in all working situations and provides unique working convenience as defined in [7]. Tool carrier is shown in the fig.1 in weighing process without tool and the figure 2 depicted the carrier in the same process with the mounted tool. The mounted tool is a mulcher Carroy.

Technical parameters of vehicle and tool are described in table 1 and table 2.

Table 1. Parameters of off-road machine

Parameter	Value	Unit
Manufacturer	Reform-Werke	
Type	Metrac H6 X	
Engine	VM-D 754 SE 3	
Tyres	33x15.50-15 BKT	
Weight	2370	kg
Weight with tool	2780	kg
Wheel base	1,995	m
Wheel track	1,630	m

Table 2. Parameters of tool

Parameter	Value	Unit
Manufacturer	DSP Production Sas	
Mark	Carroy	
Type	GF 2072 RE7F C6 2S	
Description	mulch-laying adapter	
Weight	410	kg
Length	1,0	m
Width	2,270	m
Height	1,10	m

The slope travelling ability was at 55 - 60 % in traverse lines and at 60- 65% in fall line at good driving conditions (dry ground with maximum grip). If the electronic weight transfer system is adjusted in an optimal way, working up hill of nearly 70 % can be reached on perfect conditions. This may not be the case everywhere and can only be achieved – as aforementioned – on optimal conditions and with excellent knowledge of driving and terrain [7].

Model

Mathematical model was created as a 2D simple model with situation on tilt table. The equations of model are with respect to the picture 3 and picture 4. The geometry of vehicle was defined as follow, with respect to the figures 3 and 4 :

$$t = (t_1 - \delta) \cdot \cos(\varphi) - r \cdot \sin(\varphi) - h \cdot \sin(\varphi),$$

$$H = (t_1 - \delta) \cdot \sin(\varphi) + r \cdot \cos(\varphi) + h \cdot \cos(\varphi),$$

$$\tan(\varphi) = \frac{R - r}{2 \cdot t_1 - \delta}, \quad G = m \cdot g. \text{ Where } g \text{ is gravitation acceleration.}$$

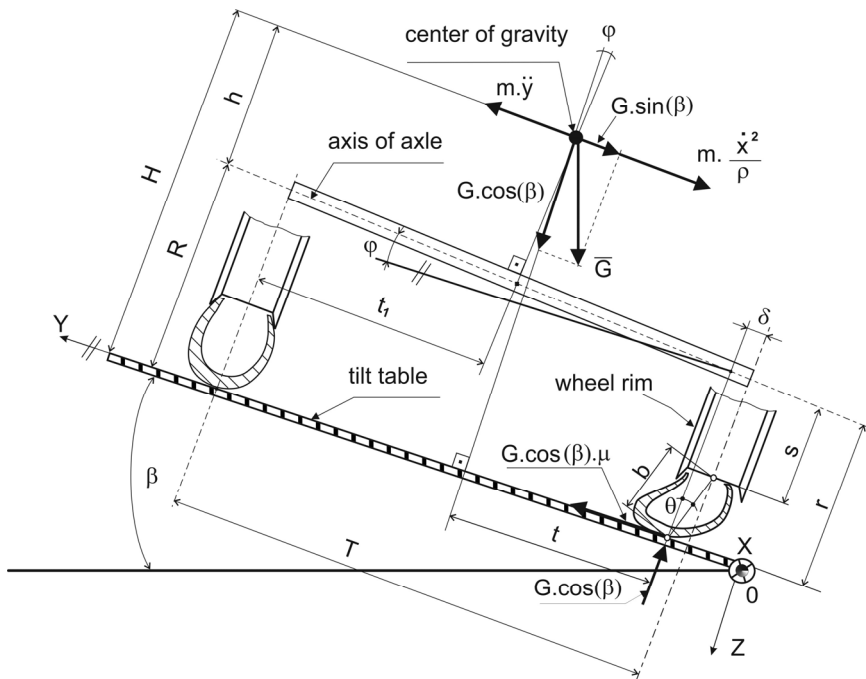


Figure 3. Vehicle on tilt table

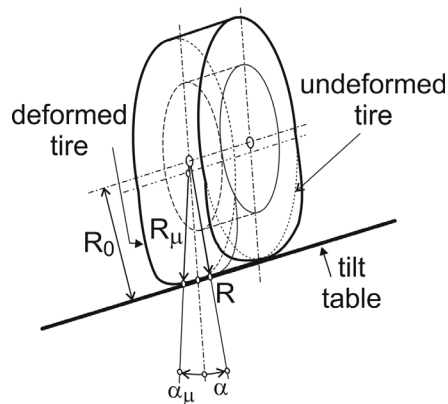


Figure 4. Tire deformation

Stability conditions

For $\dot{x} = 0; \ddot{y} = 0$,

$$\begin{aligned} G \cdot \sin \beta &= G \cdot \cos(\beta) \cdot \mu, \\ \mu &= \tan(\beta), \\ \beta &= \arctan(\mu), \\ G \cdot \sin(\beta) \cdot H &= G \cdot \cos(\beta) \cdot t, \\ H \cdot \mu &= t. \end{aligned} \quad (1)$$

Linearizing the nonlinear equations we get: $\cos \phi = 1$ and $\sin \phi = 0$, and then:

$$\begin{aligned} t &= (t_1 - \delta) - r \cdot \varphi - h \cdot \varphi, \\ H &= (t_1 - \delta) \cdot \varphi + r + h, \end{aligned} \quad (2)$$

$$\varphi = \frac{R - r}{2 \cdot t_1 - \delta}. \quad (3)$$

Combining the eq.2 and eq.3 and with the next editing we get:

$$t + H \cdot \varphi = (t_1 - \delta) \cdot (1 + \varphi^2),$$

if $\varphi^2 \ll 0$, then :

$$t = t_1 - \delta - h \cdot \varphi.$$

Yaw of tire on loaded side:

$$\delta = \frac{G \cdot \cos(\beta) \cdot \mu}{LS}. \quad (4)$$

With respect that $\frac{\delta}{H} \ll 1$ and finally get:

$$\mu = \frac{t_1}{H + \frac{G \cdot \cos(\beta)}{LS}} - \varphi. \quad (5)$$

Model of tire is described in figure 4.

The radial stiffness on loaded side of vehicle is:

$$K = n \cdot \frac{W}{R - R_s} \quad (6)$$

The radius of radially loaded tire is:

$$R_0 = R - \frac{G \cdot \cos(\beta)}{K} \quad (7)$$

The contact angle is:

$$\alpha = \arccos\left(\frac{R_0}{R}\right) \quad (8)$$

Applying of results and adhesion changing the lateral stiffness of vehicle published by [1] we get:

$$LS = \frac{(4 - \mu) \cdot R \cdot \alpha \cdot (\pi - \alpha)}{16 \cdot b} \cdot K \quad (9)$$

Yaw angle of tire on loaded side is:

$$\theta = \arcsin\left(\frac{\delta \cdot \mu}{b}\right) \quad (10)$$

Radius of loaded tire:

$$r_\mu = R_0 \cdot \left(\frac{s + b \cdot \cos(\theta)}{R}\right) \cdot \left\{1 - \frac{1}{2} \cdot \left[\left(\frac{R}{s + b \cdot \cos(\theta)}\right)^2 - 1\right] \cdot \alpha^2\right\} \quad (11)$$

Results are obtained with iterative solving of equations 1 till 11. The major result is the boundary angle of tilt table which is respect the radial and lateral stiffness of tire.

3. Results and discussion

To obtain expected results, we used the values from table 3. Technical parameters of location of center of gravity for described options we get from manufacturer [4]. The parameters of tire we also get from manufacturer.

Table 3. Input parameters for simulations

Parameter	Description	Value		Unit
		Carrier	With tool	
m	Weight	2370	2780	kg
T	Wheel track	1630	1630	mm
h	Height of center of gravity to rear axle	322	362	mm
Tires type	Tires type	33x15.50-15 BKT		
R	Radius of no-load tire	432,5	432,5	mm
RS	Static radius of tire	378	378	mm
W	Admissible load of tire	15900	15900	N
s	Radius of wheel disk	190,5	190,5	mm
b	Height of free tire section	242	242	mm
n	Number of wheels on load side	2	2	
p	Working pressure of tire	80	80	kPa
μ	Initial adhesion	0,6	0,6	
β	Initial angle of tilt table	31	31	deg

Table 4. Solved parameters

Variable	Description	Value		Unit	Solved from eq.
		Carrier	With tool		
H	Corrected height of CG	734,093	770,379	mm	2
φ	Angle of axle and tilt table	1°25'	1°43'	Deg	3
δ	Yaw of tire	49,236	53,926	mm	4
μ	Adhesion	0,974	0,918		5
K	Radial stiffness	583,486	583,486	N.mm-1	6
R0	Radius of radially loaded tire	398,332	392,421	mm	7
α	Contact angle	22°55'	24°51'	Deg	8
LS	Lateral stiffness	242,95	260,193	N.mm-1	9
θ	Yaw angle of tire	11°44'	12°53'	Deg	10
R μ	Radius of loaded tire	392,92	385,853	mm	11
β	Yaw angle of tilt table	44°15'	42°34'	Deg	2...11

Created mathematical model was applied for two options. First was for only whole carrier. The weight of operator was neglected for both options. The second option was a carrier with mounted tool – mulcher. Solved results are described in table 4. The pressure of all tires was inflated to recommended pressure. The adhesion coefficient was chosen approximately with respect to the sloped terrain with respect to [3].

Conclusion

The construction similar machines have an approximately static stability 50-60 deg. The mathematical model describes a methodology how to get an approximately values of static stability of machine with and without mounted tool. From realized

simulation we get the minimum value of angle of tilt table for machine $44^{\circ}15'$ deg. The minimal angle of tilt table with mounted tool was $42^{\circ}34'$ deg. The solved values are very near of usually declared values of the other manufacturer. The solved values valid in the state of vehicle no skidding on tilt table. The real measurement data from tilt table was not available. The change of vertical position of CG after mounting a tool has a visible effect. Inaccuracies of solved parameters are caused by linearizing of equations of model. But the distance between the real data and solved data has an effect on the labile position of vehicle. An effect of elastic properties of tire on a lateral stability of vehicle was confirmed.

References

- [1] Clark, S.K. 1971. Mechanics of Pneumatic Tires - Monograph, National Bureau of Standards Washington, USA, 1971.
- [2] Hustona, R.L. – Kellyb, F.A. 2014. Another look at the static stability factor (SSF) in predicting vehicle rollover. In.: International Journal of Crashworthiness, 2014. Vol. 19, No. 6, 567575, <http://dx.doi.org/10.1080/13588265.2014.919730>.
- [3] Li, Y.-Sun, W.- Huang, J. -Zheng, L.- Wang, Y. 2013. Effect of vertical and lateral coupling between tyre and road on vehicle rollover. In.: Vehicle System Dynamics, 2013, Vol. 51, No. 8, 1216–1241, <http://dx.doi.org/10.1080/00423114.2013.791395>.
- [4] Metrac Pruefberichte, Available at: <http://www.josephinum.at/fileadmin/content/BLT/Pruefberichte/g2008253.pdf>
- [5] Pacejka, H. 2005. Tire and Vehicle Dynamics. Butterworth-Heinemann 2005. p.672.
- [6] Pacejka, H.B. - Besselink, I.J.M.: Magic Formula Tyre Model With Transient Properties. Suppl. to Vehicle Syst. Dyn. 27 (1997), pp. 234–249
- [7] Reform - Werke, www.reform.at.
- [8] Šesták, J. – Sklenka, P. – Škulavík, L. Matematické modely terénnych vozidiel určené na popis ich správania pri práci na svahu. 1993. Universitatis Agriculturae Slovakia, Nitra. ISBN 80-7137-095-9
- [9] Šesták, J.- Rédl, J.- Markovič, R. 2000. Assessment of Side Slope Stability of Agricultural Vehicles In. : Res. Agr. Eng., 46, 2000 (2): 53-58.
- [10] Simoník, J. - Jobbágy, J. 2010. Earth-moving machinery (Stavebné stroje), 1.st.edition. Nitra: Slovenská poľnohospodárska univerzita, 2010. 187 s. ISBN 978-80-552-0514-4.
- [11]. Spencer, H.B.: Stability and control of two – wheel drive tractors and machinery on sloping ground. In: Journal of agricultural engineering research. 23(2), 1978, p.p. 169-188.
- [12] Takahashi, T.- Hada, M.- Oyama, K. Sakai. H.: 2004. New Model of Tire Overturning Moment Characteristics and Analysis of Their Influence on Vehicle Rollover Behavior. In.: Vehicle System Dynamics 2004, Vol. 42, Nos. 1–2, pp. 109–118.
- [13] Tamny, S. 1993. Operating Vehicle Roll Stability. In.: Heavy Vehicle Dynamics and Stability. SAE International, SP-1002, Detroit 1993.